NASA CR-165,601

DOE/NASA/0064-1
NASA CR-165601
AiResearch 81-18266

NASA-CR-165601
19830002078

Lightweight Electronically Commutated dc Motor for Electric Passenger Vehicles

E. F. Echolds and P. S. Walia
AiResearch Manufacturing Company
The Garrett Corporation

September 1982

NOTICE

Lightweight Electronically Commutated dc Motor for Electric Passenger Vehicles

E. F. Echolds and P. S. Walia
AiResearch Manufacturing Company
The Garrett Corporation
Torrance, California 90509

September 1982

N83-10348

CONTENTS

CONTENTS (Continued)

SUMMARY

The objective of this program was to develop a state-of-the-art, electronically commutated motor specifically designed for propulsion of electric vehicles with increased range, reduced energy consumption, and reduced life-cycle costs compared with conventional systems. The program was accomplished in two phases involving development and test of (1) a functional model breadboard converter and a rare-earth-cobalt, permanent-magnet (PM) motor, and (2) an engineering model converter and PM motor suitable for vehicle installations. The converter controls the torque and speed as in a conventional controller in addition to providing electronic commutation. The additional controls and protection required for vehicle operation are also included in the integrated package.

The motor shown in figure 1 and the converter shown in figure 2 meet the objectives established for the engineering model (i.e., 88 percent peak efficiency, a maximum output of 26 kW at 26,000 rpm, and a continuous rating of 15 kW). The efficiency value includes the losses in both the converter and motor, and hence should be compared with the efficiency of a conventional dc motor and controller in combination.

The motor and controller also regenerate power to the source during braking, with a demonstrated peak power available at the converter terminals of approximately 26 kW at 88 percent efficiency. With the system operating at 15 kW, a steady-state winding temperature of 100°C was measured at 25°C laboratory ambient temperature.

The PM motor is 163-mm (6.4-in.) in diameter and 269 mm (10.6 in.) long, and weighs 16.2 kg (35.8 lb) compared with a 15.9-kg (35-lb) objective. No target weights were established for the converter since the objective was easy access for vehicle testing and service rather than minimum package size and weight. The engineering model converter is 826 by 711 by 283 mm (32.5 by 28 by 11.13 in.) and weighs 68 kg (150 lb). About one-half the weight is due to laboratory type construction and the inclusion of capacitor banks to provide a stiff voltage source when remotely located from the power source.

Major conclusions are as follows.

(1) The combined motor and controller have a demonstrated peak efficiency of 88 percent. It has been estimated that this will result in a J227a(D) cycle efficiency of approximately 86 to 88 percent when energy available for recovery at the converter terminals is included, compared to published conventional motor and controller efficiencies (with regeneration) of 81 to 83 percent.

(2) The converter initial cost is approximately five times that of the permanent magnet motor. Converter cost can be reduced by means of LSI logic and integrated liquid-cooled semiconductor packages.
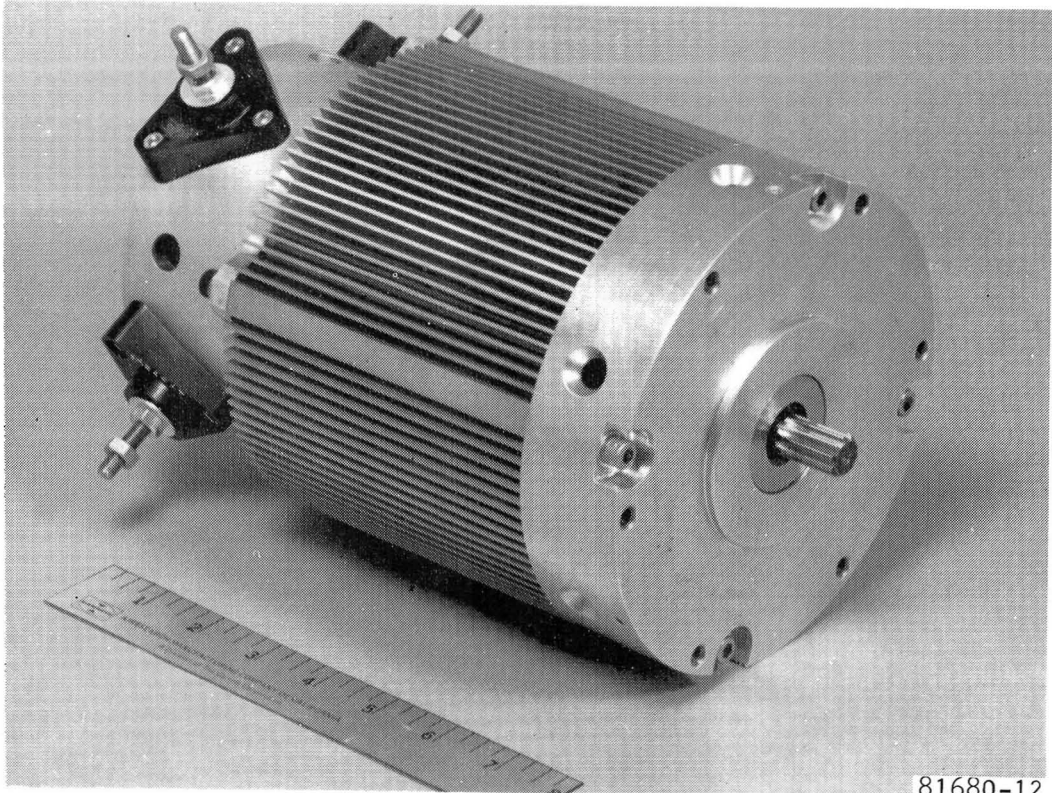
81680-12

Figure 1.--Lightweight electronically commutated dc motor.
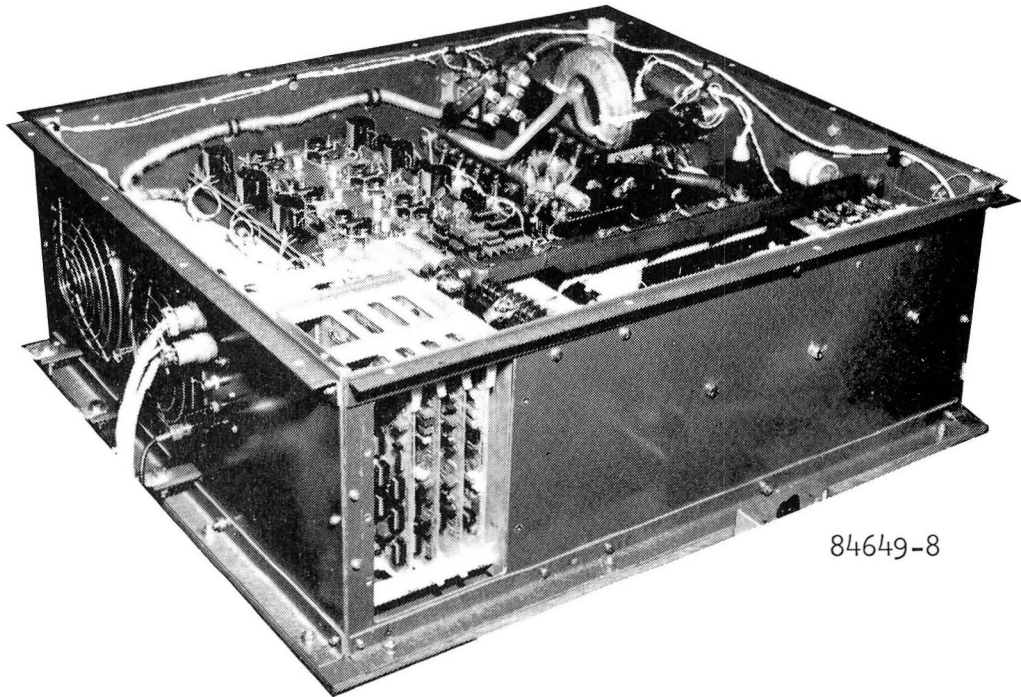
84649-8

F-34276

Figure 2.--Converter for lightweight commutated motor.

2

(3) The electronically commutated motor with a liquid-cooled converter should operate reliably without service or maintenance for the life of a passenger vehicle.

(4) The electronically commutated motor has the potential for reduced energy consumption, elimination of servicing and maintenance, and competitive initial cost when compared with a conventional brush-type motor and controller.

INTRODUCTION

To date, mechanically commutated dc motors have been used to meet most electric vehicle propulsion requirements. The motors used are usually modified designs originally developed for other applications. Electronically commutated and controlled dc motors have been developed in ratings to 134 kW (180 hp) for a variety of applications. The goal of this program is the use of this existing technology to provide an improved, electronically commutated dc motor specifically for use in an electric passenger vehicle. The application requires a lightweight, low-cost motor/converter that provides a high net efficiency over a typical driving cycle.

This report describes functional and engineering models of a motor/converter that has been designed, fabricated, and evaluated in accordance with the contractual requirements of the program. For cost reasons, the design variations used in the optimizing process were limited to those that could be accomplished by modification of an existing brushless, permanent magnet (PM), 41-kW, 40,000-rpm AiResearch motor design. The converter comprises a transistor chopper to control current and a six-pulse (six-phase) silicon-controlled-rectifier (SCR) inverter to effect commutation of the motor. This converter is a new design with a power rating typical of other converters built by AiResearch.

Program Scope

The work was organized in the following two phases.

- **Phase I:** Preliminary design and cost analysis, and the detailed design, fabrication, and test of a functional model motor/converter.

- **Phase II:** Refined design, cost analysis, fabrication, and test of an engineering model motor/converter.

Deliverable items include the functional and engineering model motors and converters.

Design Requirements Summary

The significant design requirements are summarized below.

- Voltage   120 Vdc nominal (96 V minimum)

- Output power

  Peak   26 kW (35 hp)
  Continuous   11 kW (15 hp)

- Operation   As a motor during drive and as a generator during braking

- Speed   Determined by contractor

- Gear change   One change allowed

- Efficiency   90 percent (SAE J227a, Schedule D driving cycle)

- Cooling   Air

- Ambient   -20° to +50°C

- Lubrication   Grease packed bearings

Certain additional objectives were derived through analysis to achieve the desired driving cycle efficiency with reasonable weight, and to facilitate subsequent installation in a vehicle. These are:

Speed	26,000 rpm (maximum)
Efficiency	88 percent at 26,000 rpm, 23 kW (31 hp) output
Gear change	One change assumed
Control	Accomplished by power converter in response to four possible external commands: (1) drive - brake, (2) tractive effort, (3) forward-reverse, and (4) on-off.
Accessory voltage	11 to 14 Vdc

PRELIMINARY DESIGN

Basic Design Concept

During the preliminary design task, the following essential features were selected as the design basis for the motor and its electronic controls:

A four-pole, rare-earth-cobalt permanent-magnet motor

Commutation of the motor by a six-phase silicon-controlled rectifier-inverter

Current to the motor controlled by a transistor converter (chopper)

High speed

Incorporating the high-energy magnet material into a rotating field and stationary armature design results in improved heat transfer, a low-mass rotor, and the absence of brushes or slip rings. The major limitation on the speed of the motor becomes the bearings. To permit the use of conventional grease-packed bearings, a rated speed of 26,000 rpm was selected for the design basis.

Silicon-controlled rectifiers (SCR's) were selected for use in the inverter for low cost and high reliability. Commutation of the SCR's is effected by the counter-emf (generated-emf) of the motor over the major portion of its speed range. For very low speeds, when the generated emf of the motor is low, the SCR's are force-commutated by a transistor switch controlled by a position sensor on the motor shaft. The angle of retard (firing angle), α, was selected at a nominal 120° to allow adequate margin to guarantee commutation. Circuit propagation-delay times were included in the design synthesis program. A review of the basic principles of counter-emf commutation is contained in Appendix A.

Current control to the motor is achieved by using a transistorized dc-dc converter (chopper) as a highly efficient switching regulator wherein the reference current can be varied according to torque demand. The high switching frequency needed in the chopper made the use of power transistors preferable to SCR's.

As a protection feature, provision was added for the detection and motor shutdown in the event of overspeed, which could occur if traction effort is commanded when the vehicle is in neutral. The following requirements were specified:

Detection speed shall = 1.1 x maximum speed*

Overspeed = 1.21 x maximum speed*

*Maximum speed is the maximum rotational speed of the motor during normal driving modes.

Based on torque and moment of inertia for similar machines built by AiResearch, available time for interrupting motor current between detection and overspeed is estimated to be 0.057 s.

Design Optimization

The electronic converter and permanent magnet motor combination were optimized for maximum efficiency over the SAE J227a (D) driving cycle, which is shown in figure 3. The vehicle characteristics used for analysis purposes included the following:

1350 kg (3000 lb) curb weight, including passengers; for analysis this weight is assumed to be constant regardless of changes in motor/ power converter.

Lead-acid batteries

Vehicle frontal area = 1.86 m^2 (20 ft^2)

Aerodynamic drag coefficient, C_D = 0.3

Tire rolling resistance coefficient, R_r = 0.008 N/N (lb/lb)

Rolling radius of tires = 0.29 m (11.5 in.)

$$\text{Gearbox friction loss, kW} = 0.025 \times \text{mph} \times \frac{I_{DC}}{I_{DC\ MAX}} \times \left(\frac{mph_{base}}{mph} \right)$$

NOTE: At or below vehicle base speed, use $\left(\dfrac{mph_{base}}{mph} \right) = 1.0$

Gearbox windage loss, kW = $1.2 \times 10^{-3} \times (mph)^2$

The system parameters that were optimized to meet an overall cycle efficiency are:

Lamination material

Lamination thickness

Back iron thickness

Magnet energy product

Rotor containment sleeve thickness

Machine inductance

Cooling fin height and spacing

VEHICLE SPEED, KM/HR

80
70
60
50
40
30
20
10
0

MPH

50
40
30
20
10
0

①

①

①

0   10   20   30   40   50   60   70   80   90   100   110   120   130   140
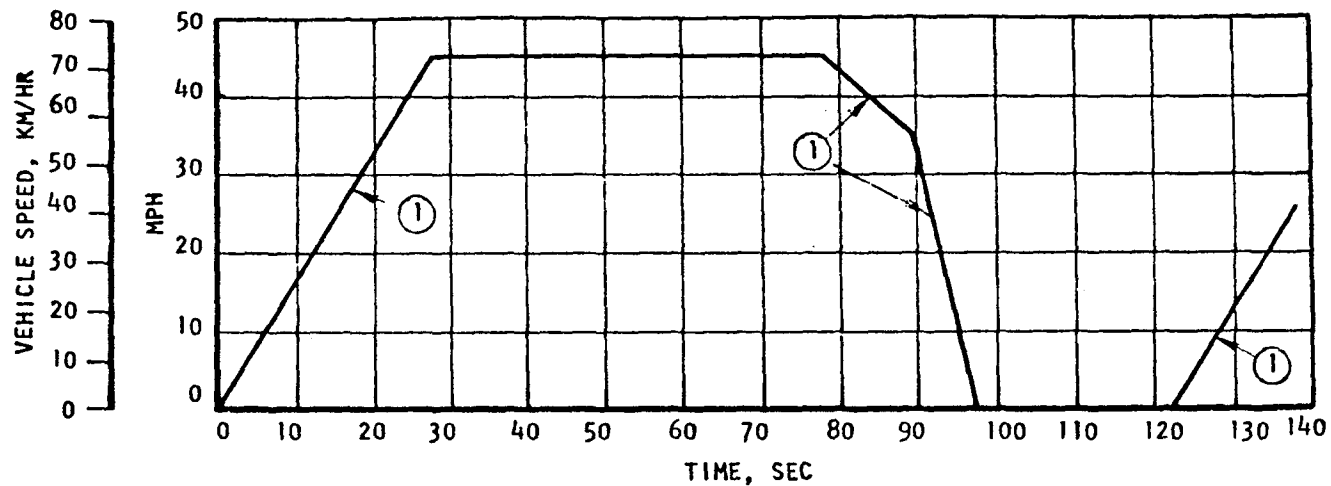
TIME, SEC

① — NON-LINEARITY PERMITTED

CHARACTERIZED BY	TESTING CYCLE	VEHICLE CRUISE SPEED		ACCEL. TIME SEC.	CRUISE TIME SEC.	COAST TIME SEC.	BRAKING TIME SEC.	IDLE TIME SEC.
		KM/NR	MPH					
Suburban Commuter Car	D	72 ± 1.5	45 ± 1	28 ± 2	50 ± 2	10 ± 1	9 ± 1	25 ± 2

S-28780

Figure 3.--SAE J-227A(D) driving cycle.

Slot fill (turns and wire size)

Machine dimensions

Converter firing angles

For this application, the optimization was accomplished using a comprehensive math model created by modifying existing computer programs to accommodate specific requirements of the system. The optimization study indicated that a modified version of an existing AiResearch motor design could be used for this application. The length of the motor was reduced, higher energy product magnet material was incorporated, and cooling fins were added. In addition, turns and wire size were changed for proper operation at the specified battery voltage. Other factors, such as lamination material and thickness and back iron thickness, were originally designed for low loss and were proper for this application. The thickness of the rotor containment sleeve was not changed in order to retain a significant overspeed capability. The driving cycle analysis program indicated the changes made provided a motor and converter combination which would meet the required cycle efficiency.

BIGMAG Program

BIGMAG is a design synthesis program for permanent magnet machines. It can be used to emulate an existing design or any desired variations of that design over any range of load and speed conditions. The program includes a SCR converter model with variable firing angle control so that the nonlinear nature of the converter/inverter current is accounted for in machine design and performance calculations. Thus, the program defines the direct current and voltage at the converter input terminals, commutation and recovery angles, apparent power factor, and converter and machine losses for any specified machine speed and current and any desired firing angle.

In addition, the program gives a complete description of machine geometry and other parameters for the stipulated base design conditions, including magnet material, ferromagnetic materials, base speed, current, voltage, current density and flux density in the stator and rotor iron, and commutation reactance.

For this system, BIGMAG was modified to include a chopper model and logic instructions so that constraints imposed by battery voltage and chopper and inverter device and interface limitations (current ratings, recovery time, frequency limits) could be accommodated; and so that losses introduced by the system controls and chopper devices could be predicted at all conditions of driving and braking.

In addition, provisions for writing the electrical system performance map into a permanent disc or tape file have been added to BIGMAG. The map file is used by the driving cycle analysis program so that at each increment of time during the cycle analysis, precise performance of a given electrical system can be looked up using an interpolation routine.

CYCLE Program

The driving cycle analysis program CYCLE is a version of an existing program updated to include the expressions for rolling resistance, gear losses, aerodynamic drag, cooling system losses, vehicle mass, and times of events unique for the specified cycle; a curve plot presenting significant data such as vehicle speed, motor speed, various energy curves, and related information; and the map file reading routine previously discussed. CYCLE calculates the vehicle performance in 0.1-s increments except during cruising at constant speed, where accuracy of the numerical integrations is not affected by the time increment. One 8-word card instructs the program to conduct a complete cycle analysis or to define performance at a specific speed and grade condition. Thus, the effect of the shift point, any gear train ratio, and mechanical braking on cycle performance for any given motor design can be readily determined.

Preliminary Design Results

A plot of a BIGMAG-designed machine analyzed by CYCLE over the J227a(D) driving cycle is shown in figure 2. Table I lists the parameters of the machine which met cycle efficiency requirements with adequate thermal capacity and reasonable weight. The required 90 percent cycle efficiency was achieved based on the following definitions:

Energy efficiency = E_{shaft}/E_{total}

E_{shaft} = total energy output delivered by motor at shaft during drive modes

E_{total} = net total energy absorbed by motor/power converter at terminals during driving and regeneration modes

From figure 4, E_{shaft} at the end of the drive mode (prior to regeneration) is 770 kW-s. E_{total} at the end of the cycle (includes regeneration) is 850 kW-s.

A detailed discussion of the energy losses involved in the operation of the vehicle over the driving cycle is contained in Appendix A.

A comparison of the effect of constant torque acceleration compared with constant power acceleration on the performance of the vehicle over the driving cycle is discussed in Appendix B.

Figure 4.--Baseline driving cycle performance.
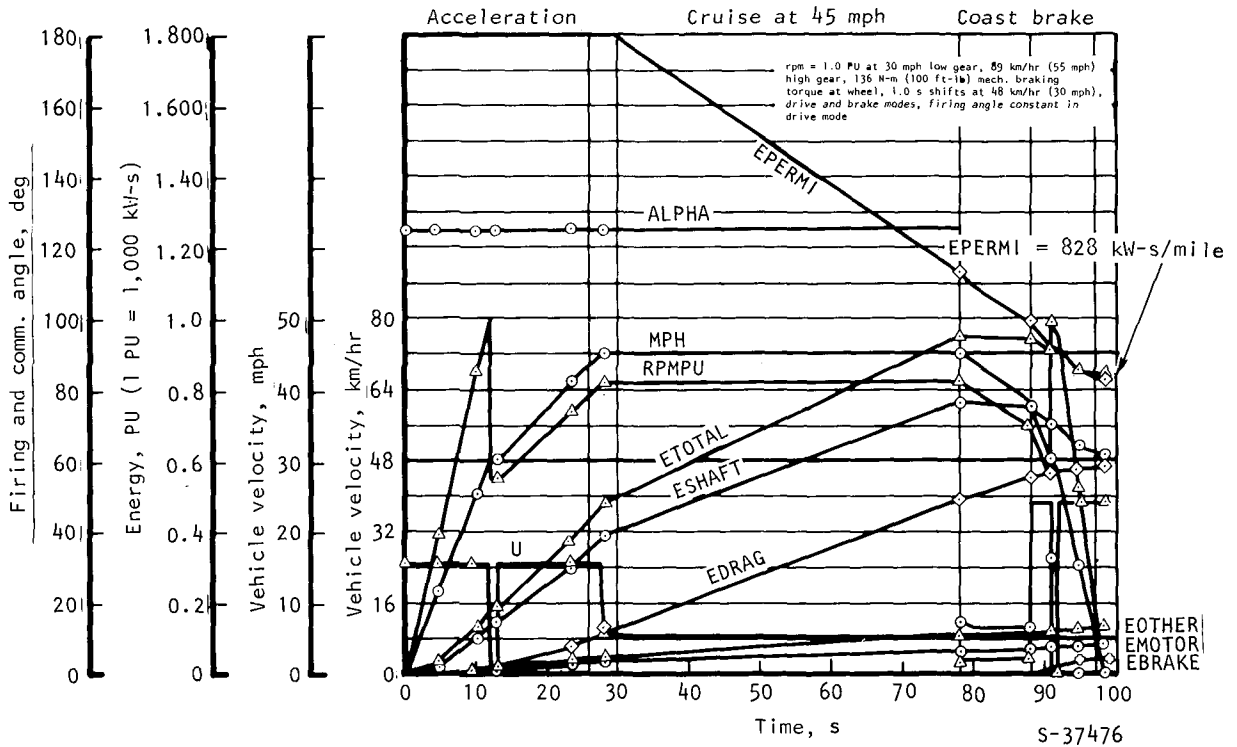
ALPHA	Converter ignition angle, deg
EBRAKE	Mechanical braking energy, PU units
EDRAG	Gearbox, rolling resistance, and aero. drag energy, PU units
EMOTOR	Energy loss in motor, PU units
EOTHER	Energy loss in controls, fan, chopper, and converter, PU units
EPERMI	Energy consumption per mile, PU units
ESHAFT	Energy at motor shaft, PU units
ETOTAL	Electrical energy at motor/power converter terminals, PU units
MPH	Vehicle speed, mph
RPMPU	Motor speed, PU units
U	Commutation overlap angle, deg

Base values

Energies	1 PU = 1000 kW-s
EPERMI	1 PU = 1000 kW-s/mile
RPMPU	1 PU = 26 000 rev/min
Gear shift time	1 s

TABLE I.--BASELINE MACHINE PARAMETERS

Parameter	Value
Voltage, Vac	55.85 V airgap, L-N, 3 phase (drive mode)
Voltage, Vdc	104.5 Vdc at 124.6 deg ignition angle and 30.86 commutation overlap angle (drive mode)
Current, A ac	190.2 A/phase
Current, A dc	246.7 A dc
Speed	26 000 rpm
Overspeed	31 460 rpm (121%)
Torque	8.603 N-m (6.345 lb-ft)
Shaft power	23.43 kW mechanical
Power input	
Converter terminals	25.828 kW dc
System terminals	27.039 kW dc
Loss summary	
Motor copper	1.13 kW
Stator iron	.248
Rotor	.280
Motor total	1.658 kW
Converter	.7402 kW
Chopper	.4938
Controls and fan	.717
System total	3.609 kW
Winding Data	24 coils connected 3 phase, 4 circuits. 4 turns per coil of 11 strands of AWG #24 HML. Pitch = 1 to 6.
Slot liner	.18 mm (.007 in.) N-K-N
Current density	21.13 A/mm^2 (13 630 A/in.^{2})
Electric loading	40.9 A·cond./mm (1038A-cond/in.)
Slot fill factor	.325
Impedances	
Base impedance	.2937 Ω
Stator leakage reactance	.0470 Ω
Stator resistance at 380°F	.0101 Ω
Commutation reactance	.0947 Ω
XAD	.0676 Ω
XAQ	.0582 Ω
Materials	
Laminations	.18 mm (0.007 in.) silicon steel
Magnets	.158 MT·A/m (19.8 MGO)(min. recommended)
Rotor yoke	4130 or 4340D steel
Weight summary	
Stator copper	0.75 kg (1.65 lb)
Stator iron	6.70 (14.77)
Rotor hoop	.35 (.78)
Magnets	1.43 (3.14)
Yoke	.65 (1.44)
Spacers	.35 (.76)
Total electromagnetics	10.23 (22.54)
Other parts*	3.07 (6.76)
Total weight	13.30 kg (29.30 lb)

*In final unit, "other parts" weighed 6.0 kg (13.3 lb) for a final total of 16.2 kg (35.8 lb)

FUNCTIONAL MODEL DESIGN

The detailed design of the functional model motor and converter was based on the optimization conducted for the J227a(D) driving cycle, as described in the previous section. The functional model system demonstrates the power capability and efficiency of the motor/converter combination in both drive and brake modes. The converter was in breadboard form and hence without some of the logic functions for protection and vehicle control ultimately incorporated in the engineering model.

Functional Model Motor Description

The functional model motor has a rare-earth-cobalt, permanent-magnet rotor; optical sensors for rotor angular position information; and a conventional three-phase stator similar to that of an induction motor. The magnets, with an energy product of 1.5×10^5 T·A/m (19.8 MGO) minimum, are radially magnetized in a four-pole configuration with spacers between the magnets to provide separation. An inconel sleeve holds the magnets and spacers in compression. A list of the significant materials is presented in table II. Dimensions and details of the machine are shown in figures 5 and 6; parts are identified in table III. The essential components of the motor prior to assembly are shown in figure 7. The motor built for test is shown in figure 8.

TABLE II. FUNCTIONAL MODEL MOTOR MATERIALS

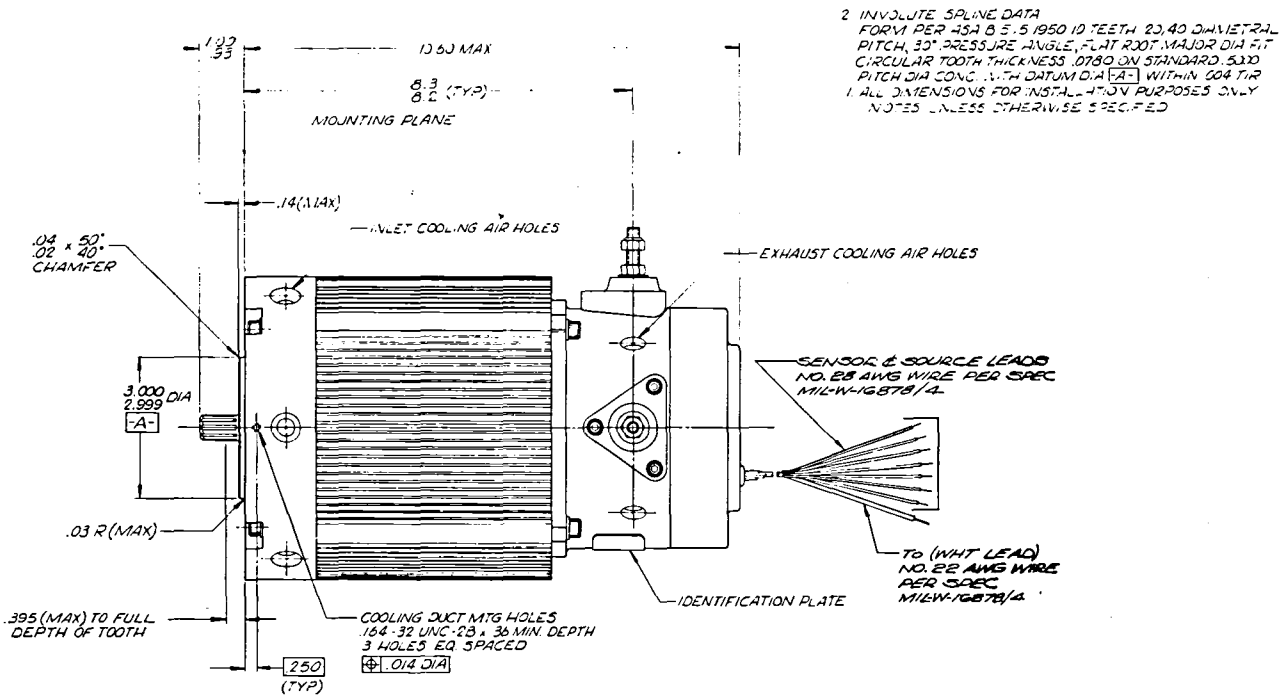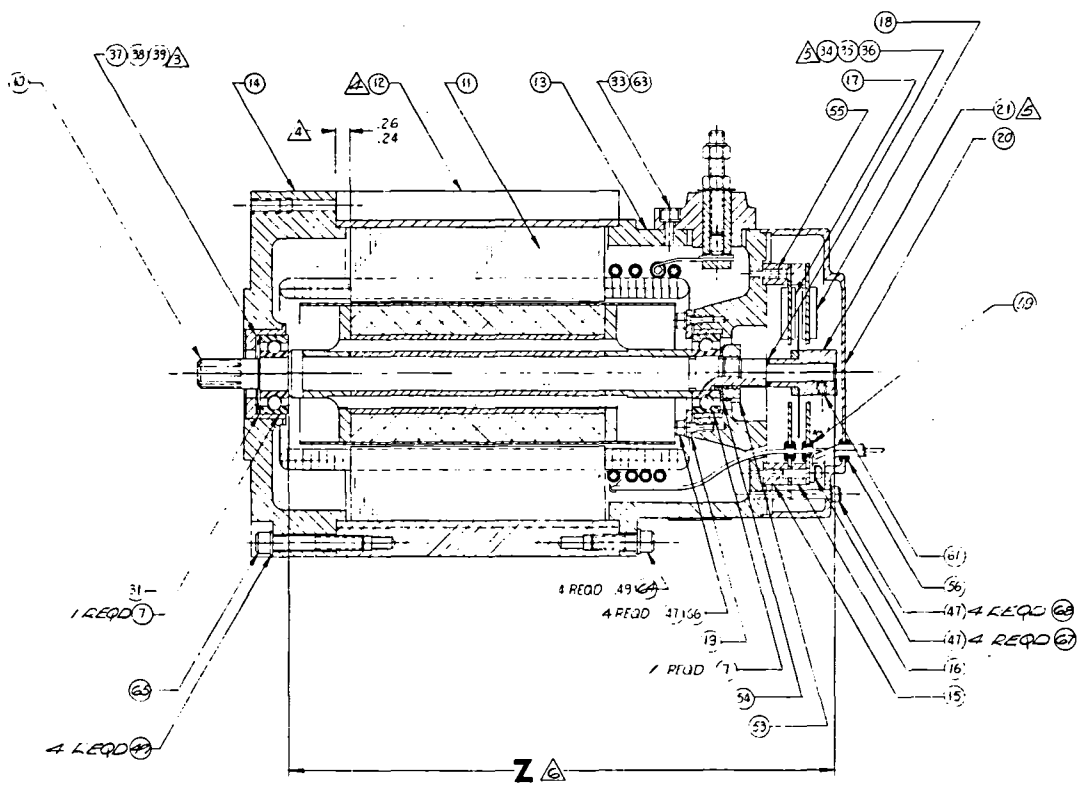| Component	Material
Shaft	Inconel 718
Magnet support	4130 steel
Magnets	Rare earth cobalt; 22 MGO energy product
Retaining sleeve	Inconel 718
Laminations	7 mil silicon steel
Slot liners	Nomex-Kapton-Nomex
Wire	Magnet wire, 220°C ML, AWG 24
Varnish	ML
Housing	2024 T3 aluminum
Bearings	SAE 52100 (races and rolling elements)
Lubrication	Mobilgrease 28

13
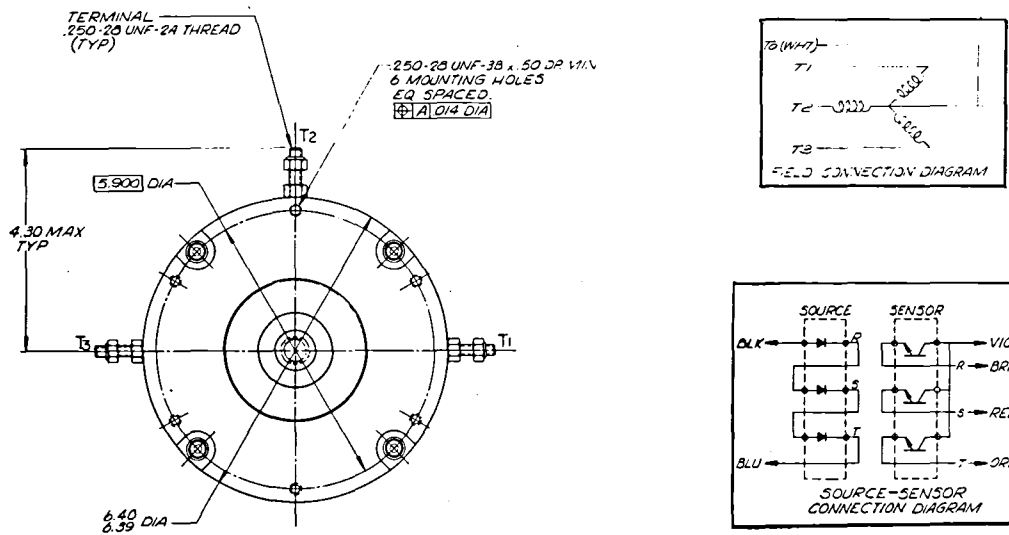
Figure 5.--Motor installation and connection details (This figure taken
from AiResearch drawing 518916).
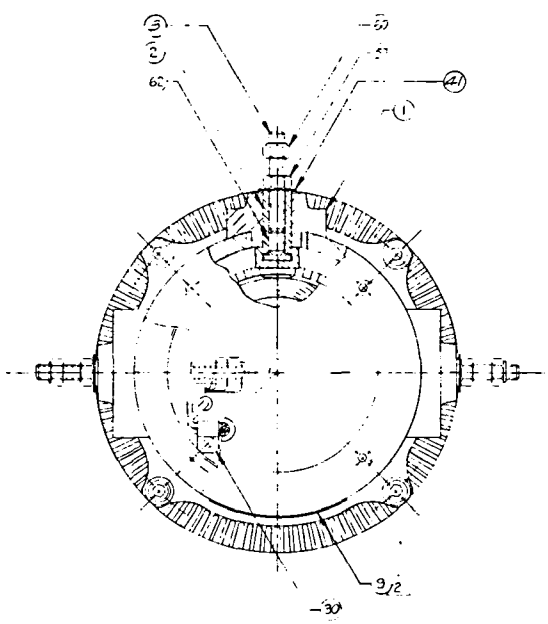
Figure 6.--Motor assembly (This figure taken from AiResearch drawing 518917).

15

TABLE III.--PARTS SHOWN IN FIGURE 6

| Find No.	Nomenclature or Description
1	Insulator
2	Terminal
3	Terminal stud
7	Bearing
9	Plate ident.
10	Rotor assembly
11	Stator assembly
12	Housing assembly
13	End bell assembly
14	End bell assembly
15	Ring sensor mounting
16	Ring source
17	Sensor assembly
18	Source assembly
19	Retainer, bearing
20	Cover sensor
21	Shutter assembly
30	Clamp loop
31	Washer, spring tension
33 to 49	Washer
53	Nut, plain round
54	Washer, lock, bearing
55	Screw
56	Grommet, rubber
57	Nut
60	Nut, self locking
61	Setscrew
62	Setscrew
63 to 68	Screw

16
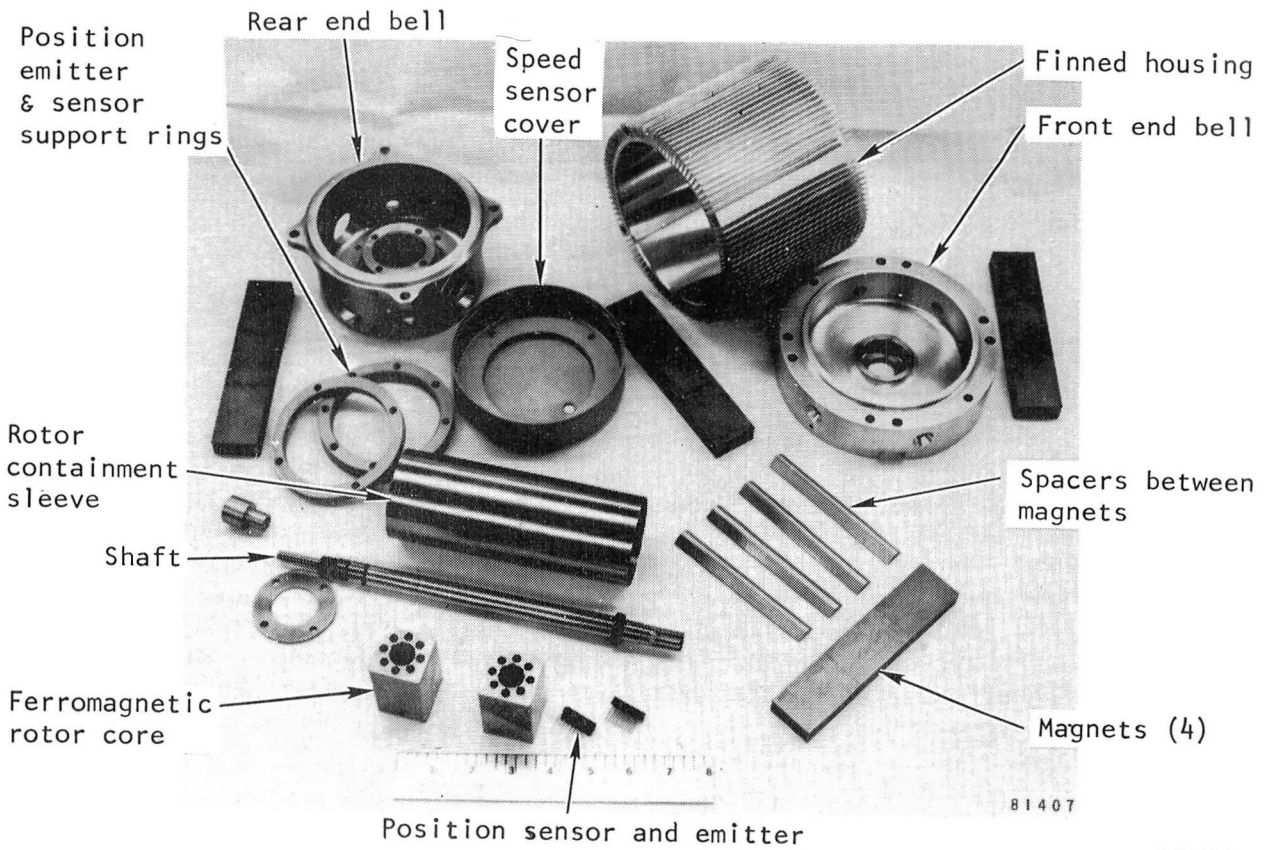
Figure 7.—Functional model motor components.

F-35162
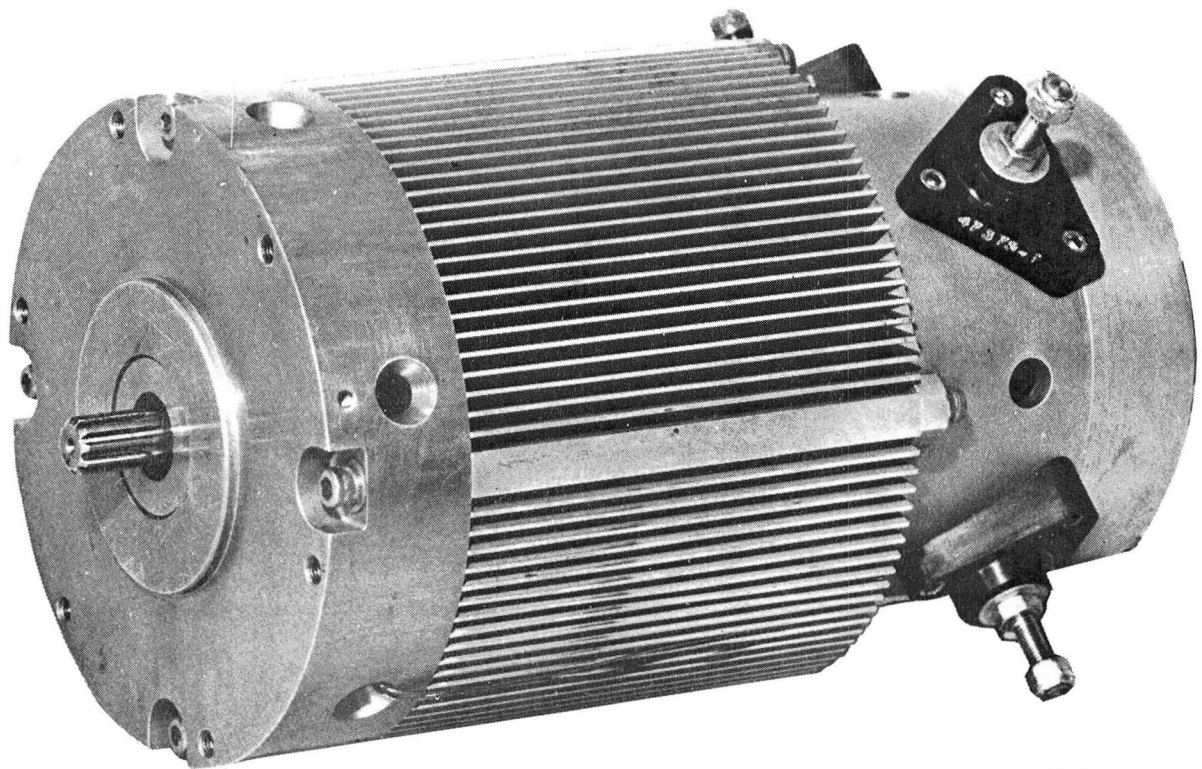
85883-2

F-36000

Figure 8.—Functional model motor.

17

Functional Model Converter

The function of the converter is to commutate and control the lightweight electronically commutated motor (lECM) over its full range of speed. The converter provides the controls for the drive and the brake modes of operation, which includes a regenerative switching scheme that returns energy to the battery during braking. The functional model converter is shown in figure 9 and the basic schematic in figure 10.

The major power elements of the converter are the upper and the lower transistor choppers Q_U and Q_L, respectively, free-wheel (FW) diodes D_1 and D_2, and a thyristor inverter Q_1 through Q_6. The primary devices used on the functional converter are listed in table IV. The lower (main) chopper controls the motor current by modulating the fixed dc voltage (battery volts). The free-wheel diodes maintain a continuous motor current by providing a path for it when the chopper is off. During this period, the current is sustained by the system inductances in the chopper, the inverter, and the motor loop. The free-wheel diodes are also a part of the regenerative scheme. The thyristor (SCR) inverter acts as a solid-state commutator for the motor.

In the drive mode, the inverter is a load commutated type in which the thyristors are turned off by the back EMF (voltage) of the motor. Since the motor is a permanent-magnet fixed-field type, the back emf is proportional to speed. Thus, at low motor speeds (less than 10 percent rated speed), when the back EMF is relatively low and is not sufficient to ensure turn-off of the thyristors, the transistorized choppers provide the means for thyristor turn-off. At motor speeds greater than 10 percent rated, the upper chopper (Q_U) is bypassed by the automatic closure of its associated contactor (SW_2). The upper chopper (Q_U) is required only during the initial start-up; the converter losses are minimized by bypassing the upper chopper at higher speeds.

In the brake mode, by opening switch SW2 and changing the SCR phase angle control, the inverter is operated as a conventional phase-delayed-rectifier (PDR), which acts to control the current or energy returned to the battery. The current path is through D_2, SW_1, the battery, D_1, and L_1 as shown in figure 10. For conditions wherein the motor back EMF is not sufficient to provide brake or regenerative energy to the battery, the motor voltage is boosted by the operation of the lower chopper (Q_L). The chopper allows for the build-up of current through D_1 and L_1, which is then transferred to the battery when Q_L turns off.

The converter is described in more detail in the engineering model discussion on page 27, and the fundamental operation of the rectifier/inverter is discussed in Appendix C.
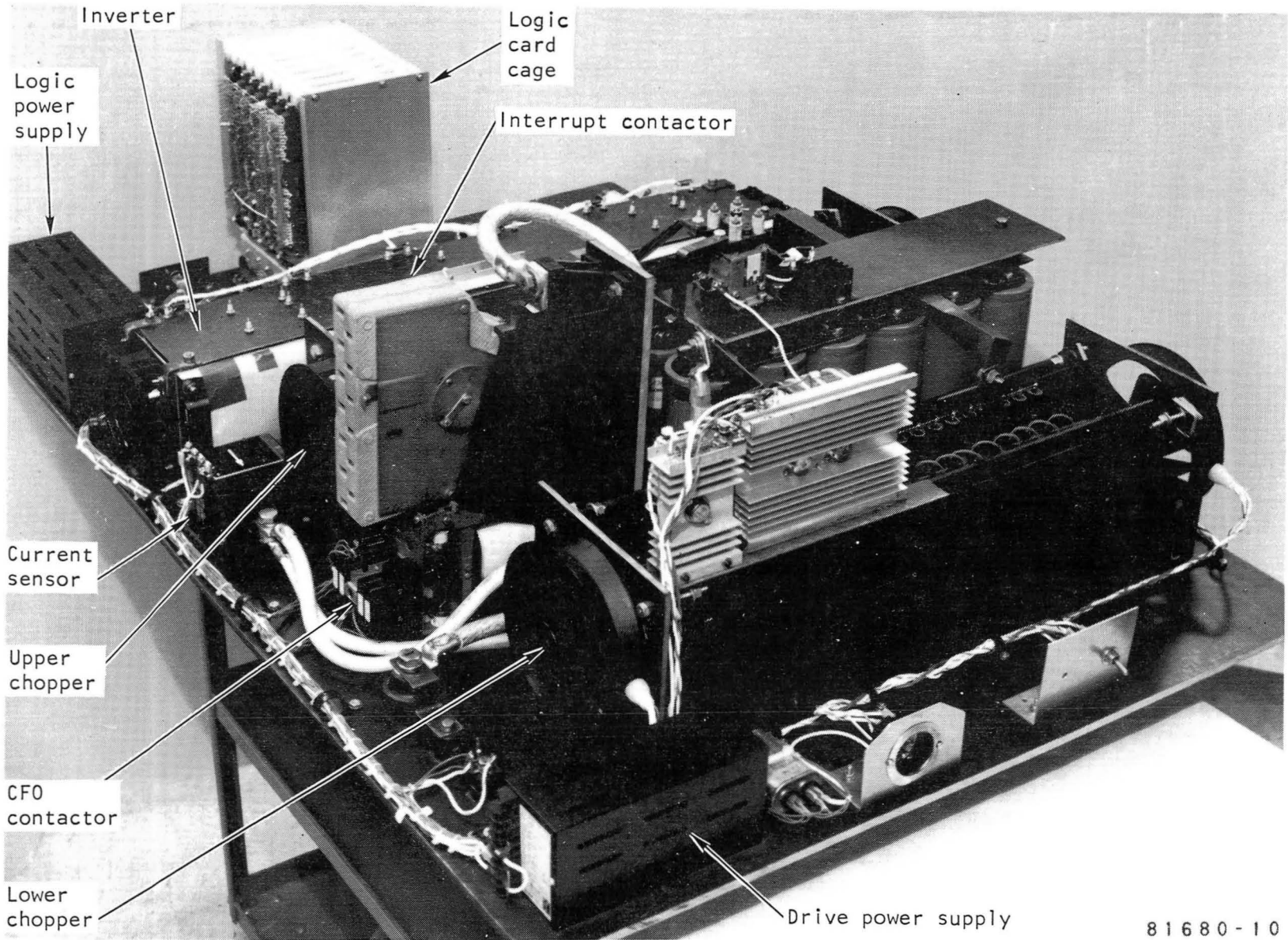
Figure 9.--Functional model converter.

Inverter

Logic
card
cage

Logic
power
supply

Interrupt contactor

Current
sensor

Upper
chopper

CFO
contactor

Lower
chopper

Drive power supply

19

81680-10

F-35160
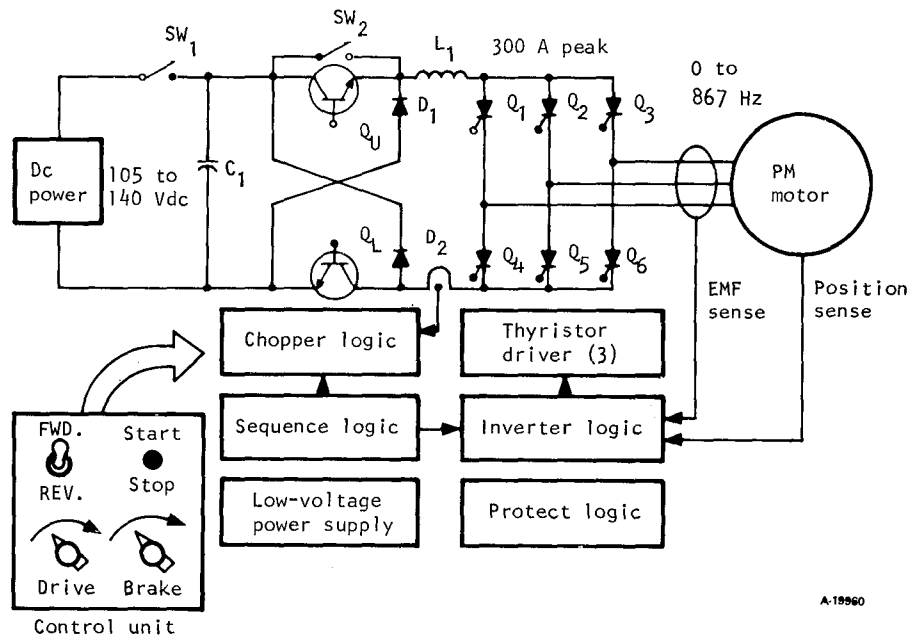
Figure 10.—Functional model converter basic schematic.

TABLE IV.—FUNCTIONAL MODEL CONVERTER DEVICES

Component	Type
Thyristors, Q_1-Q_6	G.E. 434S, 600 V, 500 A, 14 μs
Transistors, Q_U, Q_L (12 parallel, each)	Motorola MJ10015, 400 V, 50 A
Diodes (FW), D_1, D_2 (8 parallel, each)	Motorola MR874, 400 V, 50 A
Capacitors, C_1 (12 parallel)	Sprague 36D type, 6000 μF, 300 V
Interrupt contactor, SW_1	Siemens 3TC74, 400 A dc single pole
CFO contactor, SW_2	Hartmann 300 A dc double break
Logic cards	216 by 152 mm (8.5 by 6 in.), CMOS, 43 pin, ±15 Vdc power
Current sensor	Hall effect, 5000:1 current ratio
EMF sensor	Step-down control transformer
Position sensor	Photo-optical with slotted disc

FUNCTIONAL MODEL TEST

The functional model motor/converter combination was tested to determine the performance throughout the operational range in both drive and brake modes. The tractive effort was varied in four steps (25, 50, 75, and 100 percent) at each of four speeds (25, 50, 75, and 100 percent). The laboratory test setup is shown in figure 11. The efficiency of the chopper/inverter/motor was determined by measuring the dc input power, using conventional meters, and the mechanical output power using conventional torque and speed measurement devices.

The measured efficiencies shown in figures 12 through 15 include all converter and motor losses, except for approximately 175 w of power required for the 12-v logic power supplies. The continuous rating of the motor was determined by steady-state operation until temperature stabilization. The required 11 kW continuous rating was verified. For the functional model, the rated speed was determined to be the speed at which the motor delivered the rated steady-state power of 11 kW with rated current supplied to the motor. This speed was found to be 22,000 rpm; hence the designated 100 percent speed is 22,000 rpm. The thermal response of the machine winding, end bell, and exit air temperature are shown in figure 16. An externally mounted fan delivering approximately 4250 l/min airflow and drawing 120 W was used. The cooling requirements are discussed in Appendix D.

A-19962

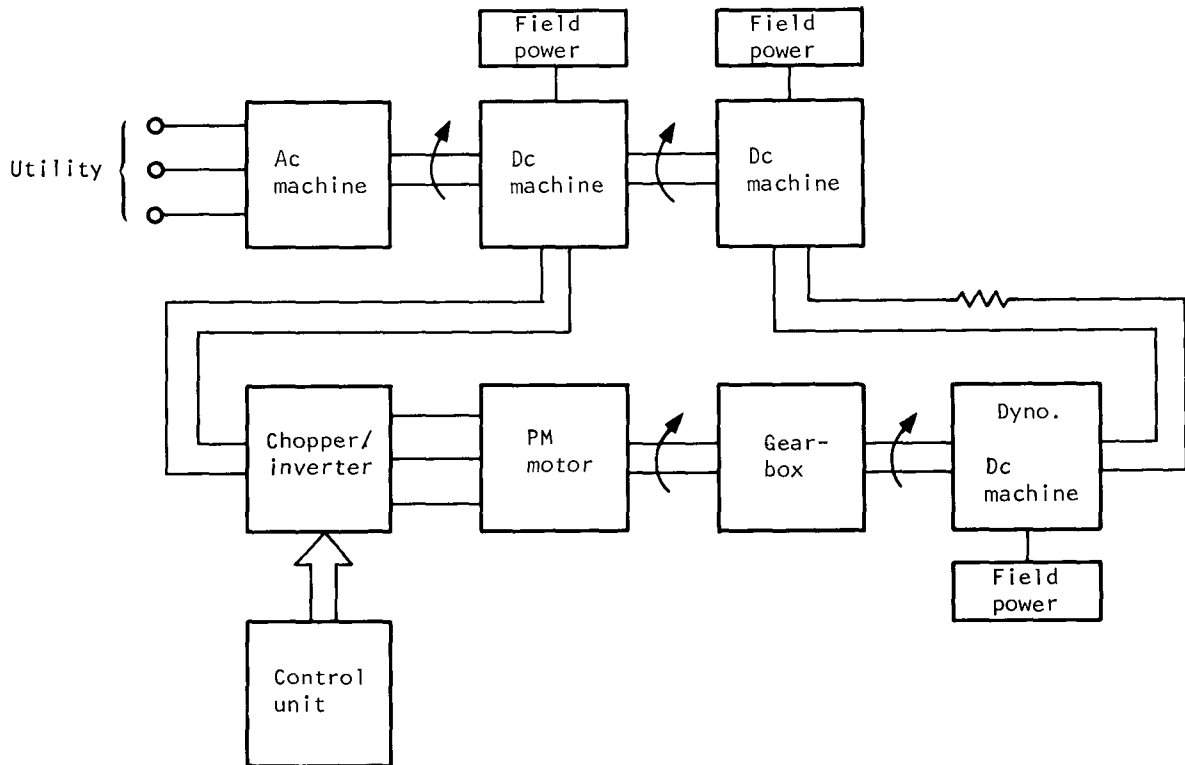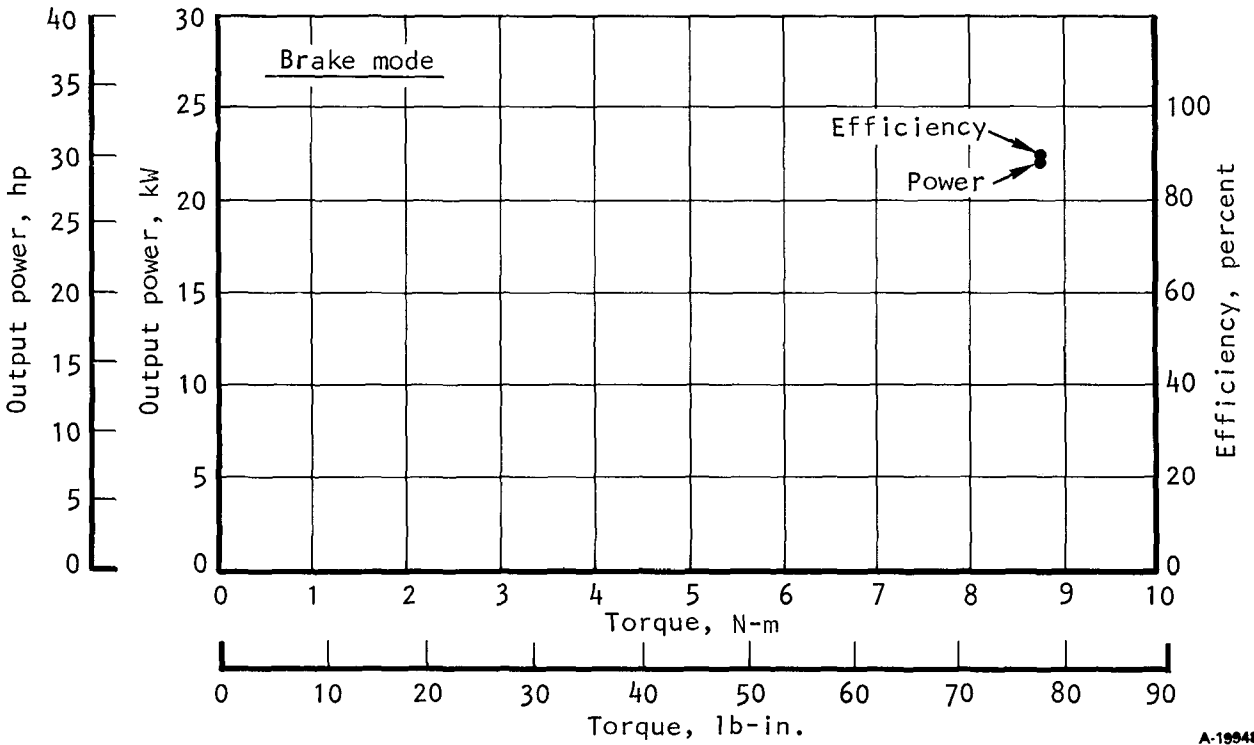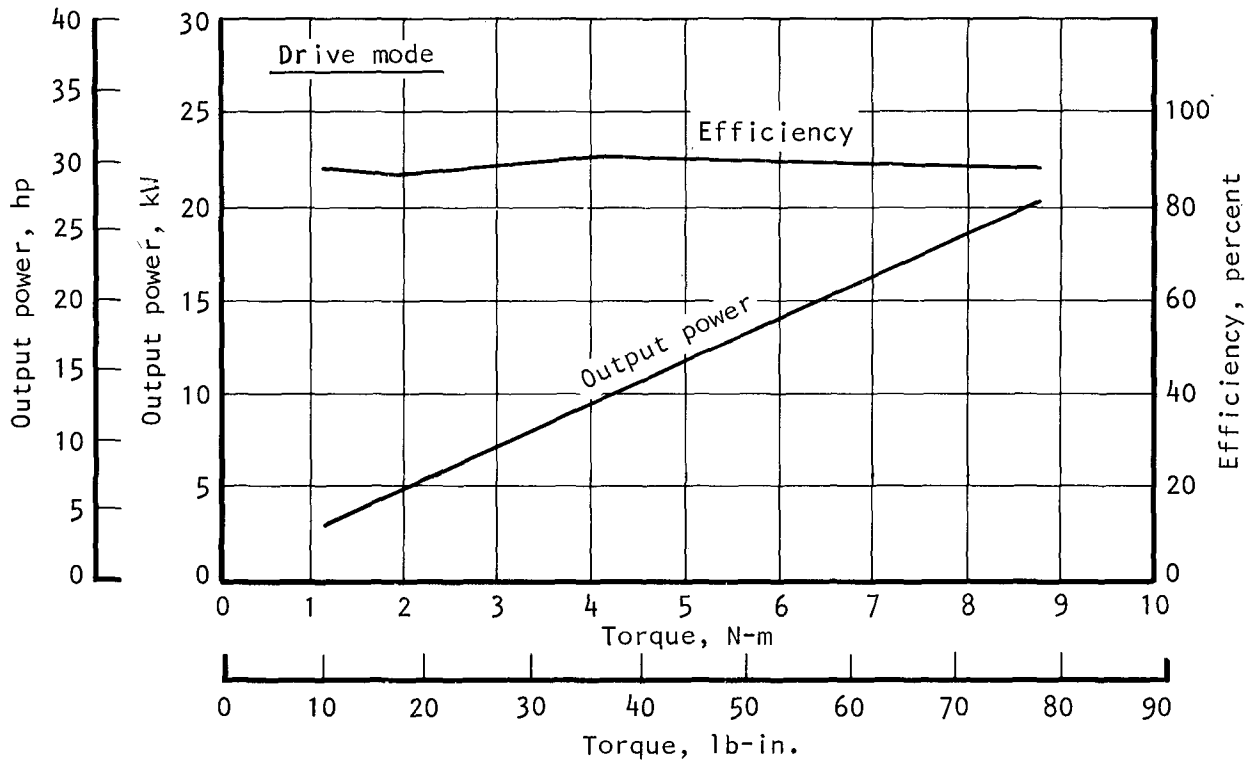Figure 11.--Laboratory test rig block diagram.
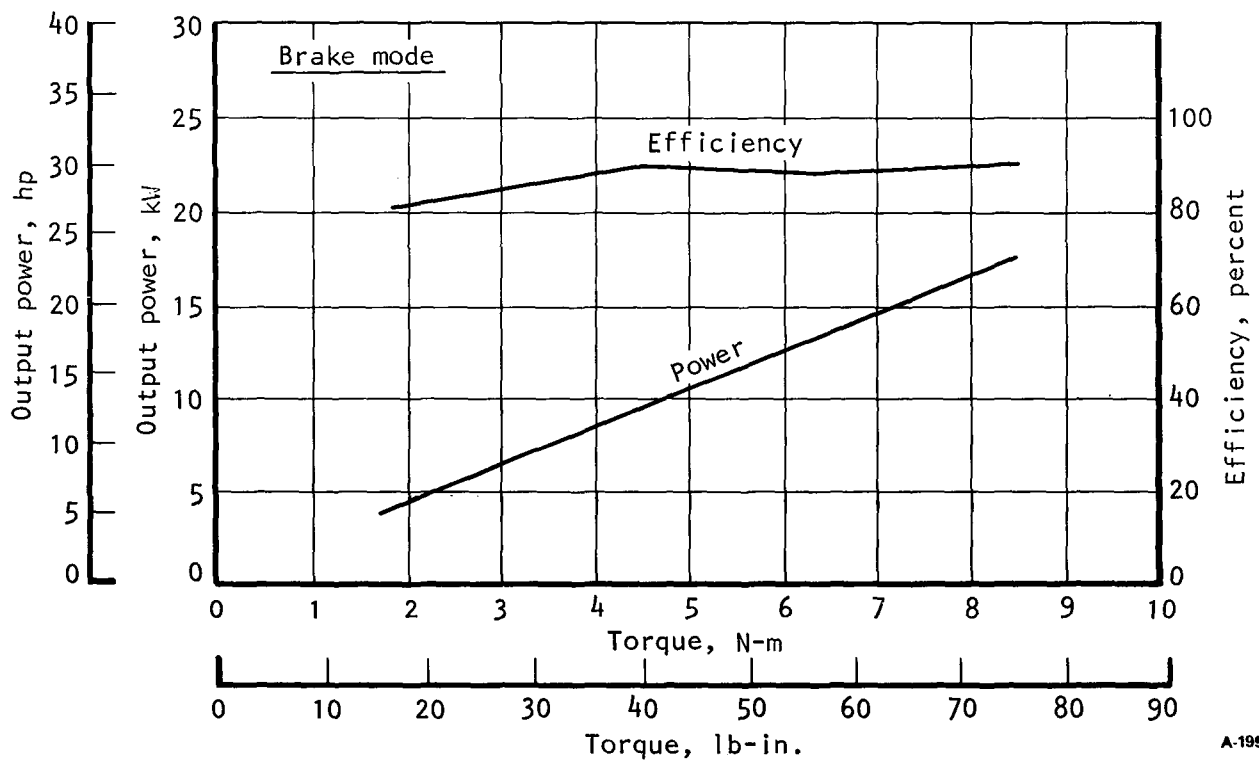
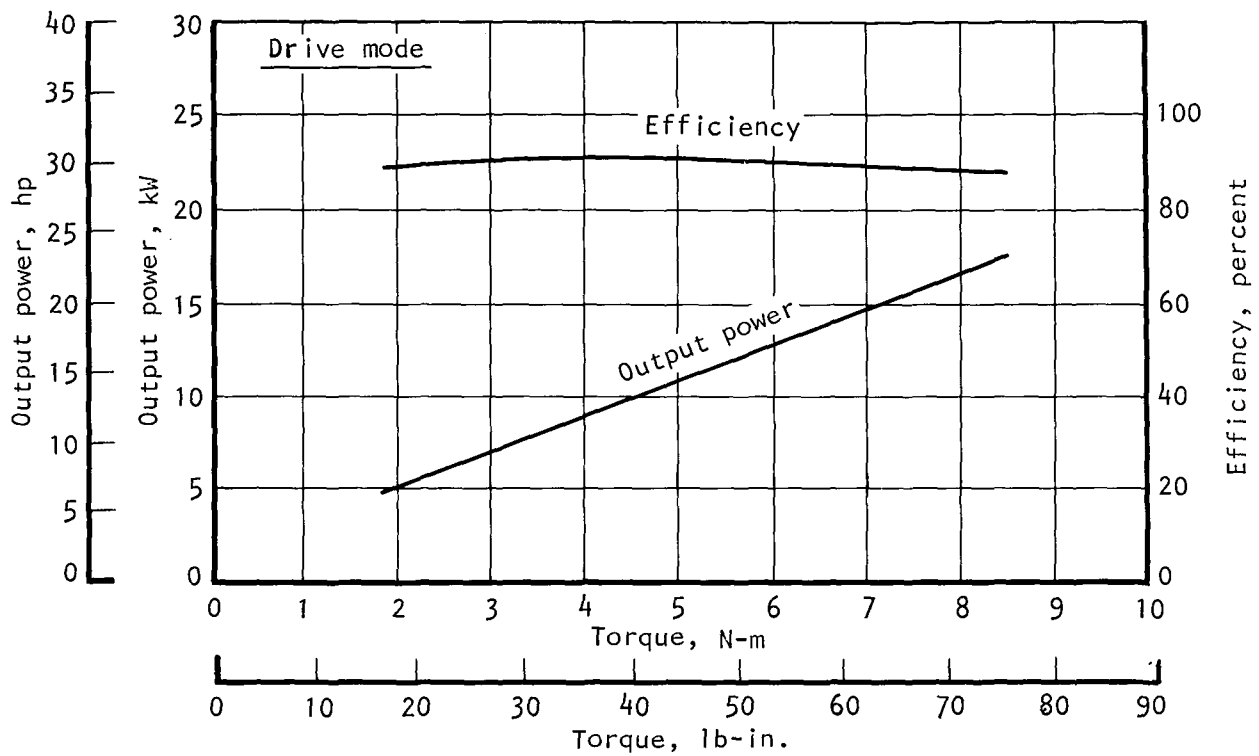Figure 12.--Functional model performance at 22,000 rpm.

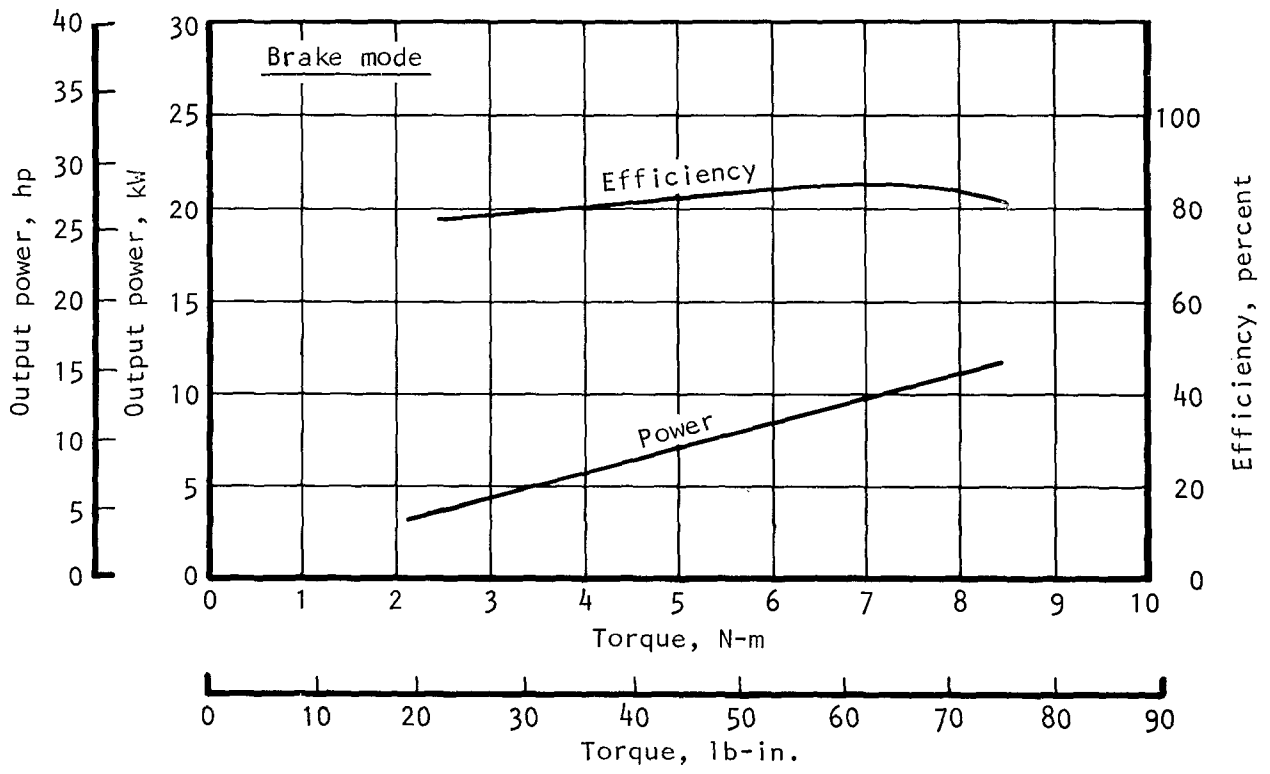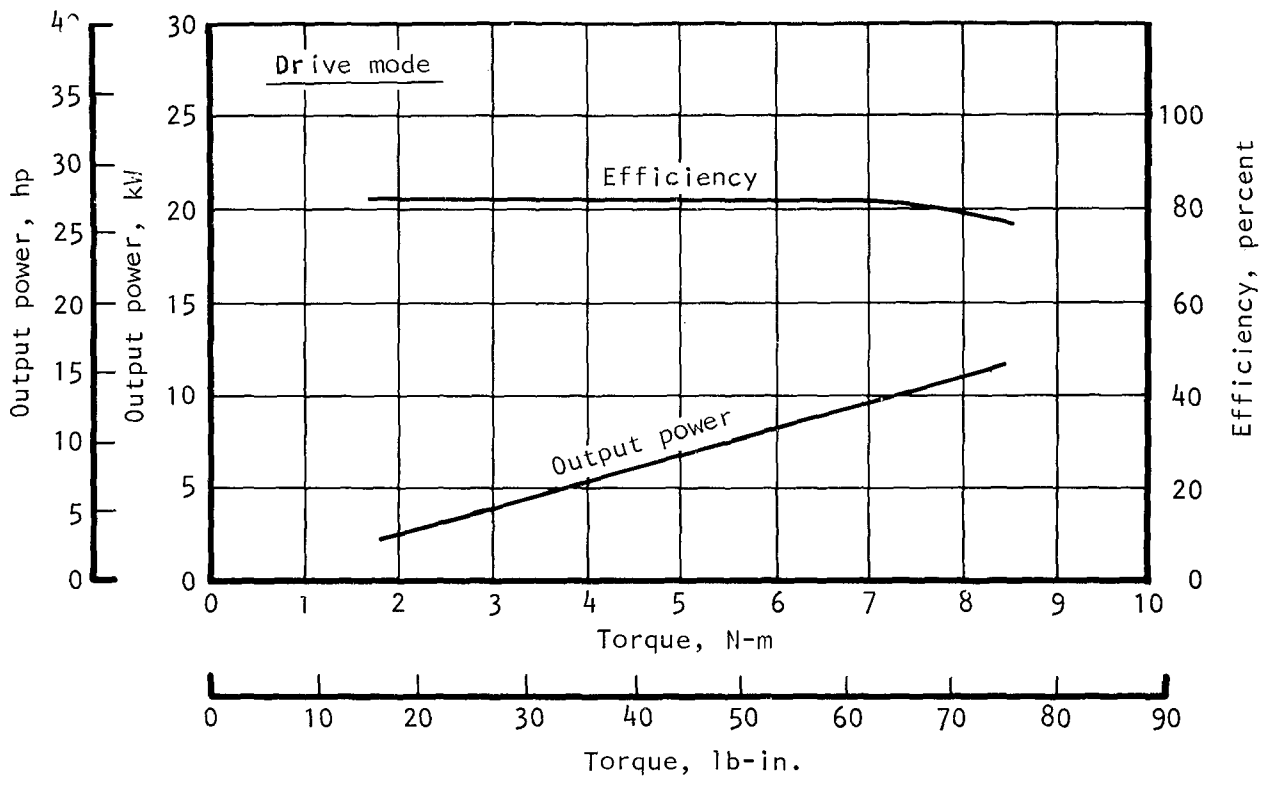Figure 13.—Functional model performance at 19,500 rpm.

A-19946 -A

Figure 14.--Functional model performance at 13,000 rpm.
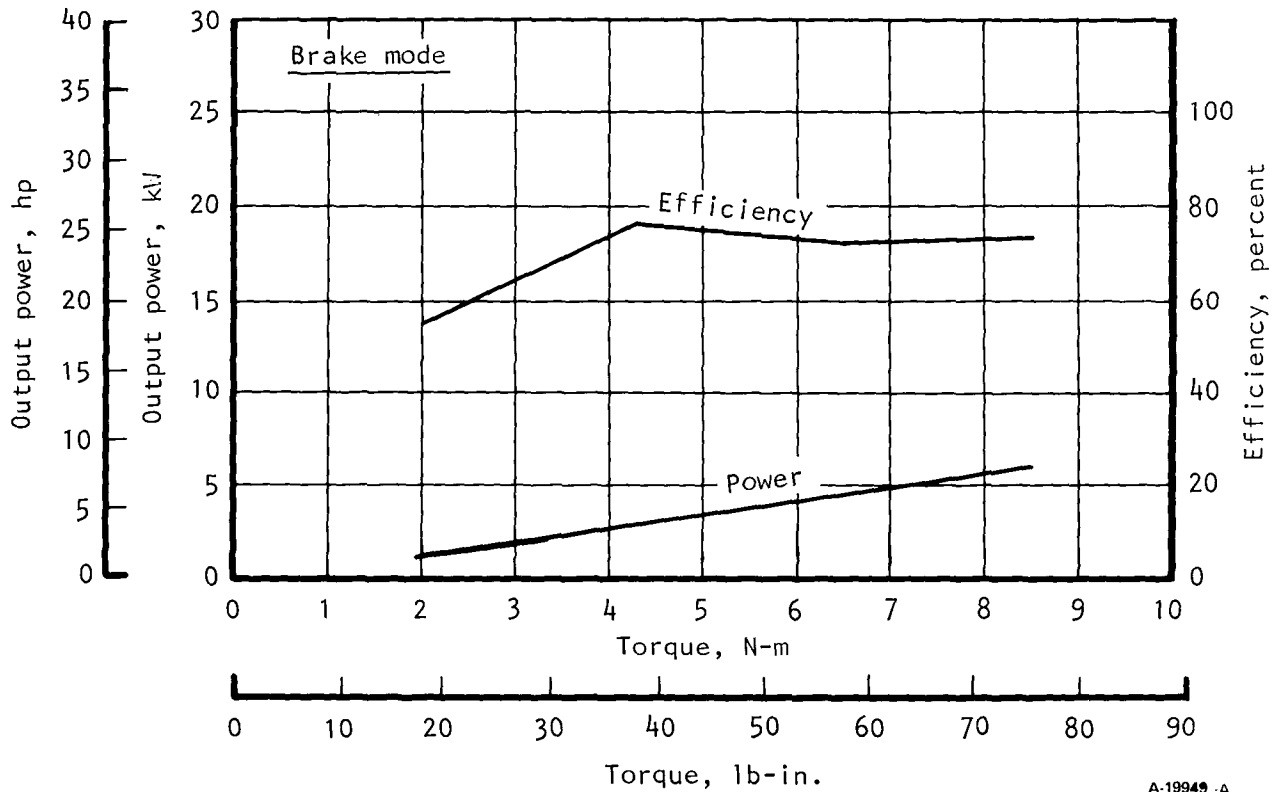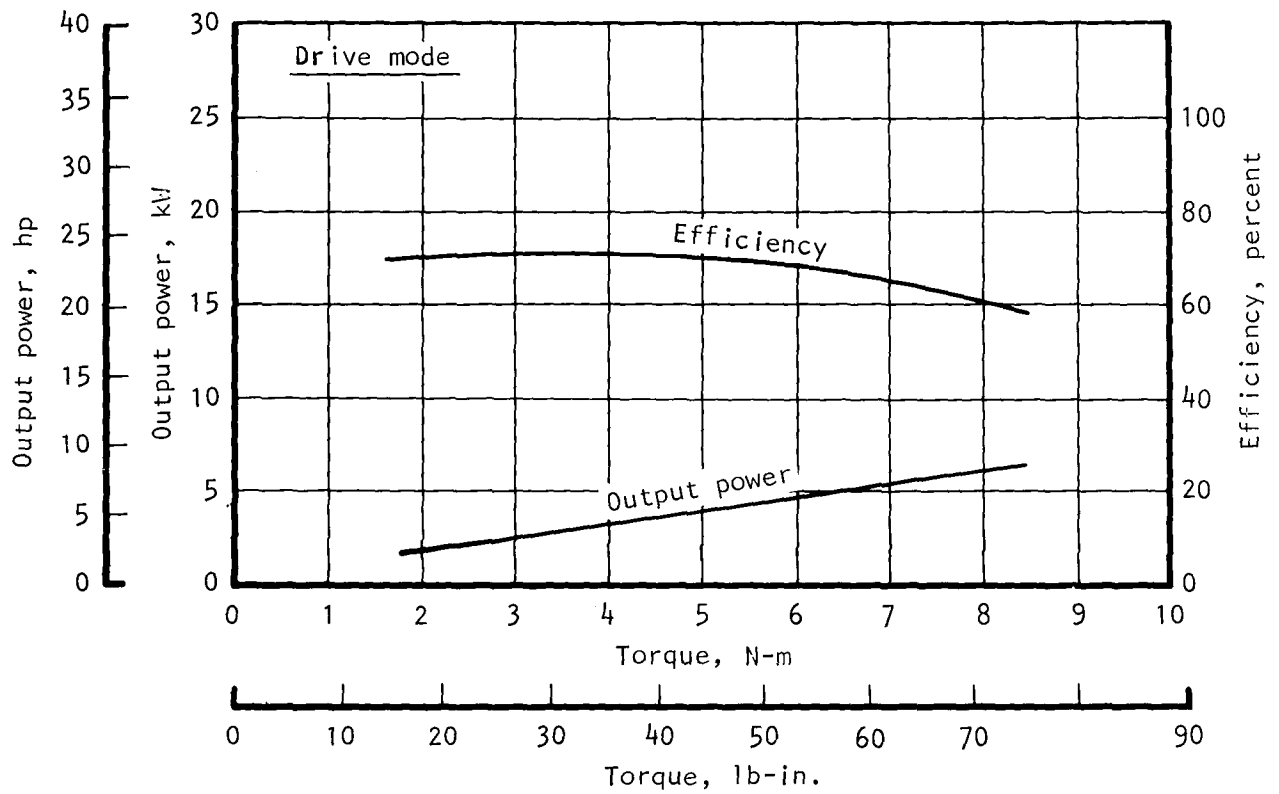
A-19951 -A

Figure 15.—Functional model performance at 6500 rpm.
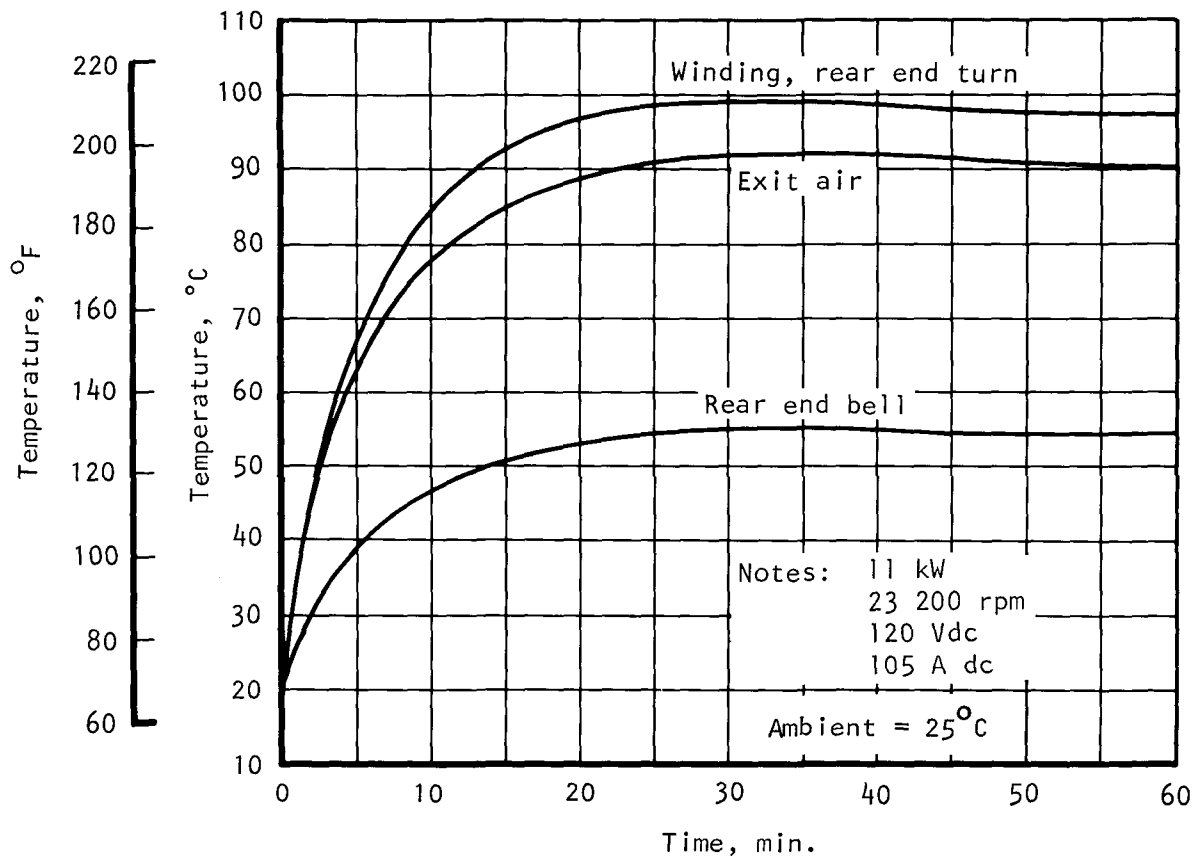
A-19949 -A

Figure 16. Functional model motor temperatures.

A-19945

26

ENGINEERING MODEL DESIGN

The engineering model motor and converter were designed for 26 kW peak and 15 kW continuous power. Functional model power rating was 23 kW peak and 11 kW continuous. This improvement was incorporated in view of current estimates of vehicle requirements, and to obtain full advantage of the motor capabilities.

The engineering model converter was packaged for installation in a test vehicle, and incorporates several protection and control features deemed necessary for vehicle operation. The packaging was arranged for easy access during test rather than minimum size and weight.

The engineering model rotating machine is identical to the functional model, as shown in figure 5, except for a winding change from 4 turns per coil of 11 strands of 24 AWG wire to 3 turns per coil of 14 strands 24 AWG wire. This winding change results in increased speed to allow full motor performance with magnets that are about 10 percent higher in energy product than originally planned. The winding change also allows an increase in machine rating to 26 kW peak and 15 kW continuous.

The results of testing of the functional model showed that the rated power was achievable at a motor speed of 22,000 rpm. Since the motor was capable of 26,000 rpm, the higher power ratings could be achieved without an increase in magnet size or motor size by making the indicated winding change. This would allow the motor to exceed the requirements of the SAE J227a, Schedule D, Driving Cycle.

Recognizing that the shaft speed of this motor is substantially higher than normally encountered in an electric vehicle traction motor, a separate study was made to determine the additional weight and loss of efficiency resulting from the addition of a speed reducer. It was found that a gear reducer that reduced the shaft speed to 5,000 rpm would have an efficiency of 98 percent and would add less than 1.8 kg (4 lb) to the motor. The results of this study are presented in Appendix E.

The function of the engineering model converter is the same as in the functional model--to provide the commutation and controls for the light-weight electronically commutated motor. The engineering model converter is shown in figure 17; the basic schematic is shown in figure 18. The control features provided by the converter are vehicle application oriented and are listed in table V.

84649-8

Drive
power supply

Logic
power supply

Logic
card
cage

Dc link
inductor

Chopper
components
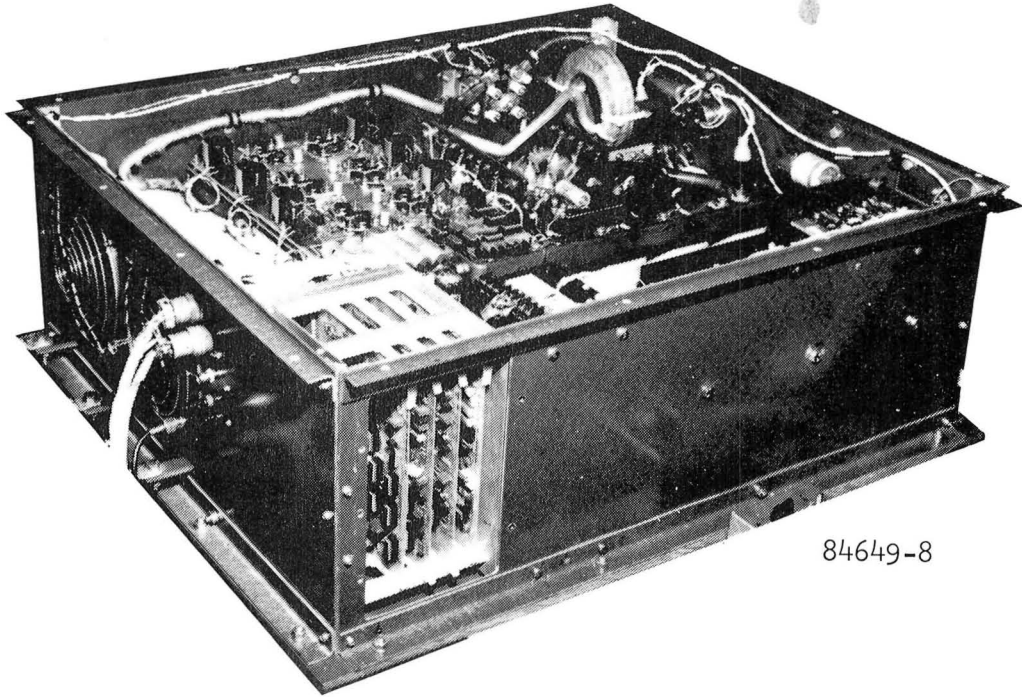
Inverter
components
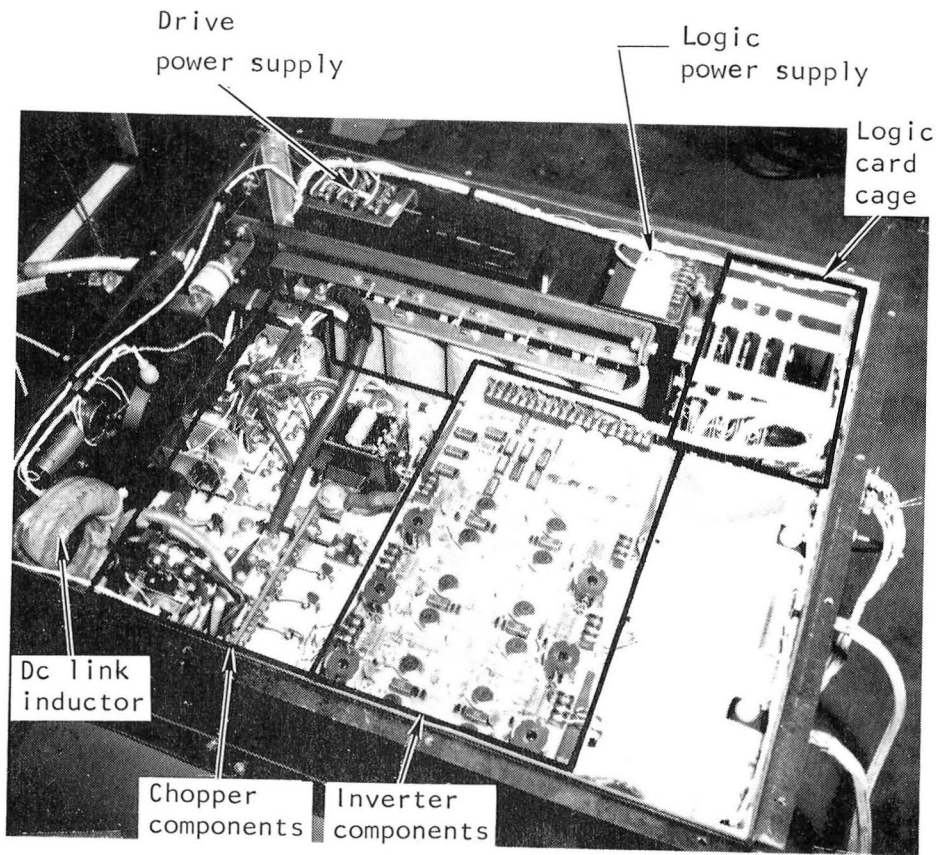
Figure 17. Engineering model converter.

F-35163
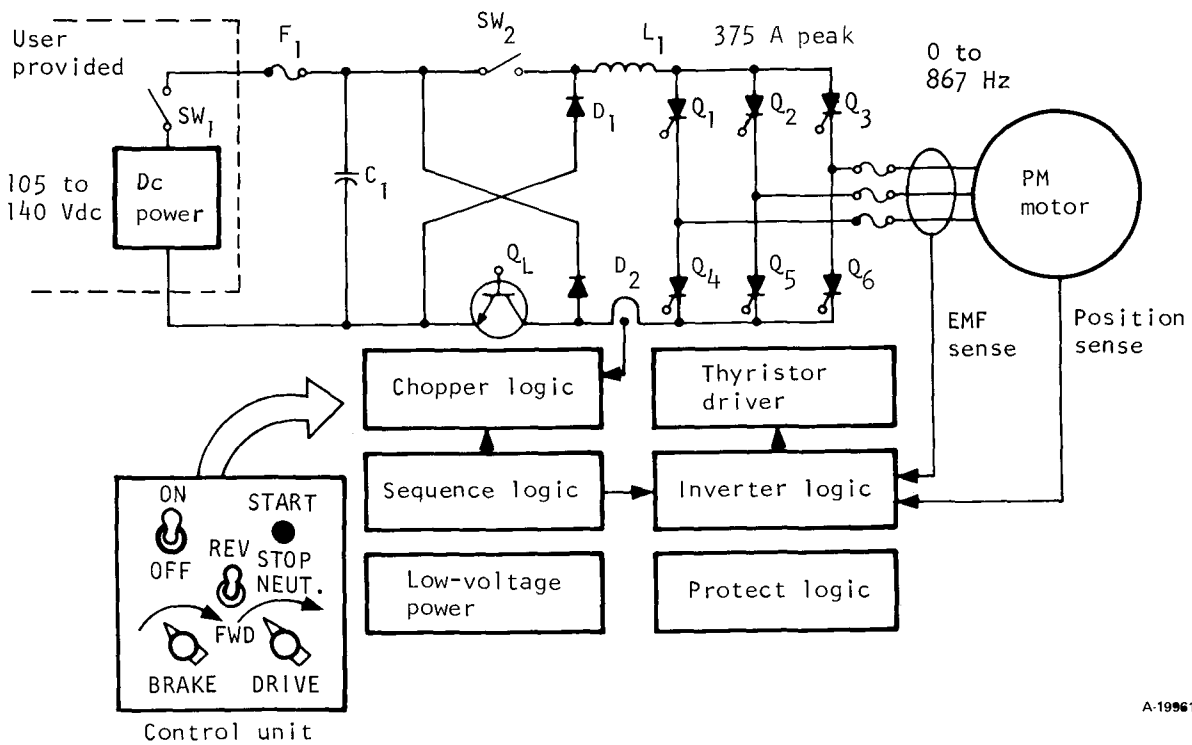
Figure 18.--Engineering model converter basic schematic.

TABLE V.--CONVERTER CONTROL FEATURES (VEHICLE APPLICATION ORIENTED)

- Five functional controls: (1) drive
  (potentiometer), (2) brake (potentiometer),
  (3) forward/reverse (switch), (4) on/off
  (switch), and (5) start/reset (pushbutton)

- Brake command overrides drive command

- Speed limited reverse mode ($\sim$10%)

- Normal DR/COAST/BK transitions are jerk-limited:
  zero to maximum or maximum to zero torque in 0.5 s

- For emergency situations, rapid DR/BK transitions
  are non-jerk-limited (i.e., the commanded torque
  is immediately reduced to zero)

- 12 Vdc logic power ($\sim$25 A)

- Built-in tach and synch signals

- Eight automatic protection features
  (listed in Table VI)

29

Engineering Model Converter Modifications

The engineering model design was accomplished by making four major changes to the functional model as described below.

Elimination of upper chopper.--As is evident from the engineering model converter schematic, there is only one transistor chopper used, while two are used in the functional model converter. The upper chopper, which has been eliminated, was provided to assist in rapid turn-off of the inverter thyristors during the start mode (less than 10 percent rated motor speed) when the back emf is low and not sufficient to provide thyristor turn-off. Tests showed that with the upper chopper removed, thyristor turn-off could be achieved by turning off the single (lower) transistor chopper each time thyristor turn-off is desired. The duration of this turn-off interval is programmed with the motor speed to provide sufficient time to ensure thyristor turn-off under worst-case conditions.

Package for lower size and weight.--The engineering model converter was packaged in a smaller enclosure than that used for the functional model. In accomplishing this, accessability to various components was emphasized for measuring currents and voltages to allow evaluation of the engineering model design. The controller weighs 68 kg (150 lb) and its dimensions are 82.6 by 71.1 by 28.4 cm (32.5 by 28 by 11.2 in.), but its size and weight can be further reduced considerably by methods listed in the improvement assessment recommendations section.

Transistor change.--Transistors were evaluated and changed from fourteen Motorola Model MJ10016 transistors to five Fuji ET-133 Darlington transistors, as described under the transistor chopper description. The change from the Motorola to Fuji type transistors was based on the following considerations: (1) use of a new, proven power transistor; (2) increase in power rating using minimum number of power transistors; (3) inherent increase in reliability due to use of fewer power transistors; (4) increase in chopper efficiency due to decrease in transistor switching losses; and (5) increased transistor switching frequency to minimize the rating or size of the series inductor (L_1).

Completion of the control logic.--The control logic was completed in the following areas. The drive/brake sequence logic and the protection logic were implemented. A list of the automatic protection features is given in table VI. Improved transistor drive circuitry was implemented to satisfy the new power transistor drive requirements. The logic for the drive circuit was also redesigned to eliminate the electrical noise problems due to the switching of high voltages and currents.

Converter Description

An electrical schematic of the engineering model converter is shown in figure 19. The major elements that constitute the converter are discussed below, and the primary devices used are listed in table VII. All component designators discussed below are referenced to the electrical schematic shown in figure 19.

TABLE VI.--MOTOR/CONVERTER AUTOMATIC PROTECTION FEATURES

```
* Dc overcurrent:  not to exceed 420 A → pause → 0.2 s
     shutdown

● Motor overspeed:  not to exceed 28,600 rpm → pause (drive
  mode only)

● Transistor heatsink overtemperature:  >100°C → pause

● Transistor saturation sensor:  >5μs turn-on → 20 μs pause
  → restart

* Logic power supply monitor (+15, +5, +12):  10 to 20 percent
  tolerance → shutdown

* Torque command and feedback monitor:  overscale → pause
  → 0.2 s → shutdown

● Forward/reverse interlock:  zero current and zero speed
  before change

● Forward/reverse check:  improper command → pause


* Logic card LED annunciated
```

TABLE VII.--ENGINEERING MODEL CONVERTER DEVICES

```
● Thyristors:  G.E. 434S, 600 V, 500 A, 14 μs

● Transistors:  Fuji ET133, 520 V, 100 A (5 parallel)

● Diodes (F.W.):  Motorola MR876, 600 V, 50 A (8 parallel)

● Capacitors:  Sprague 36D type, 6000  F, 300 V (5 parallel)

● Drive/brake switch:  Hartmann 300 A dc double break

● Logic cards:  216 by 152 mm (8.5 by 6 in.), 43 pin,
              CMOS, +15 Vdc power

● Current sensor:  Hall effect, 5000:1 current ratio

● EMF sensor:  Step-down control transformer

● Position sensor:  Photo-optical with slotted disc
```
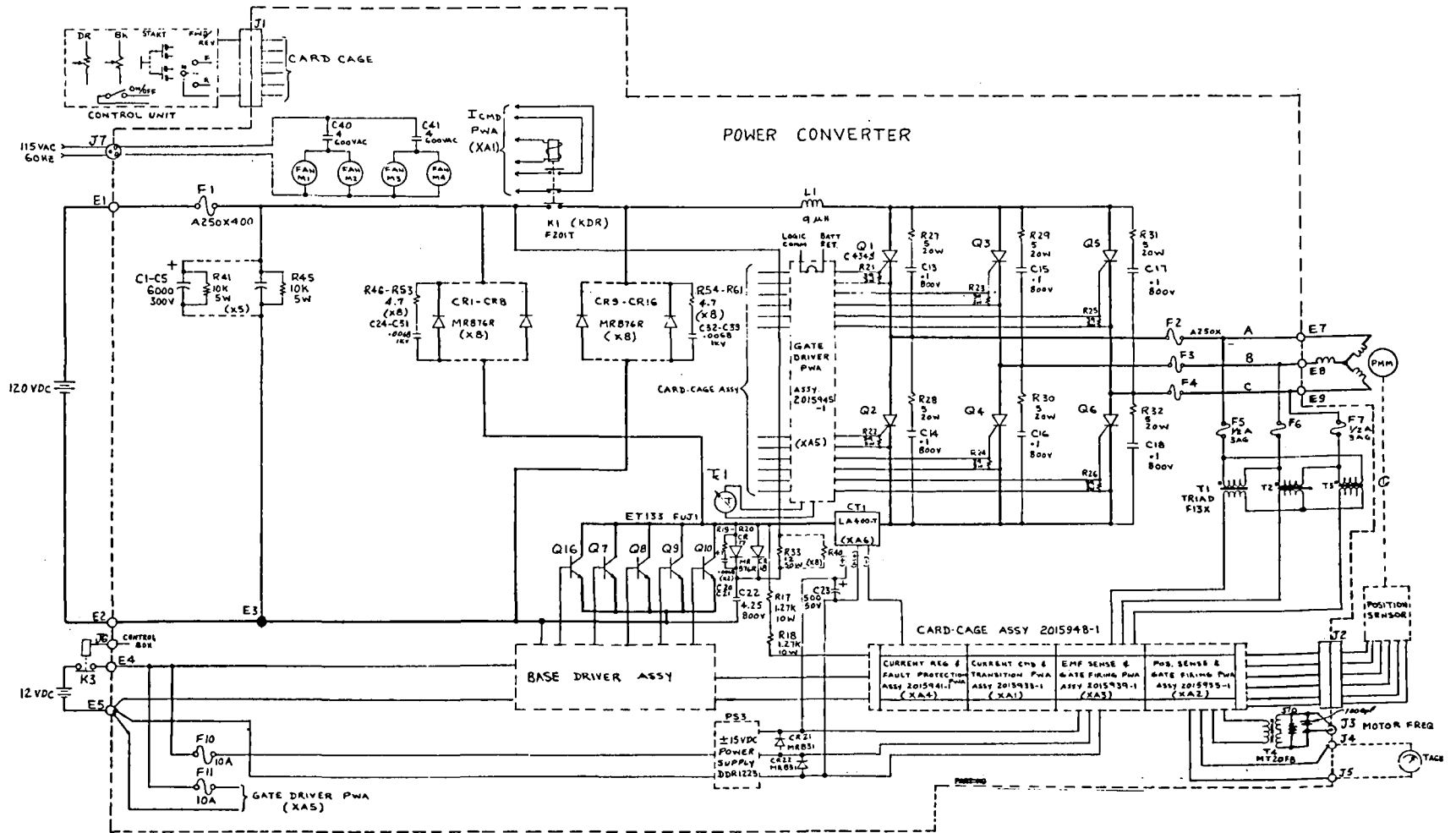
Figure 19.--Power converter electrical schematic.

Transistor chopper.--The chopper performs three important functions:

(1) It regulates the voltage to the inverter.

(2) It provides current control to the inverter.

(3) It provides for turn-off of the inverter thyristors at low motor speeds.

The transistor chopper modulates the fixed battery voltage in response to a current command to perform the above functions. The current command is initiated by the drive and brake controls on the control unit and is processed through the control logic to provide a base drive control for the chopper.

The chopper is a variable-frequency, variable-duty-cycle type, and is capable of switching up to 375 A peak current. Regulation is achieved by ripple control of approximately 2 percent around the commanded current with an upper frequency limit of 16 kHz. A brief description of various components of the chopper is given below.

Power transistor selection: Various transistors were tested and evaluated for this application on the AiResearch dedicated transistor test console using AiResearch funding. Some of the devices that were considered are (1) Toshiba Model 2SD648, (2) G.E. Model D67DE5, (3) Motorola Model MJ10016, and (4) Fuji Model ET-133.

Comparing the test and evaluation data, it was evident that the Fuji ET-133 Darlington would yield the smallest and most efficient chopper. Thus, the Fuji ET-133 was selected to be the power transistor for the engineering model chopper. Further, the test and evaluation data indicated that a minimum of four of these devices in parallel would be required to provide the necessary 375 A peak, 16-kHz switching capability. A fifth device in parallel was added to provide the short-circuit current capability. These devices are referenced as Q7-Q10 and Q16 in the converter electrical schematic.

Base Drive: Due to their fast switching speeds and low drive requirements, MOS-FET devices were selected to provide the base drive for the power transistors. Special attention was given to the base drive scheme to achieve rapid rise and fall times for the power transistor switching, thereby minimizing the switching losses for the chopper transistors.

Snubber circuit: The clamp circuit comprises CR17-CR18, C22, and R33-R40, and provides a safe switching locus for the power transistors. Special consideration was given to the packaging of the snubber to optimize its usefulness.

Thyristor (SCR) inverter.--The inverter performs the important function of providing solid-state commutation for the IECM permanent-magnet dc motor. The inverter is a line-commutated type except at motor speeds less

than approximately 10 percent of the rated speed (start mode). During the start mode, the inverter thyristor turn-off, which is required six times each electrical cycle, is effected by providing a turn-off or "blanking" pulse to the transistor chopper every 60 electrical degrees.

Thyristors and snubbers: The inverter thyristors are referenced as Q1-Q6 in the converter electrical schematic. R27-R32 and C13-C18 form the RC snubber network for the thyristor protection.

Gate drive: The control logic utilizes signals from the rotor position sensors to generate the gate drive signals that activate the inverter thyristors in the correct sequence of rotation. The control logic also takes into consideration various protection conditions, firing angle command (internally generated), back EMF sense signals, etc. to generate the gate drive logic signals, which are provided to the gate driver assembly (XA5), as shown in figure 19.

Free-wheel diodes.--The free-wheel diodes maintain a continuous motor current by providing a conduction path for it when the chopper is off. During this period the current is sustained by the system inductance in the chopper, inverter, and motor loop. The free-wheel diodes also perform an important function during the regenerative brake mode. During this mode, they provide a path for the energy to be returned to the battery (dc voltage source).

Control logic.--The primary function of the control logic is to interface with the commands from the control unit and feedback signals from the rotor position sensor, back EMF sensors, current feedback, etc., and then to generate drive/brake, forward/reverse, and protection commands used to create drive signals to the chopper and inverter. The control logic is packaged on four printed wiring board assemblies that are enclosed in a card cage. The card cage assembly and the four printed wiring assemblies (XA1-XA4) are shown in figure 19.

Power supplies.--Power supplies PS1-PS3 supply the 5 Vdc and -5 Vdc for the chopper base drive and ±15 Vdc for the control logic and the current sensor.

Current sensor.--The current sensor, CT1 on the schematic shown in figure 19, provides an isolated current feedback to the control logic. It is used to monitor (1) the chopper current when the chopper is on or (2) the free wheel current when the chopper is off. The current sensor operates on the Hall-Effect principle and provides accurate current feedback for the chopper current control.

Cooling.--The engineering model converter uses an integral forced air cooling arrangement for the chopper, inverter, and free wheel diode assemblies. These assemblies are the major heat dissipating elements in the converter. The forced air cooling is provided by four Rotron-Caravel fans. Two of these fans are for air inlet into the heatsinks and the other two are for exhaust. Each fan is capable of providing 100 cfm of

airflow. The chopper transistors and the free wheel diodes are mounted on a modified Wakefield 511 aluminum extrusion. This is a high-fin-density heatsink and provides approximately 0.08 m^2 (130 in^2) of cooling surface per linear inch of extrusion. To minimize the contact resistance between the chopper transistor and the heatsink mounting surfaces, a conducting thermal compound is employed. The thyristors for the inverter are pressed between aluminum-finned extruded heatsinks which provide an extended cooling surface for the thyristors. Again, a thin layer of thermal compound is used between the thyristor and the heatsink mounting surfaces.
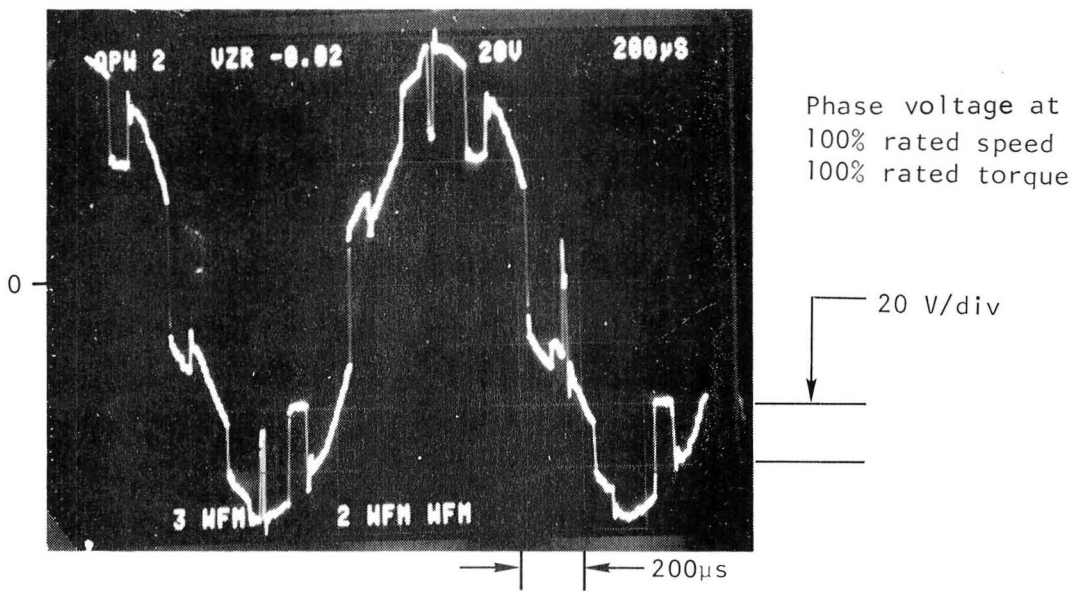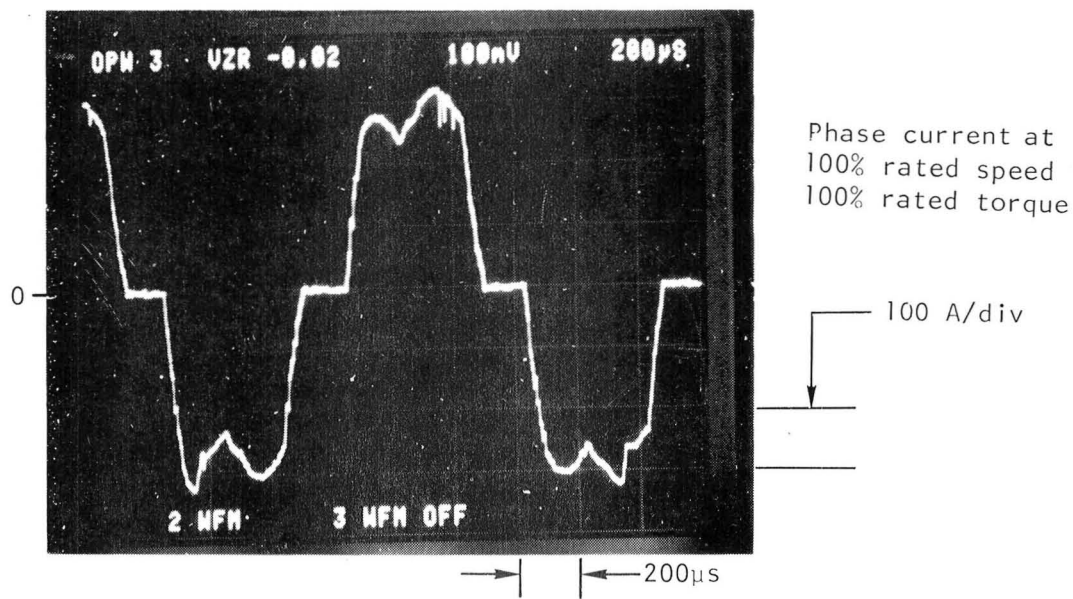
Control unit.--The control unit provides vehicle application oriented controls. These controls consist of drive, brake, forward/reverse, on/off, and start/stop, as indicated in basic schematic of the engineering model (figure 18). The control unit can be detached from the converter by disconnecting a connector.

Dc-link inductor.--The engineering model permanent-magnet dc motor has relatively low inductance per phase. A 9-μH inductor was inserted between the chopper and the inverter to provide the dv/dt protection for the inverter devices operating in conjunction with their R-C snubber networks. This also allows the choppper switching frequency to be established at 16 kHz.

Typical waveforms.--Final testing of the converter and motor included waveform analysis to ensure proper operation in both the drive and brake modes. Figures 20 through 23 show typical converter output voltage and current waveforms at the various conditions summarized in table VIII. The curves for phase voltage show the switching transients superimposed on the approximately sinusoidal wave shapes. The current curves show the modulation of the chopper as it maintains the required average current level for the load.

TABLE VIII.--WAVEFORM SUMMARY

Figure	Mode	Waveform	Motor	
			Speed, percent	Torque, percent
17	Drive	Current	100	100
17	Drive	Voltage	100	100
18	Drive	Current	100	50
18	Drive	Voltage	100	50
19	Drive	Current	50	100
19	Drive	Current	25	100
20	Brake	Current	100	100
20	Brake	Current	50	100

Phase current at
100% rated speed
100% rated torque

100 A/div

Phase voltage at
100% rated speed
100% rated torque

20 V/div

A-19957

Figure 20.--Converter output waveforms for driving mode.

Phase current at
100% rated speed
50% rated torque

100 A/div

500µs

Phase voltage at
100% rated speed
50% rated torque

20 V/div

500µs
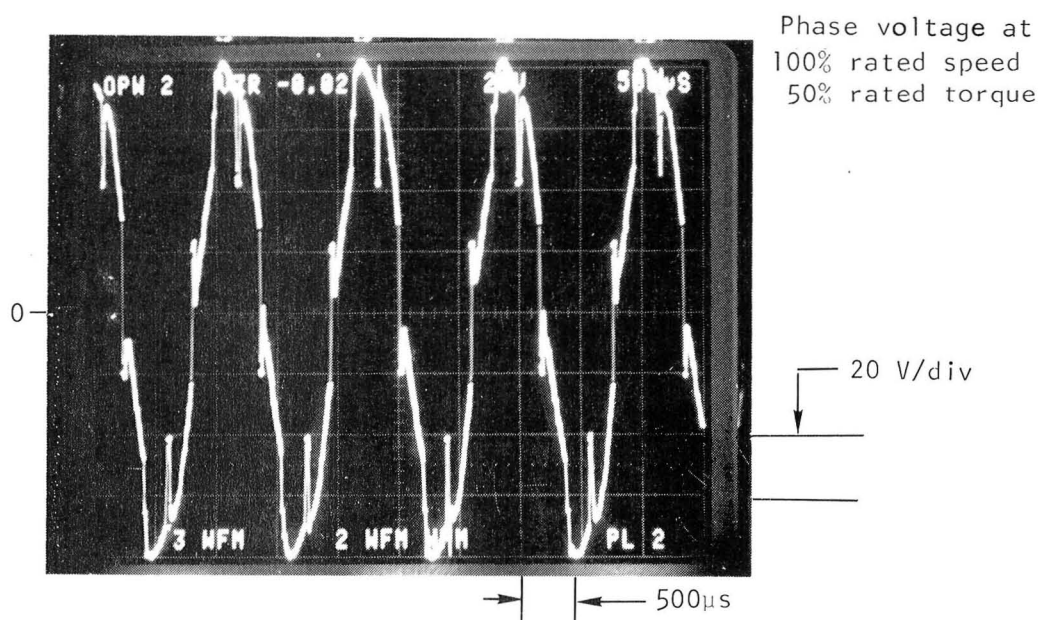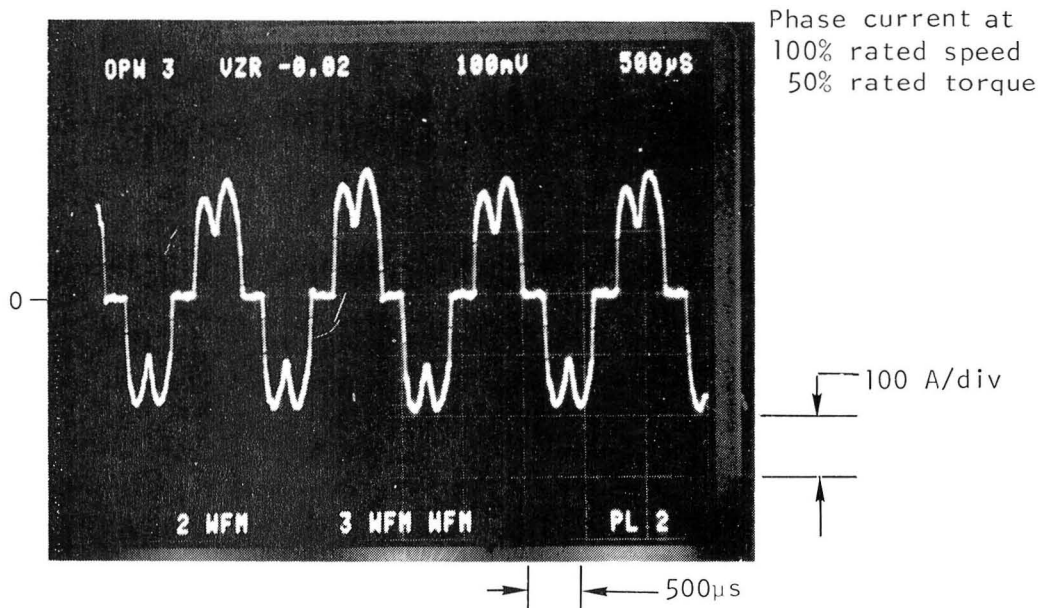
A-19955

Figure 21.--Converter output waveforms for driving mode.

Phase current at
50% rated speed
100% rated torque

100 A/div

500μs

Phase current at
25% rated speed
100% rated torque

100 A/div

1 ms
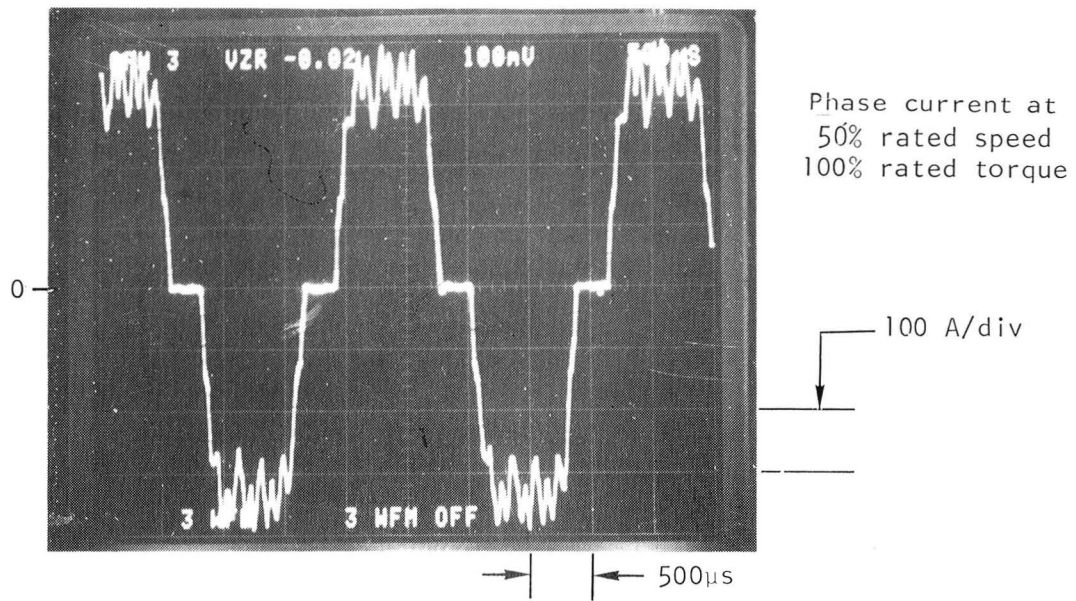
A-19958

Figure 22.--Converter output waveforms for driving mode.

Phase current at
100% rated speed
100% rated torque

100 A/div

200µs

Phase current at
50% rated speed
100% rated torque

100 A/div

500µs
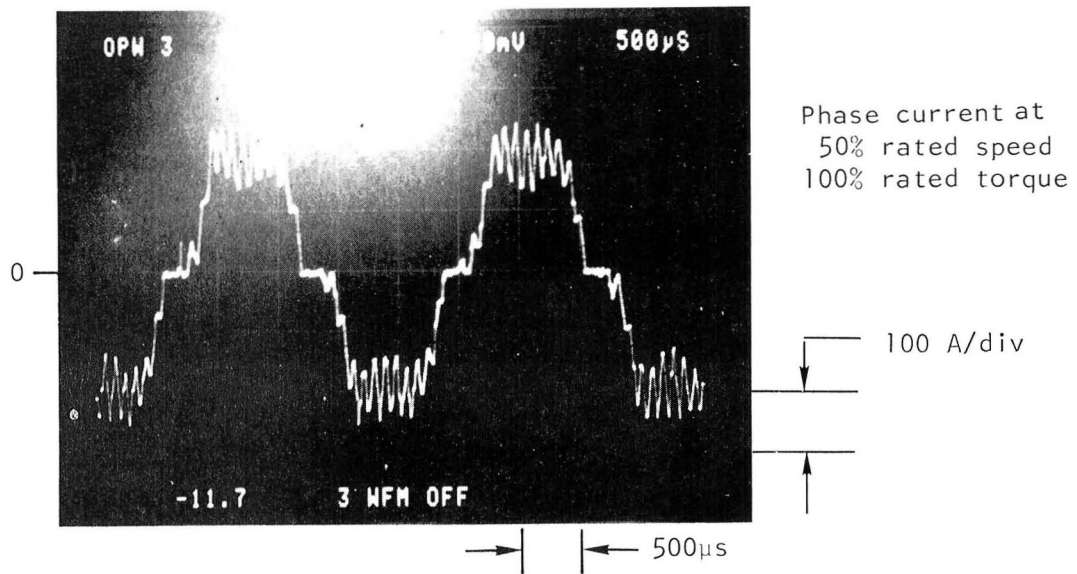
A-19956

Figure 23.--Converter output waveforms for braking mode.

ENGINEERING MODEL TEST

The engineering model was tested under the same loading conditions as the functional model; the tractive effort was varied in four steps (25, 50, 75, and 100 percent) at each of four speeds (25, 50, 75, and 100 percent). The laboratory setup is shown in the schematic of figure 24 and the photographs of figure 25. In the drive mode, the 480-V, 3-phase i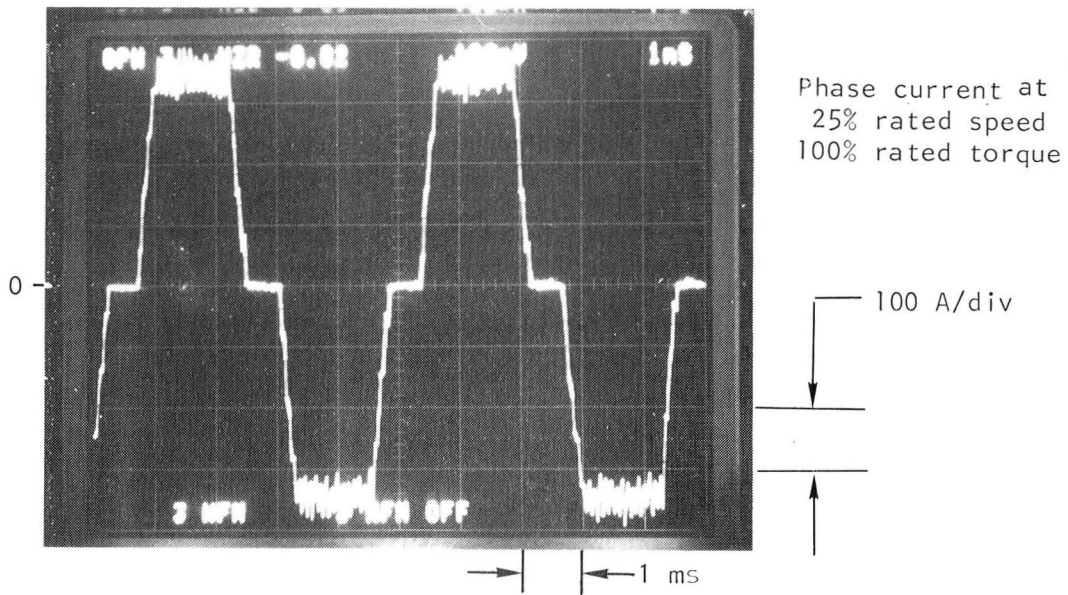nput power is transformed, rectified, and filtered to provide the required dc voltage to the converter. The motor output shaft is geared down and coupled to a dc machine acting as an absorption dynamometer. In the brake mode, the dc machine acts as a drive motor to provide the input power to the IECM motor. The electrical output from the converter is absorbed by a 26-kW resistive load bank. The measured test results are shown in figures 26 through 29. For the convenience of the reader wishing to use these results for further analysis, these data are presented in tabular form in Appendix G. All protective and vehicle control functions were checked for proper operation. The temperature rise profile for continuous operation at 15 kW output is also shown in figure 30. Wh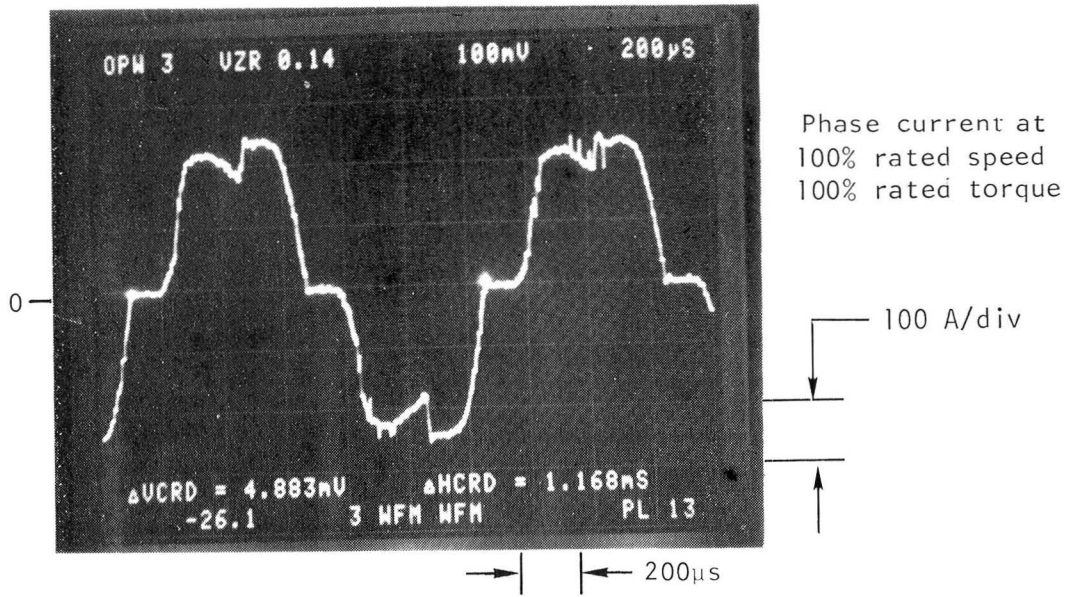en steady-state temperature was achieved, one minute of operation at 26 kW resulted in a final winding temperature of 135°C, which is well within the 200°C maximum rated allowable winding temperature.

Operation of the test stand included simulated vehicle start, acceleration, drive, coast, brake, and stop modes. Transitions from low-speed position sensing to higher speed back emf sensing, or visa versa, was smooth with no detectable hesitation or jerky motion. Slow transitions from the drive to brake, or visa versa, were equally smooth. Rapid drive-brake-drive transitions, which by design are not jerk-limited, were simulated by the controls in a manner equivalent to the sudden releasing of the accelerator pedal and applying the brakes.

The efficiency of the chopper/inverter/motor was determined by measuring the dc input power using conventional meters, and the ac output power of the converter using the Tektronix Oscilloscope/Waveform Calculator Model 7854. The Tektronix instrument utilizes high frequency digital waveform processing necessary for the accurate measurements of the quasi-sine wave produced by the inverter. The efficiency of the machine was determined by measuring the input ac power using the Tektronix oscilloscope and the mechanical output power using conventional torque and speed measurement devices.

40
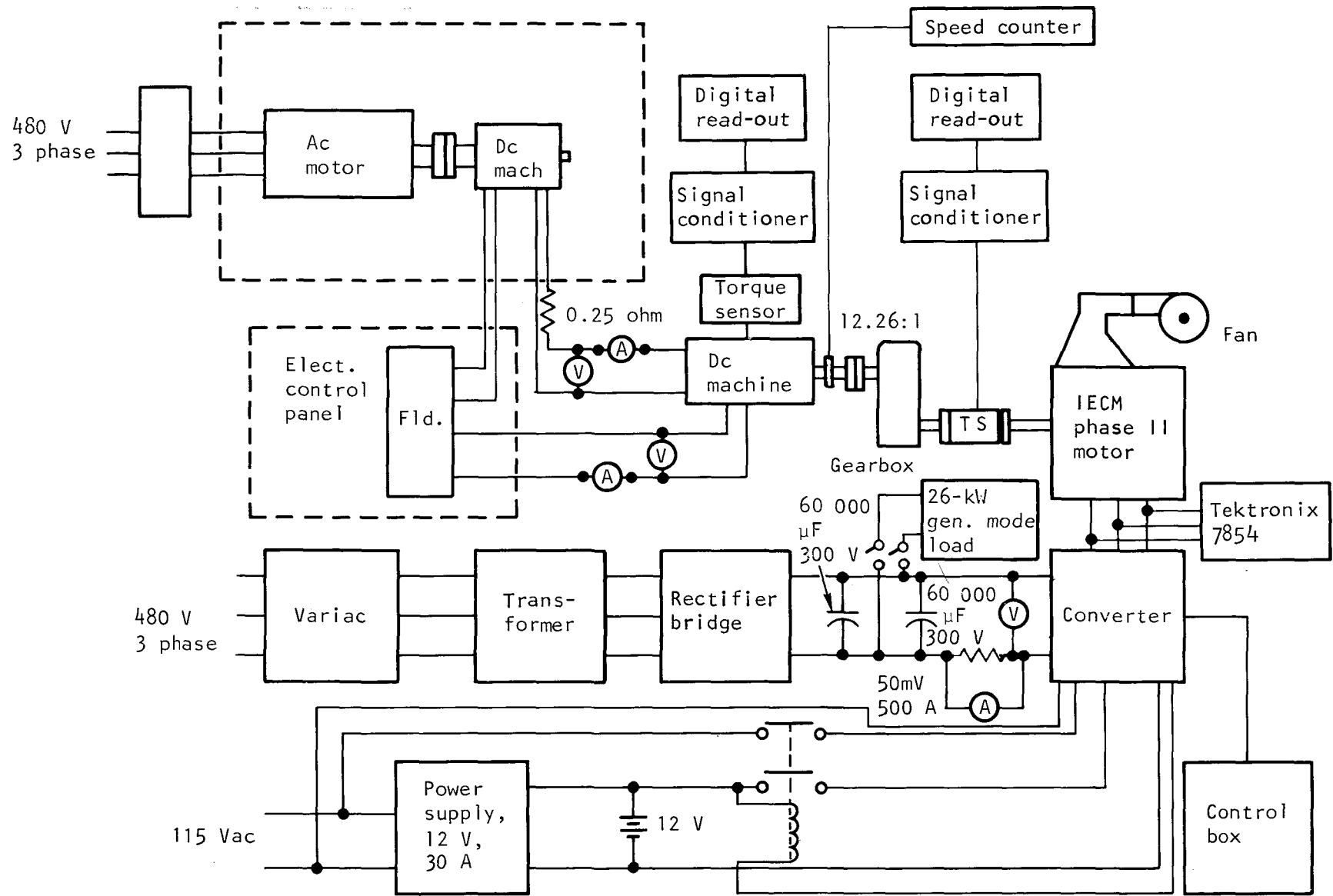
Figure 24.--Test setup for engineering model, motor/converter.
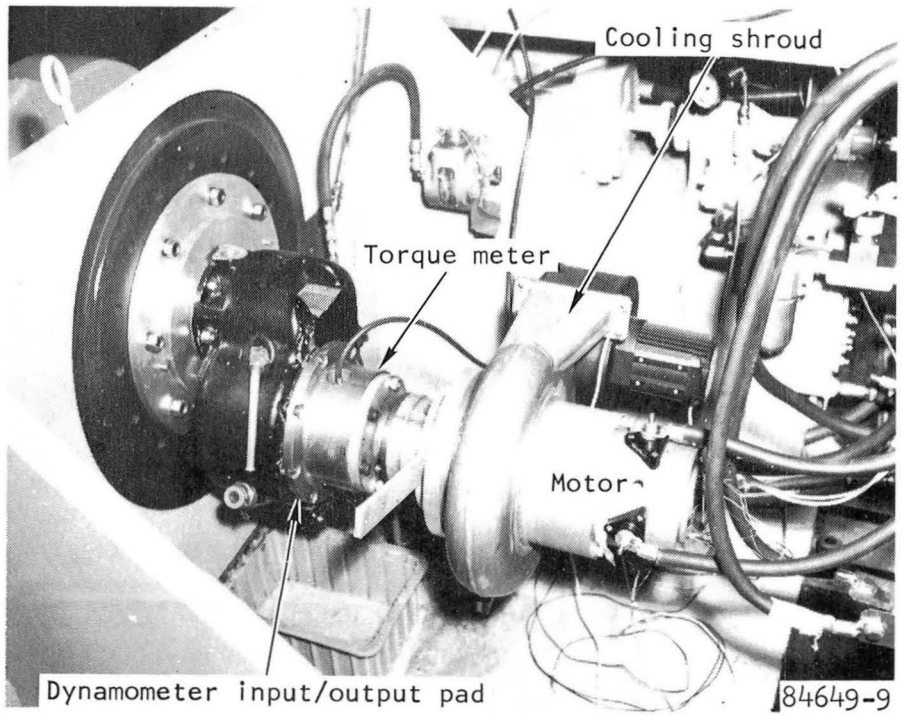
A-19959
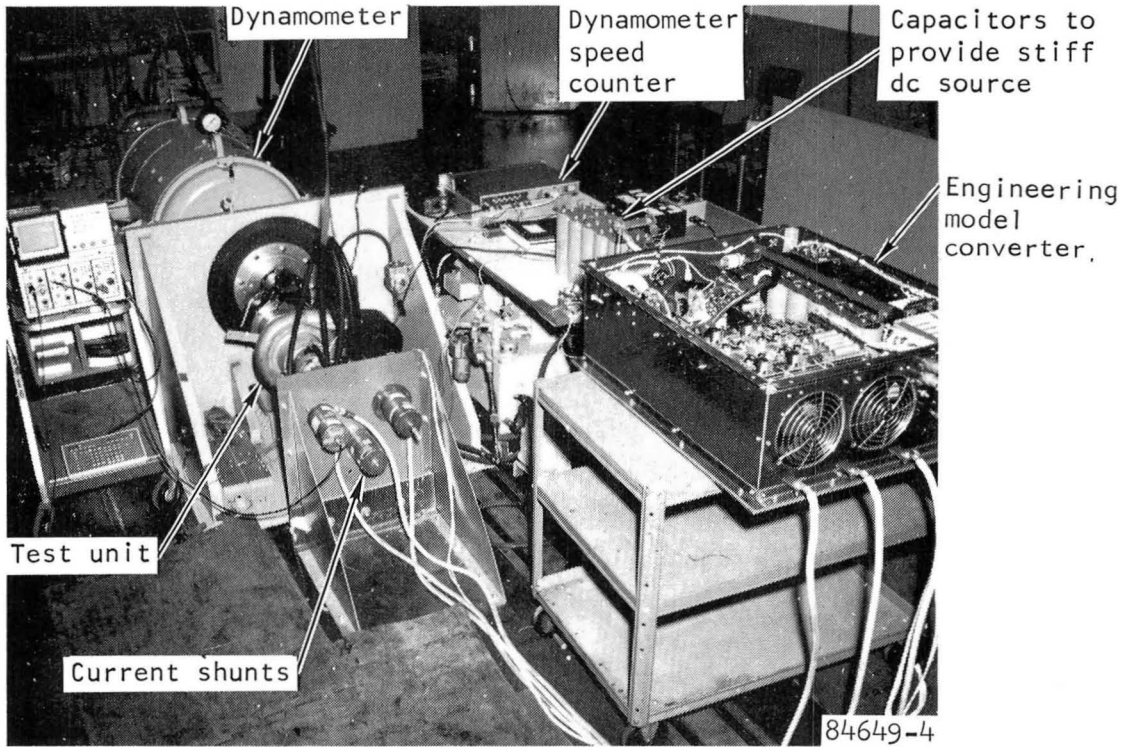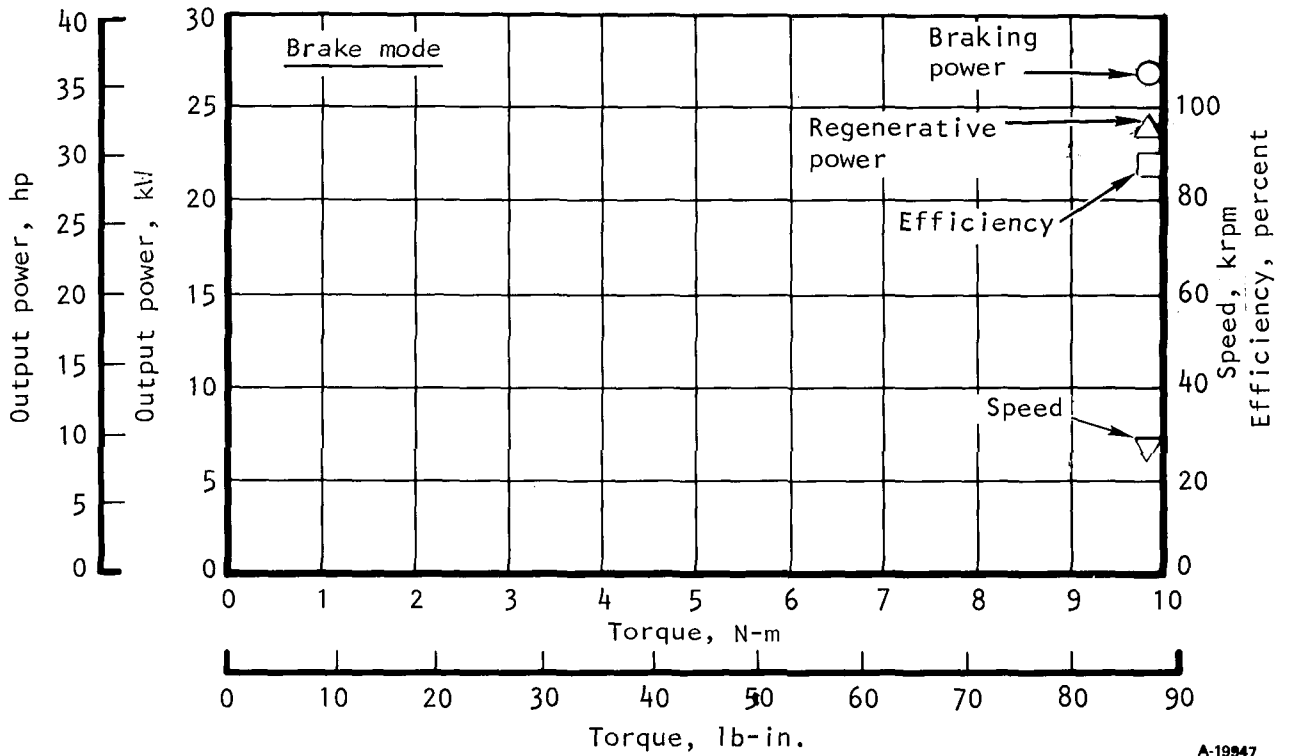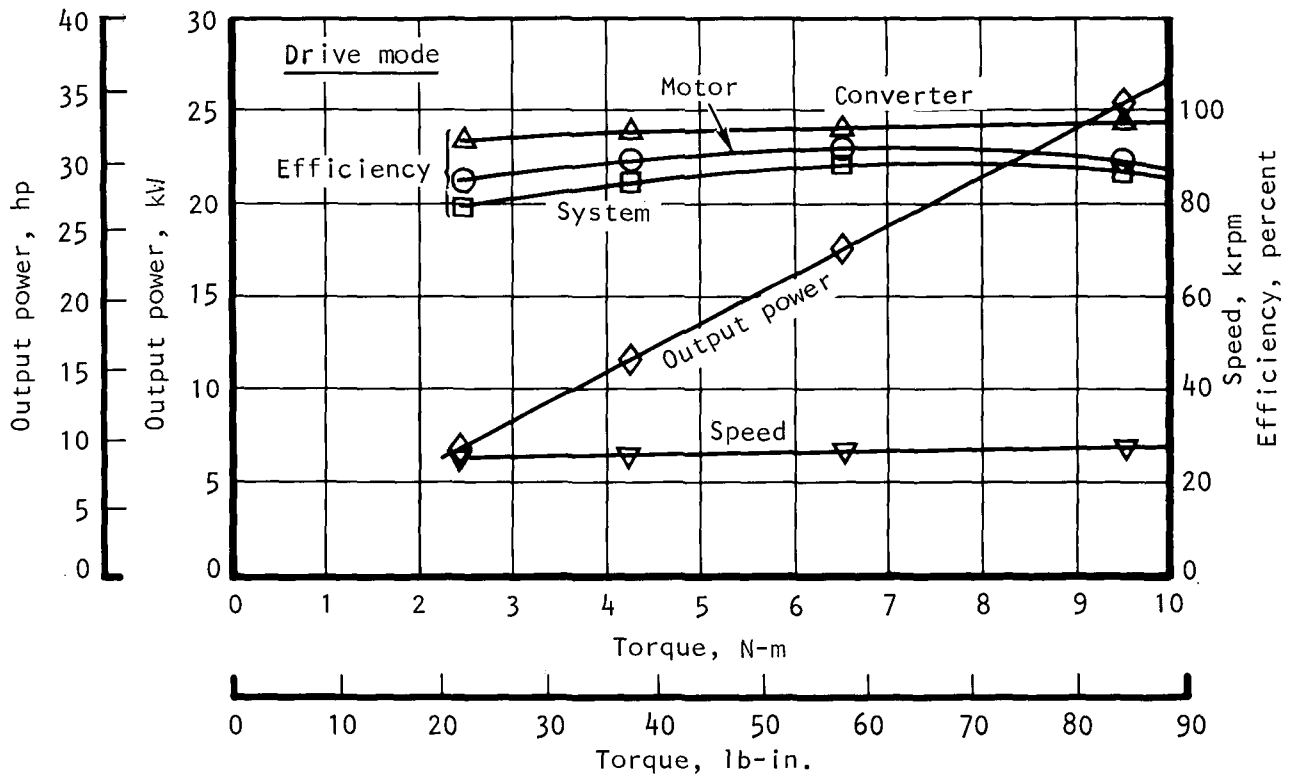
Figure 25.--Laboratory setup.

F-35161

Figure 26.--Engineering model performance at 100 percent speed.

43
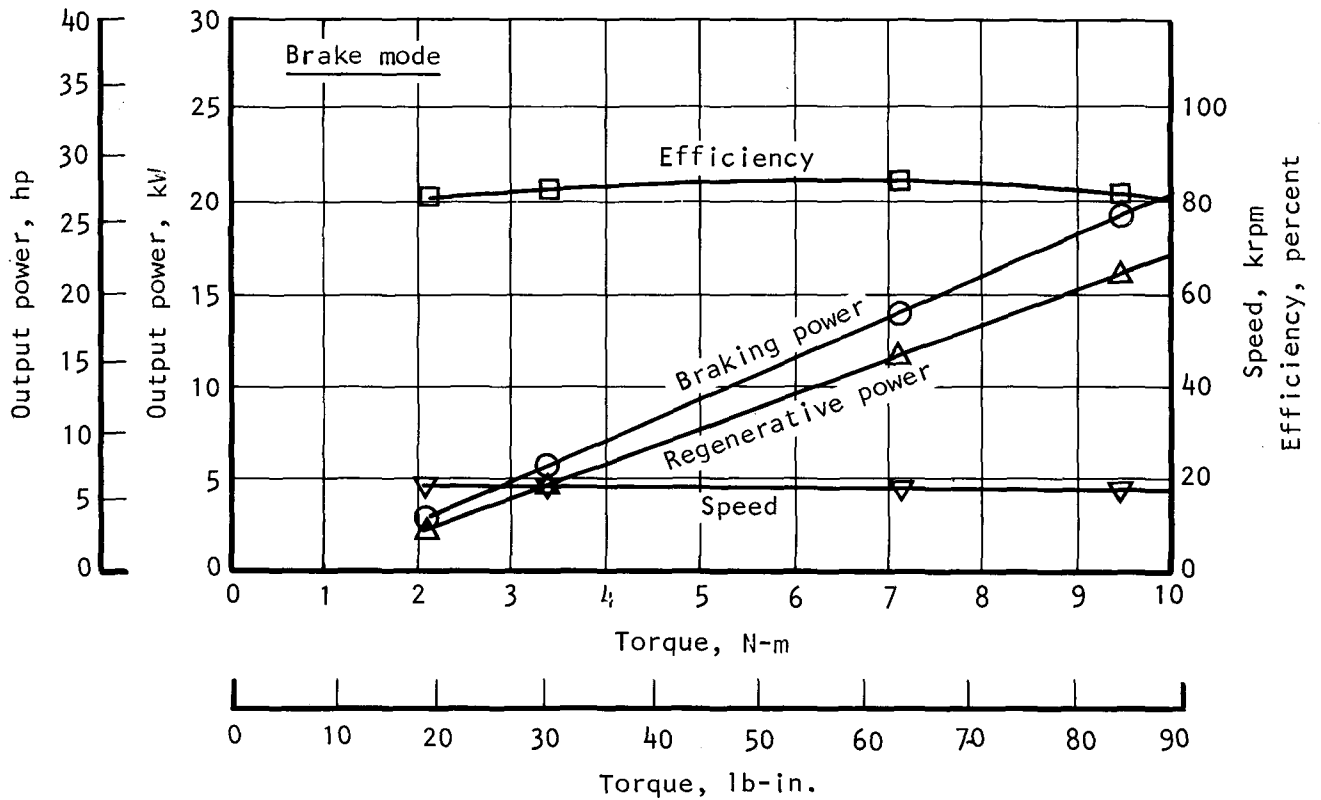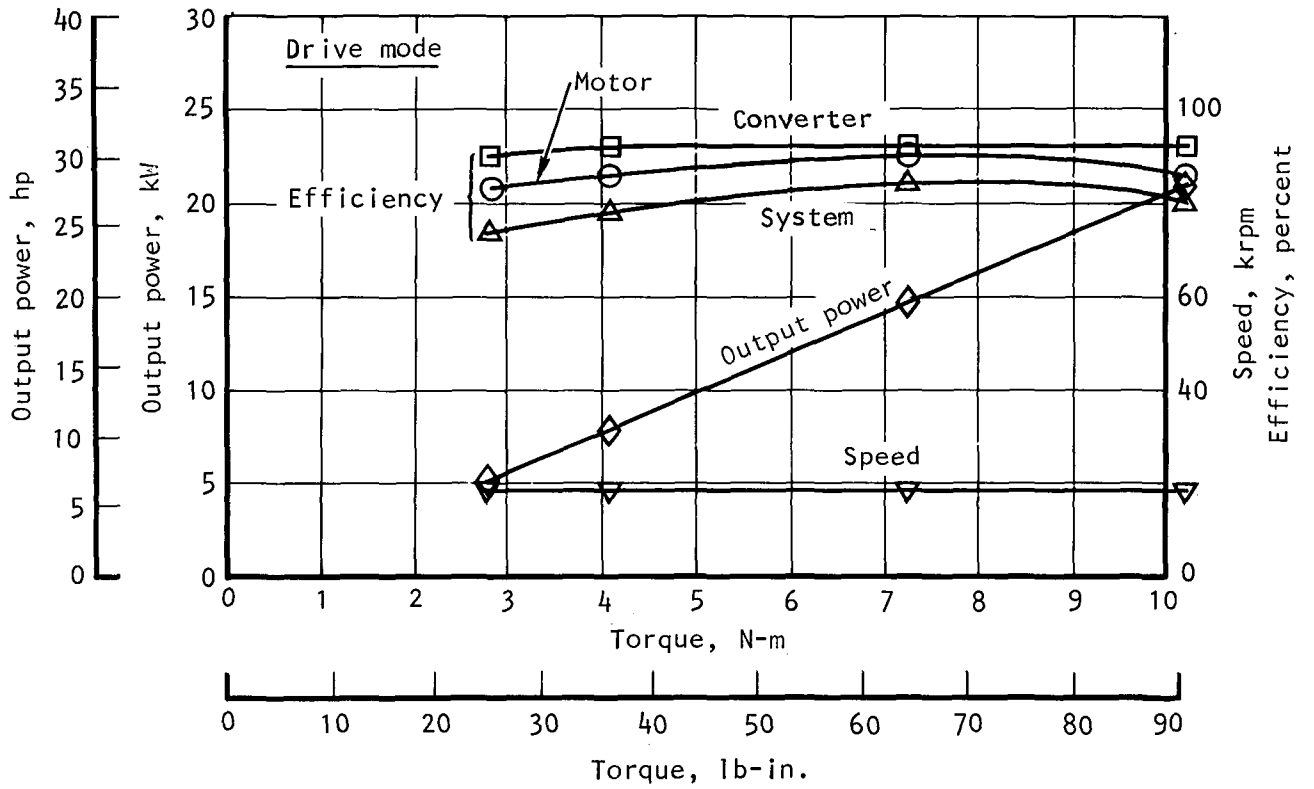
Figure 27.—Engineering model performance at 75 percent speed.

A-19950
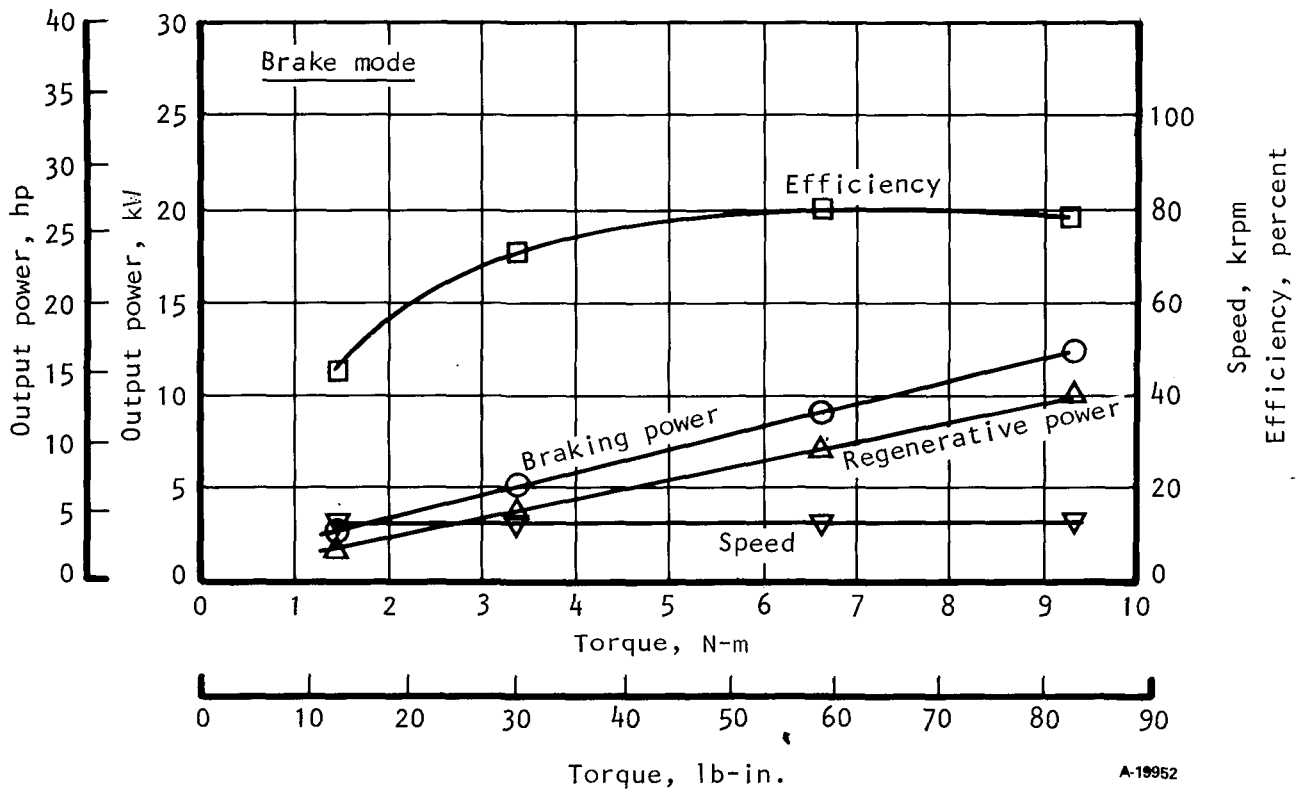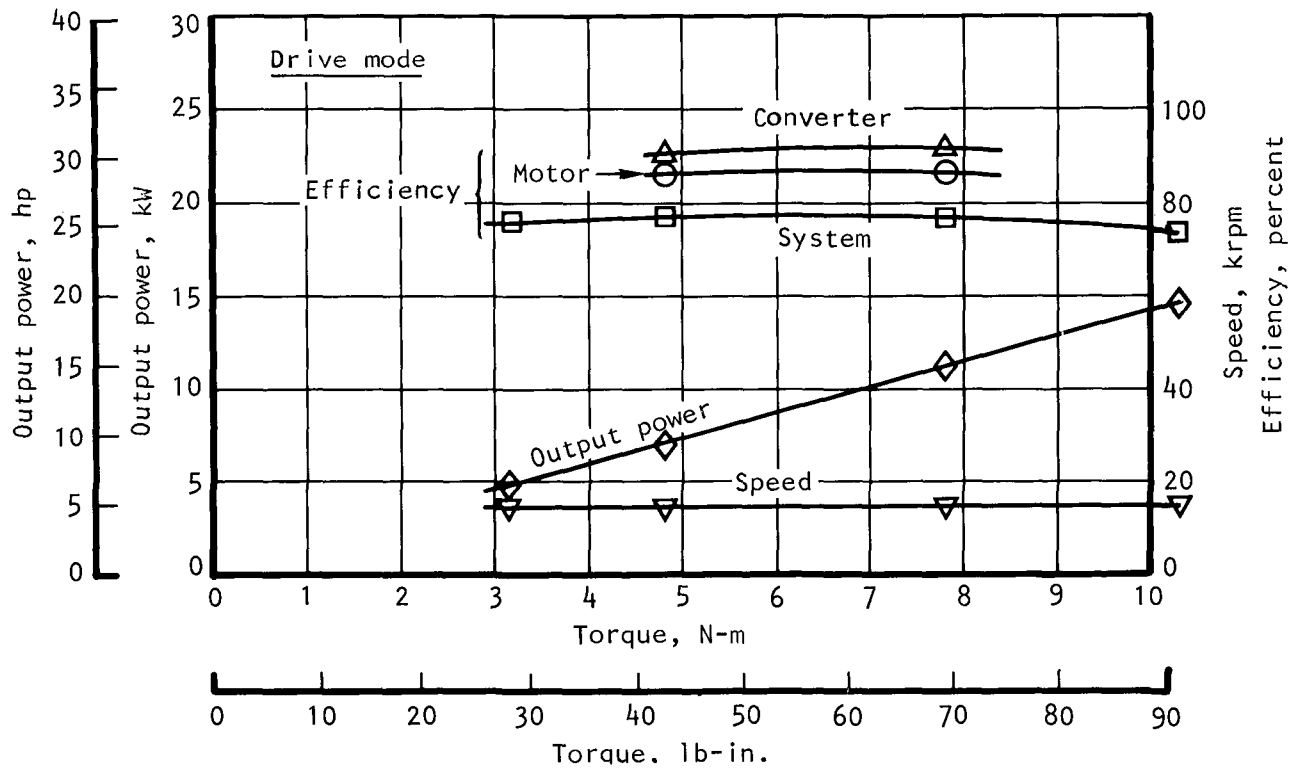
Figure 28.—Engineering model performance at 50 percent speed.
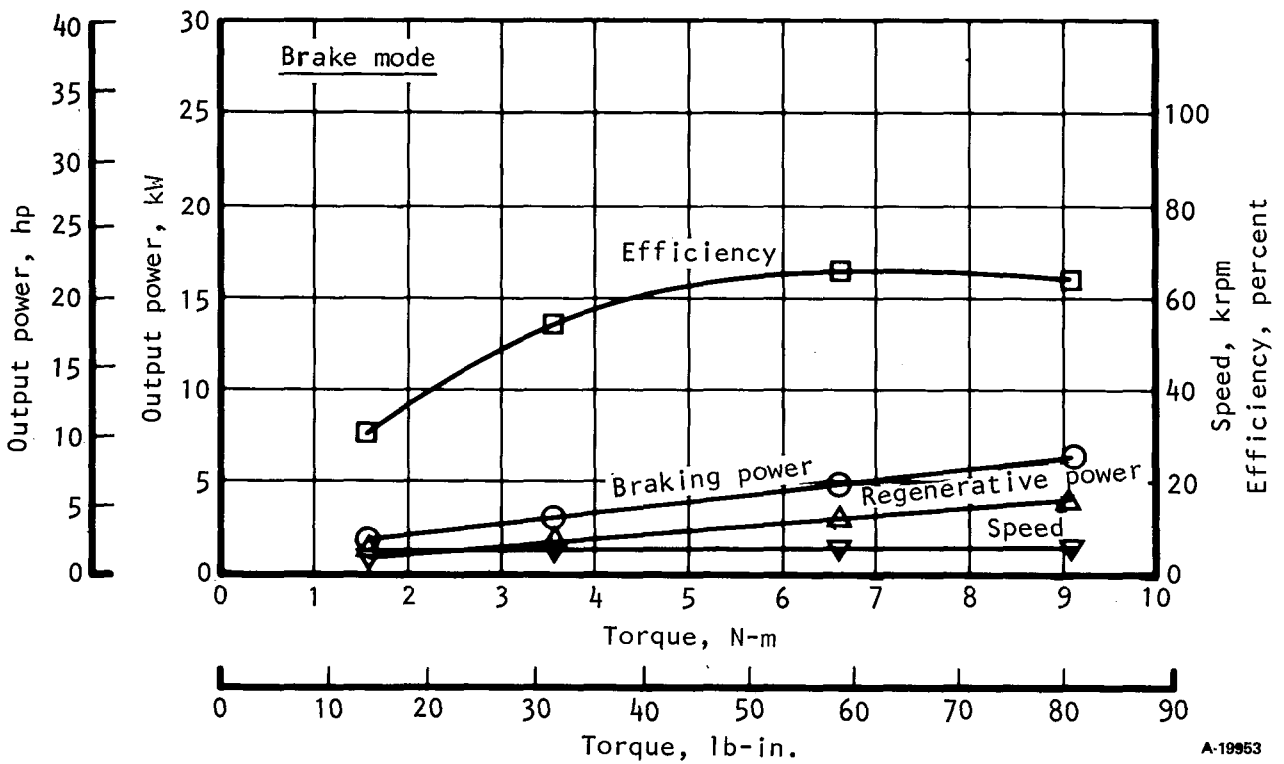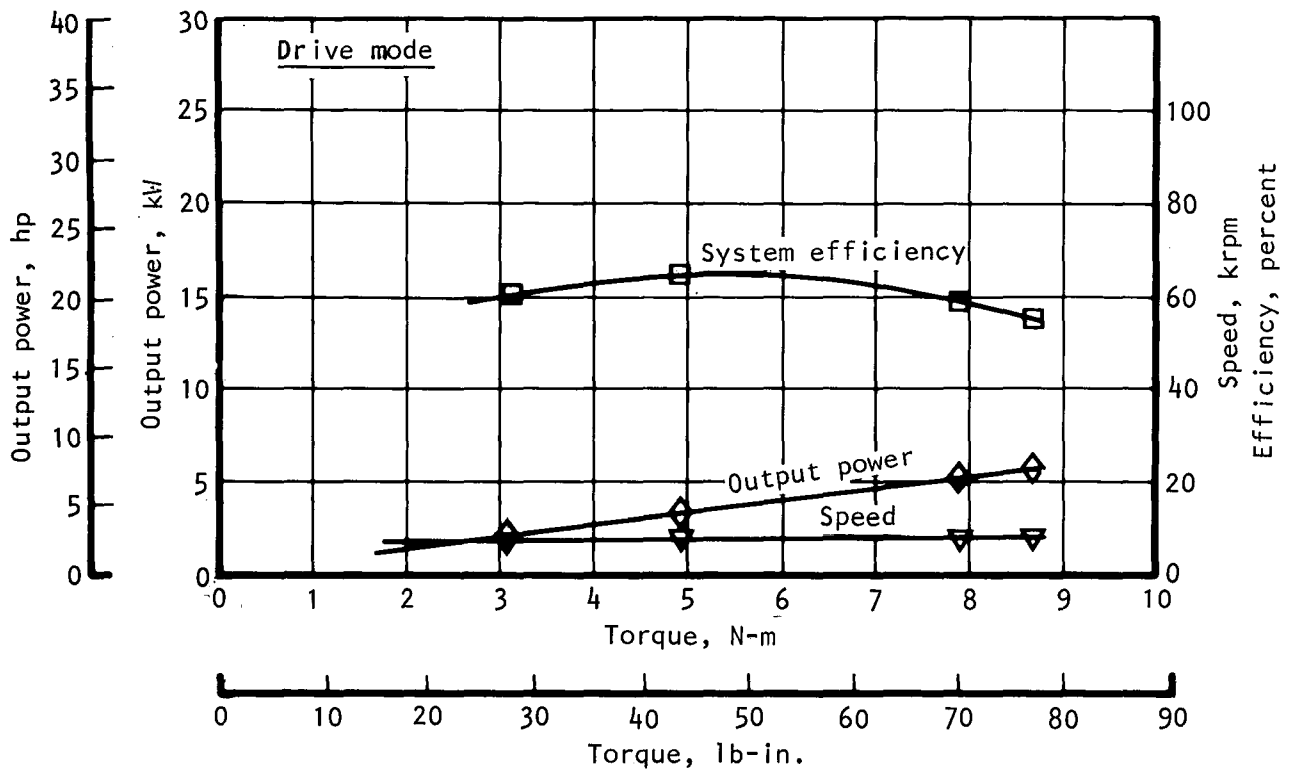
Figure 29.—Engineering model performance at 25 percent speed.
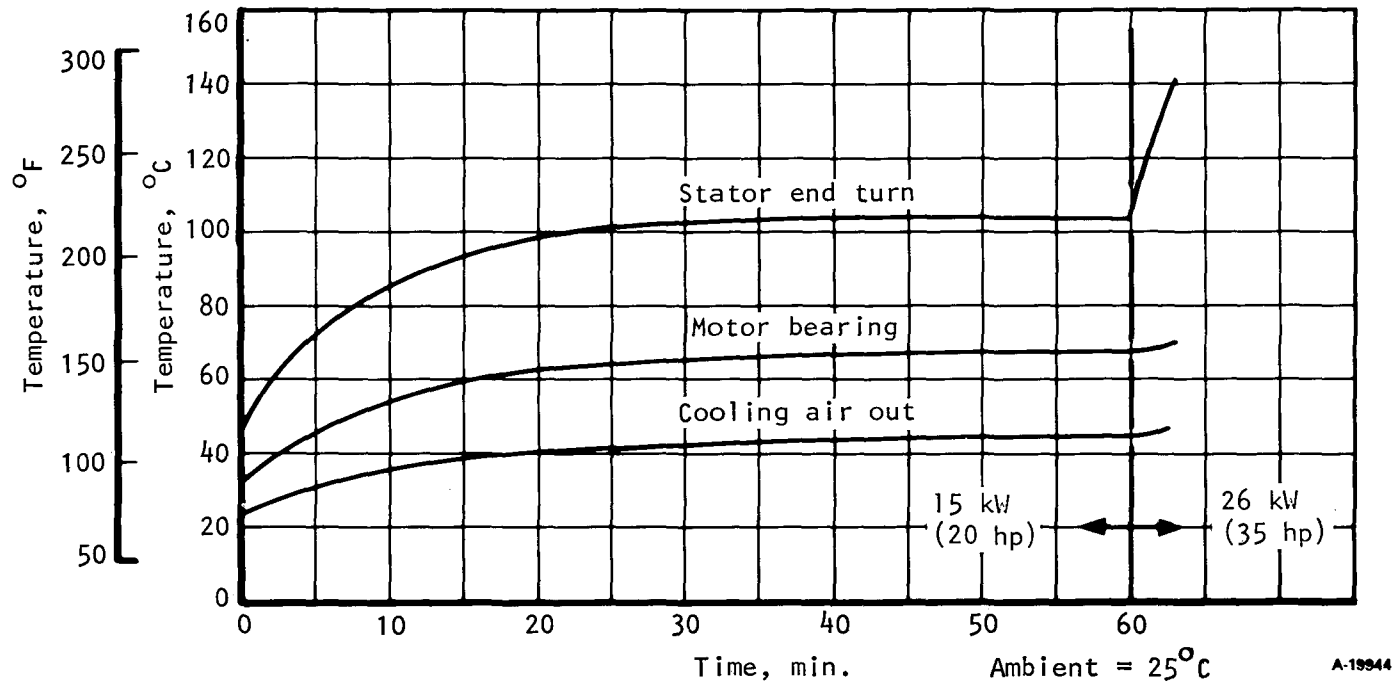
Figure 30.--Engineering model motor thermal evaluation.

47

IMPROVEMENT ASSESSMENT

A study has been completed to determine possible improvements that can be made to reduce the size, weight, and cost, and improve the performance and reliability of the motor and converter. The suggested improvements are listed in table IX. The major improvement is a change to liquid cooling for the converter.

Cost estimates (in 1978 dollars) at the completion of phase 1 of the program are shown in table X. The estimate indicates that the signifi-cant costs are associated with manufacture of the converter. The recommen-dations if incorporated will allow a significant reduction in parts count, and reduce the amount of labor for mounting and connecting components. Cost estimates for a liquid cooled configuration cannot be made until a design is available in sufficient detail to allow accurate estimating. A converter cost reduction of 50 percent is suggested as an objective if all cost-related recommendations are incorporated.

TABLE IX.--IMPROVEMENT POSSIBILITIES

- Increase peak power to 30 to 35 kW: Improve vehicle performance

- Design for minimum magnet material: Reduce cost

- Liquid-cooled power semiconductors: Reduce cost, size, and weight

- Adjustable firing angle: Optimize torque/ampere

- Dc interface and current sensing: Minimize component size and weight

- Optimized logic power supplies: Design for application

- Optimized "blanking" pulse width: Maximize torque at low speeds

- Input dc monitoring: Optimize for battery characteristics

- Integrated logic: LSI for lower cost, size, and weight

- Automatic motor synchronization during shift: Minimize clutch wear

TABLE X.--MOTOR MANUFACTURING COST ESTIMATE (1978 DOLLARS)

	Motor	Converter
First cost at 10,000 units per year		
Magnet material (motor only)	152	-
Raw material, purchased parts, subcontracted items	85	1360
Labor	65	290
	$302	$1650
First cost at 100,000 units per year		
Magnet material (motor only)	152	-
Raw material, purchased parts, and subcontracted items	60	1200
Labor	40	160
	$252	$1360

APPENDIX A

DETERMINATION OF ENERGY LOSSES

Energy Efficiency

Energy efficiency has been defined as the total mechanical energy delivered at the motor shaft over a driving cycle divided by the total electrical energy put into the motor over a driving cycle. This definition is interpreted as

$$\eta_E = \frac{E_S}{E_M}$$

where η_E = energy efficiency

E_S = total energy delivered from the motor to the motor shaft during the drive modes of the cycle

E_M = energy absorbed by the motor from the battery during drive modes minus the energy delivered by the motor to the battery during regeneration

Symbols

G_D sum of gearbox losses during drive modes

R_D sum of losses to rolling resistance during drive modes

A_D sum of losses to aerodynamic load during drive modes

K_D sum of kinetic energies added to vehicle during drive modes

M_D sum of all losses in motor/power converter during drive modes

M_R sum of losses in motor/power converter during regeneration modes

G_R sum of gearbox losses during regeneration

R_R sum of losses to rolling resistance during regeneration

A_R sum of losses to aerodynamic load during regeneration

H_R sum of losses to hydraulic/mechanical brakes during regeneration

K_R sum of kinetic energies removed during regeneration

B_D energy extracted from battery during drive mode

B_R energy delivered to battery during regeneration

S_D sum of energies delivered to shaft during drive (energy flow from motor to shaft)

S_R sum of energies delivered to shaft during regeneration (energy flow from vehicle to shaft)

Substituting these symbols:

$$E_S = S_D$$

$$E_M = B_D - B_R$$

the equation for energy efficiency becomes:

$$\eta_E = \frac{S_D}{B_D - B_R}$$

where $S_D = G_D + R_D + A_D + K_D$

$$S_R = K_R - (G_R + R_R + A_R + H_R)$$

$$B_D = S_D + M_D$$

$$B_R = S_R - M_R$$

$$B_D - B_R = G_D + R_D + A_D + K_D + G_R + R_R + A_R + H_R - K_R + M_D + M_R$$

Notes: (1) The change in potential energy is assumed to be zero.

(2) Energy to and from the motor (B_D and B_R) is determined at the terminals of the motor/power converter.

(3) With reference to the SAE J227A(D) cycle in figure 31, drive modes occur during periods 1, 2, and 3. Regeneration occurs during period 5. Period 4 is defined by the cycle as a "coasting" period. However, to obtain maximum energy recovery, regeneration should also occur during period 4.

(4) More efficient regeneration during period 5 can be achieved by dividing the period into high- and low-gear deceleration. This would result in higher motor speeds at low vehicle speed. However, the driver would be required to make the downshift at the right time or a complex automatic transmission would be needed.

Gearbox Losses

Experience has demonstrated that a gearbox efficiency of 92 percent is a reasonable value for steady-state running under moderate loads. With this value as a base, along with available test data that indicate the nature and apportionment of losses, vehicle gearbox losses can be estimated for various

52
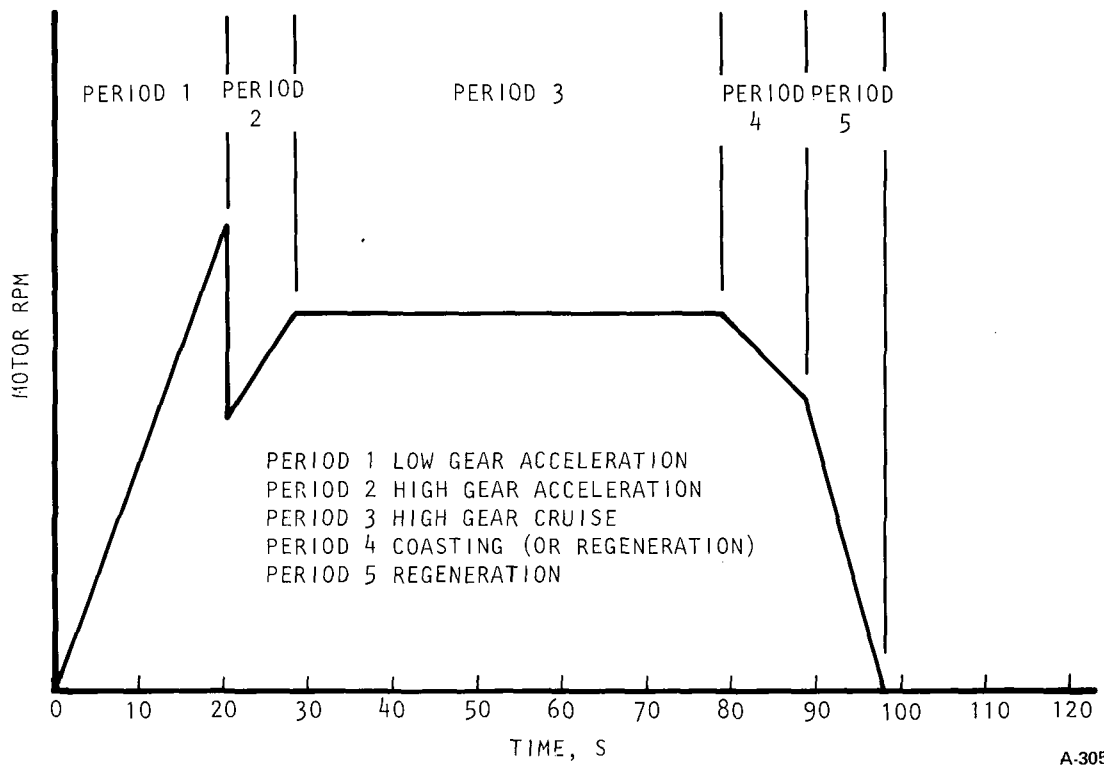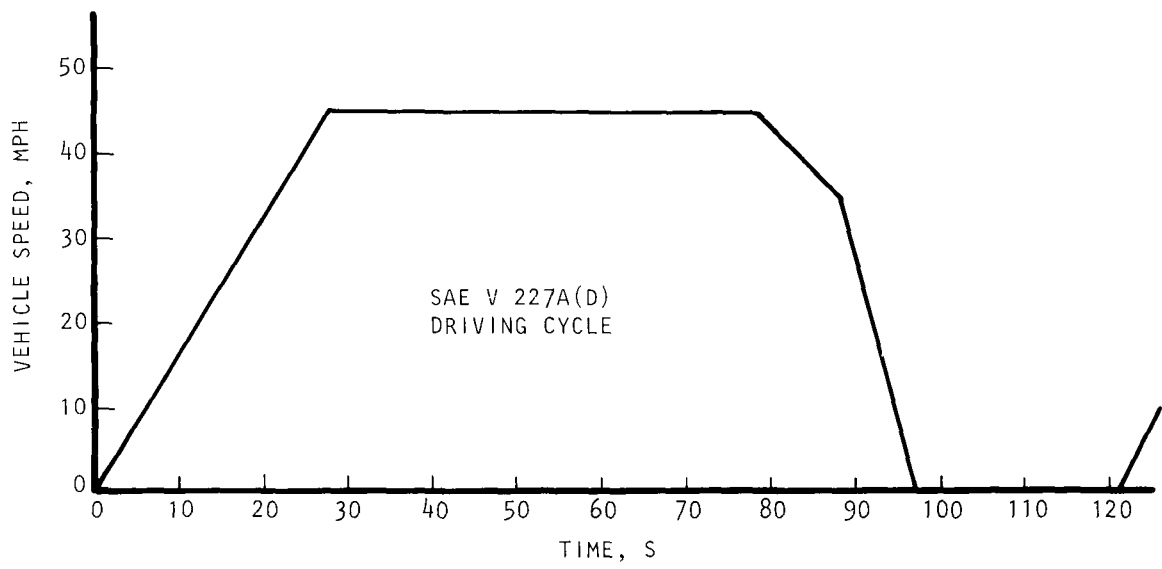
Figure 31.—Operating modes.

PERIOD 1 PERIOD 2 PERIOD 3 PERIOD 4 PERIOD 5

PERIOD 1 LOW GEAR ACCELERATION
PERIOD 2 HIGH GEAR ACCELERATION
PERIOD 3 HIGH GEAR CRUISE
PERIOD 4 COASTING (OR REGENERATION)
PERIOD 5 REGENERATION

A-30589

operating conditions. Gearbox losses are divided into friction (seals and gear-to-gear) and churning of the gears in the oil. Tests conducted by Rockwell on an R-140 axle and on a gearbox for the Standard Light Rail Vehicle and by Hurth on a Canadian Light Rail Vehicle gearbox showed that losses are a function of speed and torque as follows:

Friction power loss, $F_{loss} = f_1 (N \times T)$

Churning power loss, $C_{loss} = f_2 (N^2)$

where N is an input or an output rotational speed and T is the corresponding torque.

For the passenger vehicle motor, at speeds above base speed,

$$T = f_3 \left[\left(\frac{I_{DC}}{I_{DC\ MAX}} \right) \times \left(\frac{N_{BASE}}{N} \right) \right]$$

For speeds below base speed, $\dfrac{N_{BASE}}{N} = 1.0$

Base speed, N_{BASE}, is defined as:

(1) For a conventional separately excited, wound field motor, base speed is the full-load operating speed of the machine where the armature and field are subjected to their respective full-rated voltages. Speeds above base speed are achieved by field weakening.

(2) For a permanent magnet machine, base speed is the full-load operating speed where full-rated voltage is applied to the stator winding. Speeds above base speed are achieved by changing the firing angle in the inverter.

Note that $N = k_1 \times S_V$, where S_V is vehicle speed.

Substituting in the loss equations:

$$F_{loss} = k_2 \times S_V \times \frac{I_{DC}}{I_{DC\ MAX}} \times \frac{S_{V\ BASE}}{S_V}$$

$$C_{loss} = k_3 \times S_V^2$$

The test data also showed that at rated load

$$\frac{F_{loss}}{C_{loss}} \approx \frac{1}{2.1}$$

54

Rated load for the electric vehicle application is based on a 1361 kg (3000 lb) vehicle traveling at 56.3 km/hr (35 mph) on a 10 percent grade.

Constants k_2 and k_3 above were selected to correspond with the probable 92 percent overall efficiency, the F_{loss}: C_{loss} ratio established by the test data, and the electric vehicle rated load. The resulting equations are:

$$\text{Gearbox friction loss, kw} = k_2 \times S_V \times \frac{I_{DC}}{I_{DC\ MAX}} \times \frac{S_{V\ BASE}}{S_V}$$

where $k_2 = 0.0155$ kW per km/hr or 0.025 kW per mph

Note: (1) For vehicle speeds above base speed, use formula as shown.

   (2) For vehicle speeds at or below base speed, use:

$$\frac{S_{V\ BASE}}{S} = 1.0$$

Gearbox windage loss, kw $= k_3 \times (\text{mph})^2$

where $k_3 = 4.63 \times 10^{-4}$ kW per $(\text{km/hr})^2$ or 1.2×10^{-3} kW per $(\text{mph})^2$

A sample calculation for the electric vehicle rated load condition is presented below.

Vehicle speed = 56.3 km/hr (35 mph) on a 10 percent grade

$S_{V\ BASE} = 17.1$ km/hr (27.5 mph)*

$I_{DC} = I_{DC\ MAX}$

Vehicle frontal area = 0.186 m^2 (20 ft^2)*

Aerodynamic drag coefficient = 0.3*

Rolling resistance coefficient = 0.008*

Gearbox friction loss $= 0.025 \times 35 \times 1.0 \times \dfrac{27.5}{35} = 0.69$ kW

Gearbox windage loss $= 1.2 \times 10^{-3} \times (35)^2 = 1.47$ kW

---

*Assumed from other vehicle programs.

Aerodynamic load =   83.2 Newtons   (18.7 lb)

Rolling load   =   106.8   (24.0)

Grade load   = 1334.4   (300.0)

Road load   = 1524.4 Newtons (342.7 lb)

Road power (i.e., gearbox output) = $\dfrac{342.7}{550}$ × 51.33 × 0.746 = 23.86 kW

Total required gearbox input = 23.86 + 1.47 + 0.69

                             = 26.02 kW

Gearbox overall efficiency = $\dfrac{23.86}{26.02}$ = 0.92

APPENDIX B

COMPARISON OF CONSTANT TORQUE
VS. CONSTANT POWER ACCELERATION
FOR THE DRIVING CYCLE

Figure 32 shows the driving cycle (SAE J227A(D)) performance of the baseline machine. This machine is operated at a current density of 2.112 × 10^7 A/m^2 (13,624 A/in^2) and has a commutation reactance of 0.322 percent, a rated voltage of 55.85V$_{L-N}$, and a rated current of 190.2 A ac (247 A dc).

Figure 33 shows the driving cycle performance for a machine designed to provide approximately constant power acceleration commencing at the time that motor speed is 0.5 per unit. This results in a 23.6 percent increase in motor weight. This machine is designed to have the same current density at 1 per unit current and the same per-unit reactance as the baseline machine. Consequently, a new lamination configuration was required. In this design, core density at rated load was made the same as that for the baseline. It was necessary to increase the rated current to 258.4 A ac (335 A dc) and slightly reduce rated voltage, which is constrained by the battery voltage-current characteristic. This resulted in a dc current in the chopper that exceeds the device capabilities of the baseline system, 300 A dc maximum. Therefore, two additional transistors would be required in the chopper to accommodate this machine.

The energy consumed by the constant power system over the cycle is somewhat less than that for the baseline machine, primarily because of the greater power rating of the machine, which during regeneration allows more recovery of mass energy so that less braking torque is needed to complete the cycle within 98 s. It will be noted that at completion of the acceleration to 28 km/hr (45 mph), the energy consumption is slightly higher for the constant power system. At the end of the 28-km/hr (45 mph) cruise and the coast period, the energy consumed is equal for both the baseline and constant power systems.

Figure 34 shows the performance for a constant torque acceleration using a machine the same as the baseline machine as far as rated current, voltage, and reactance are concerned, but with the lamination constraint removed so that the current density in the stator windings could be reduced to a point--1.046 × 107 A/m^2 (6750 A/in^2)--where a machine weight is obtained equal to the machine weight incurred for the constant power cycle. In this case, the device ratings in the chopper are not exceeded, current being the same as that in the baseline system, 247 A dc.

At the end of the regeneration cycle, energy consumed is slightly higher than in the constant-power case of figure 33; this is again entirely attributable to better energy recovery during regeneration. However, energy recovery could be improved for this cycle (without exceeding the 300-A chopper limit) by operating at 1.21 per unit current during regeneration. In such a case, the system depicted in figure 33 would have better performance,

Figure 32.--Vehicle and motor performance vs time, baseline machine.
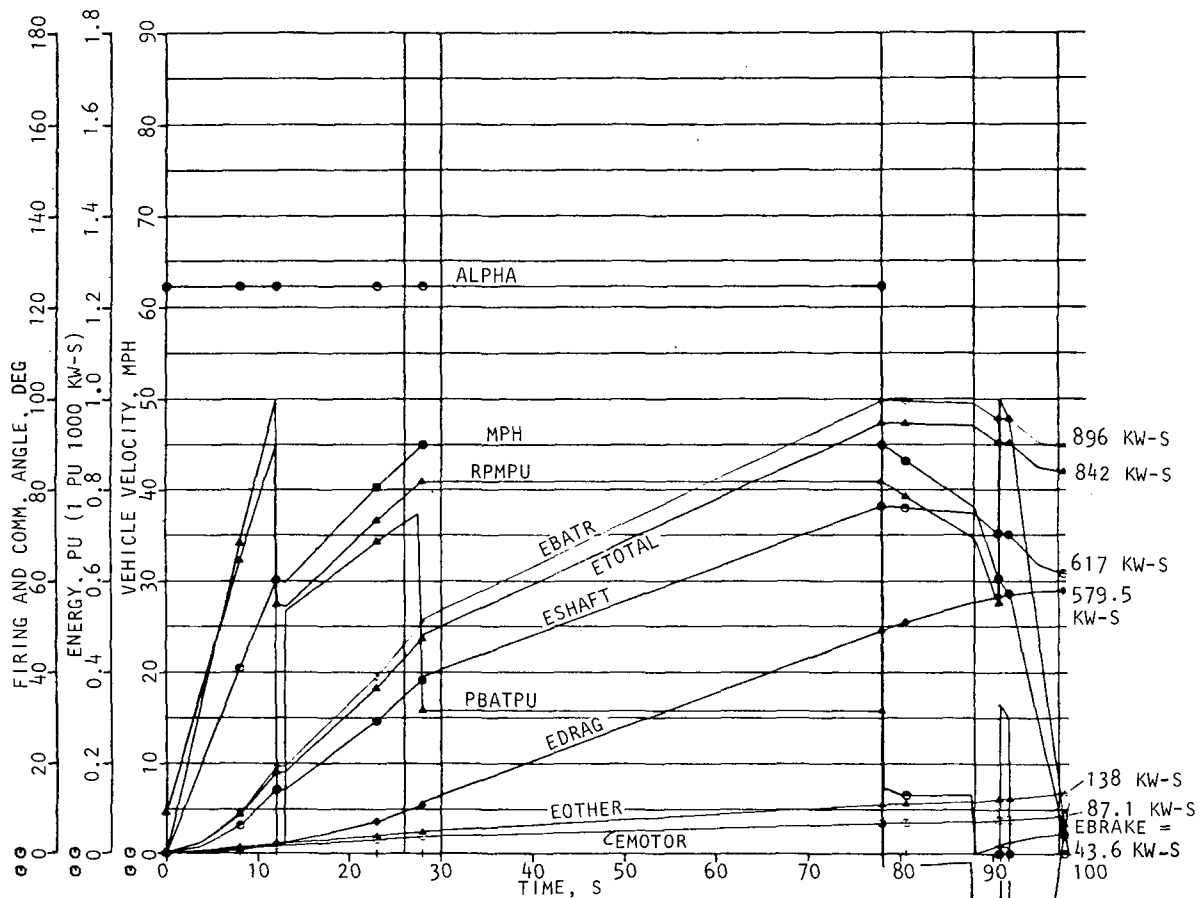
BASELINE DESIGN, CONSTANT TORQUE, 13,634 A/IN^2
28.8 LB, 100 FT-LB BRAKING TORQUE
PBATPU = POWER AT BATTERY TERMINALS, PU, BASE = 30 KW
EBATR = TOTAL SYSTEM ENERGY INCLUDING LOSS INSIDE BATTERY, PU
          BASE = 1000 KW-S
          BASE AMPERES = 190.2 (246.7 A DC)
          BASE VOLTS = 55.85 V$_{L-N}$ (104.5 V DC)
          BASE SPEED = 26,000 RPM
NOTE: BASE VALUES, ETC., SAME FOR FIGURES 33 AND 34 UNLESS NOTED.

A-30689

58
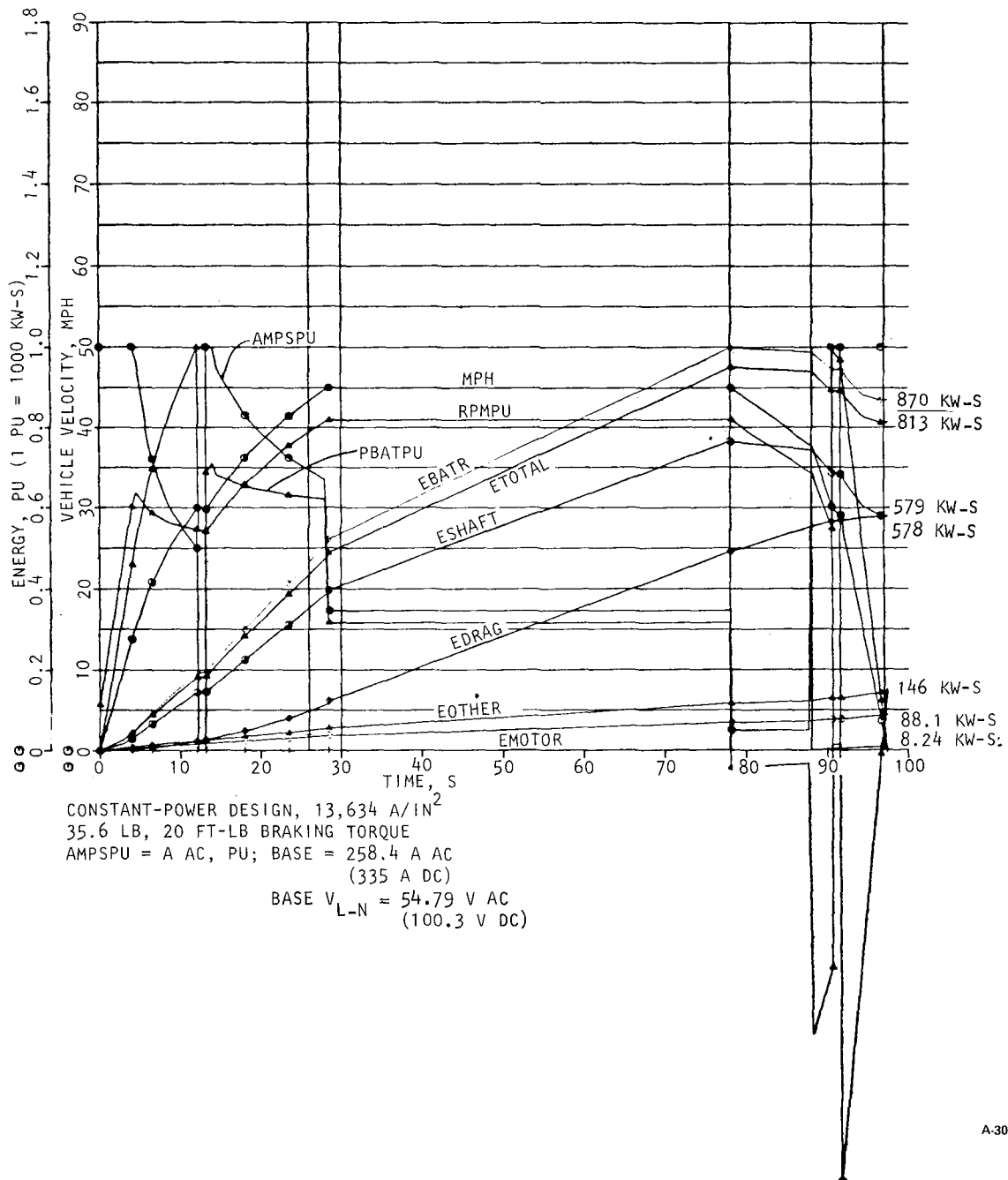
Figure 33.--Vehicle and motor performance vs time, constant-power design.

Figure 34.--Vehicle and motor performance vs time,
constant torque design.

and the energy consumed at any previous time during the cycle as well as the heat energy to be dissipated from the motor is always less than for the other systems.

A constant-torque acceleration is preferable for a motor of a given size and weight as far as the chopper, converter, and motor are concerned. With respect to battery life or performance, no basis is available for preferring either constant-torque or constant-power acceleration. The power flow at the battery terminals is obviously more nearly constant during acceleration in the system depicted in figure 33, but during regeneration, the figure 33 power spikes are larger than in the cases of figures 32 and 34.

Driving Cycle Performance Legend

ALPHA	Converter ignition angle, deg
EBRAKE	Mechanical braking energy, PU
EDRAG	Gearbox, rolling resistance, and aerodynamic drag energy, PU
EMOTOR	Energy loss in motor, PU
EOTHER	Energy loss in controls, fan, chopper, and converter, PU
EPERMI	Energy consumption per mile, PU
ESHAFT	Energy at motor shaft, PU
ETOTAL	Electrical energy at motor/power converter terminals, PU
MPH	Vehicle speed, mph
RPMPU	Motor speed, PU
U	Commutation overlap angle, deg

Base values:

   Energies: 1 PU = 1000 kW-s

   EPERMI: 1 PU = 1000 kW-s/mile

   RPMPU: 1 PU = 26,000 rev/min

   Gear shift time: 1 s

APPENDIX C

SIX-PULSE CONTROLLED RECTIFIER-INVERTER OPERATION

Basic Circuit Description

Efficient operation of the permanent magnet (PM) machine as both a motor and a generator is achieved by the circuit that can be designated as a six-pulse, double-way controlled rectifier-inverter, often called a three-phase bridge rectifier (ref. 1). This circuit, shown in figure 35a, provides conduction in both directions in each phase winding of the motor. Whether the circuit operates as a rectifier or inverter is determined by the firing angle, α (angle of retard), as illustrated in figure 35b. As shown in this figure, maximum output occurs at $\alpha = 0°$ for rectifier operation and $\alpha = 180°$ for inverter operation.

Circuit operation in both the controlled rectifier and inverter modes is affected by the PM machine inductance. This reactance acts to form notches in the otherwise ideal sinusoidal waveforms. For example, figures 36a and 36b show typical line-to-neutral and inverter SCR voltage, waveforms for an inverter firing angle of 120°. The waveforms are idealized since they neglect switching transients and assume perfect SCR's as well as ripple-free dc current. However, they do include the effect of the PM motor inductance, which acts to delay the transfer of current from one conducting SCR element to the next. This results in a time period defined as the overlap angle, μ, during which the SCR being turned off and the SCR being turned on are both conducting.

For reliable inverter operation, an additional time period must be provided to allow sufficient time for the SCR to regain its blocking state, that is, to turn off. This time is defined as margin angle, γ, as illustrated in figure 36a.

Counter-emf Commutation

For inverter-PM motor interface, special attention must be paid to the transfer or commutation of current between the motor windings. For line-commutated inverters, this process must be started early enough in the particular cycle to ensure that sufficient turnoff time is available for the SCR.

Figure 37 illustrates the conditions for current transfer from the C+ to the A+ phase of the PM motor. The constant current (I_D) is initially being conducted through SCR C+ to SCR B-. Firing of SCR A+ causes a circulating current, i_A, which acts to reduce the current through SCR C+ to zero in sufficient time to allow the PM motor counter-emf of e_c and e_a to reverse bias SCR C+, thus providing its necessary turnoff time, that is, $e_c > e_a$. The cycle then continues with SCR A+ conducting the load current I_D.
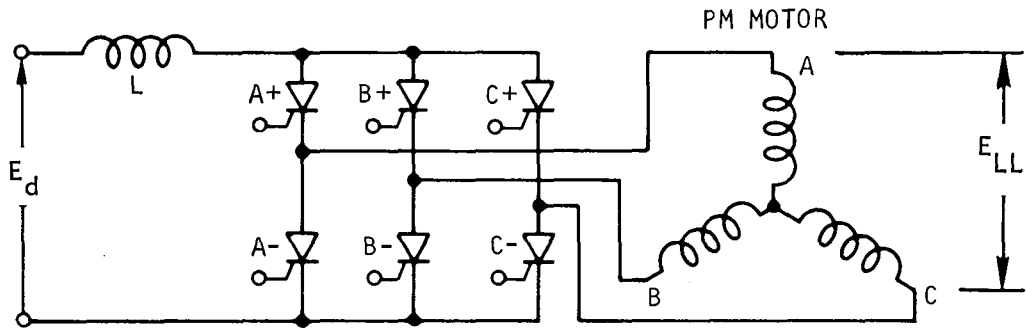
a. Six-pulse controlled rectifier and line-commutated inverter.
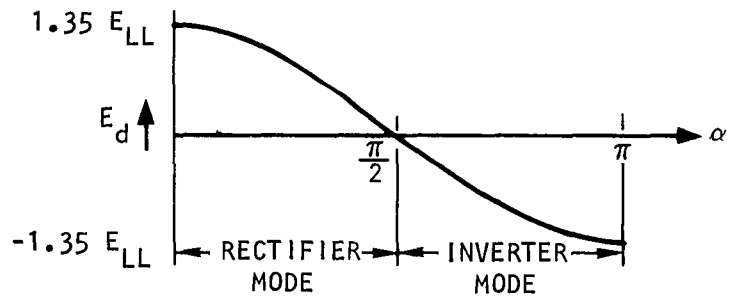
b. Average dc voltage, E_d vs. firing angle, α.

A-32566

Figure 35.--Six-pulse controlled rectifier-inverter.
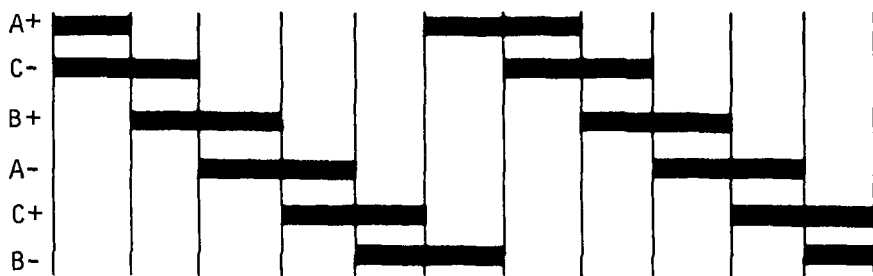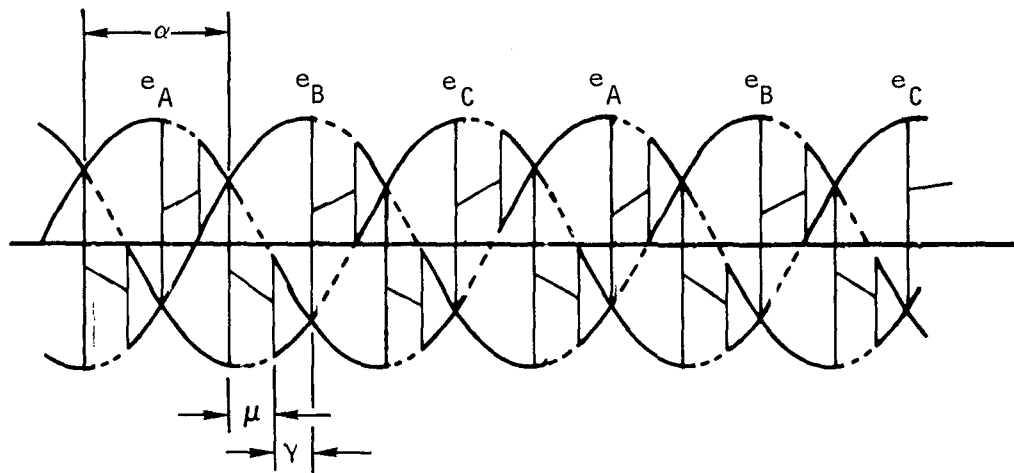
a. Idealized phase voltages and SCR firing sequence for angle of retard, α ; overlap, μ ; and margin, Y ; shown for SCR A+.
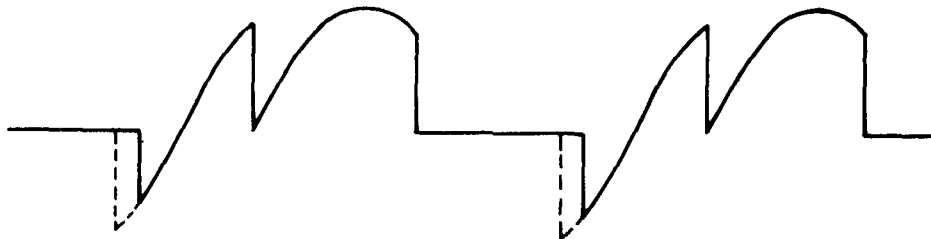
b. Voltage across SCR C—.

A-32174

Figure 36.--Six-pulse, line-commutated inverter with
α = 120°, μ = 30°.
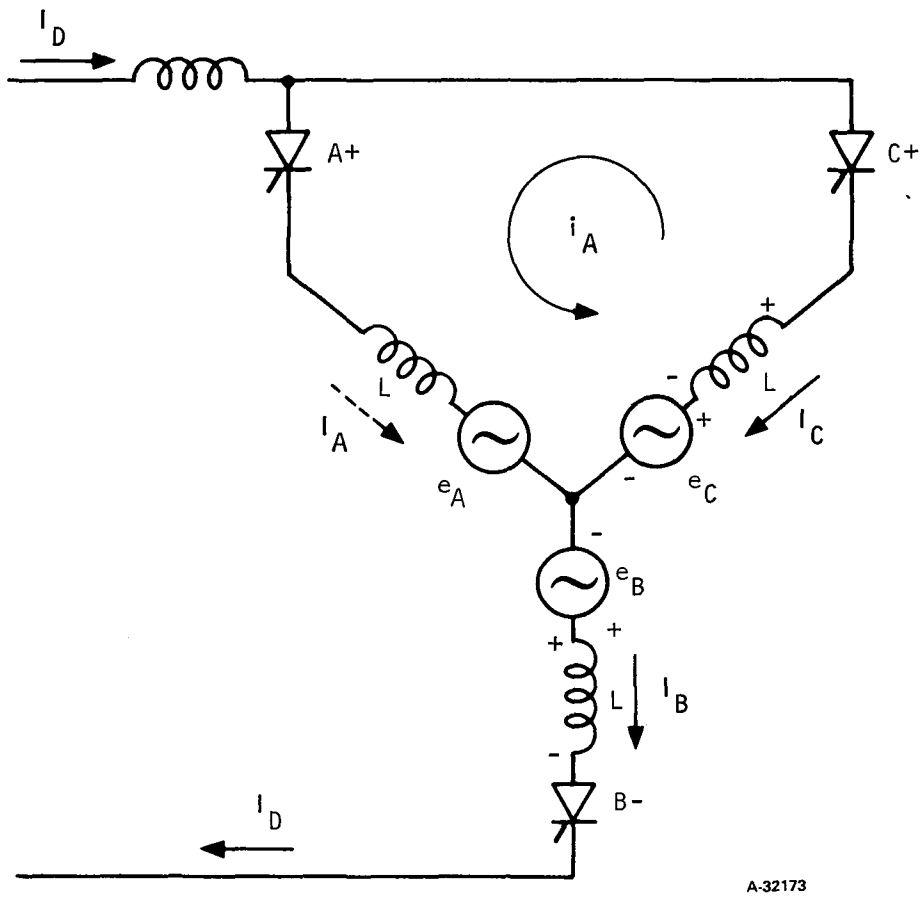
Figure 37.--Commutation circuit for SCR C+.

Figure 38 illustrates the circuit waveforms with phases C and B conducting until $\omega t = \alpha$, at which point SCR A+ will be turned on in order to transfer conduction to phases A and B. When A+ is fired, and until commutation is complete at $\omega t = \alpha + \mu$, a short-circuit current, shown as i_A on figure 37, circulates between phases A and C because of the difference between the phase voltages. At the instant of firing, the current in SCR A+ is zero and begins to increase, while the current in SCR C+ begins to decay as shown in figure 38. i_A is the current through SCR A+, and $i_C = I_D - i_A$ is the current through SCR C+. The equations for the currents are given by

$$i_A = \frac{1}{L} \int_{t = \frac{\alpha}{\omega}}^{t = \frac{\alpha + \mu}{\omega}} (e_c - e_a) dt \qquad (C1)$$

$$i_C = I_D - i_A = I_D - \frac{1}{L} \int_{t = \frac{\alpha}{\omega}}^{t = \frac{\alpha + \mu}{\omega}} (e_c - e_a) dt \qquad (C2)$$

$$i_A = 0; \quad i_C = I_D \qquad\qquad t < \frac{\alpha}{\omega}$$

$$i_C = 0; \quad i_A = I_D \qquad\qquad t > \frac{\alpha + \mu}{\omega} \qquad (C3)$$

It is also apparent from the above equations and figure 38 that the maximum current that can be transferred corresponds to the time integral of the voltage that is available for the transfer, measured from the instant of firing to the instant of voltage reversal. The firing angle (α) and the overlap angle (μ) are determined by satisfying equations C1 and C2 with a satisfactory margin of safety, γ. These two angles are functionally interrelated and are, in addition, a function of the dc source voltage, the motor phase voltages, the maximum current level, and the machine inductances. The following equations have been obtained (ref. 2)

$$\cos \mu = 1 - X_L \text{ (PU)} \qquad (C4)$$

$$X_{L,PU} = \omega L \frac{I_d}{\sqrt{6} E_a} \qquad (C5)$$

$$\frac{E_d}{E_{do}} = \frac{\cos \alpha + \cos(\alpha + \mu)}{2} \qquad (C6)$$
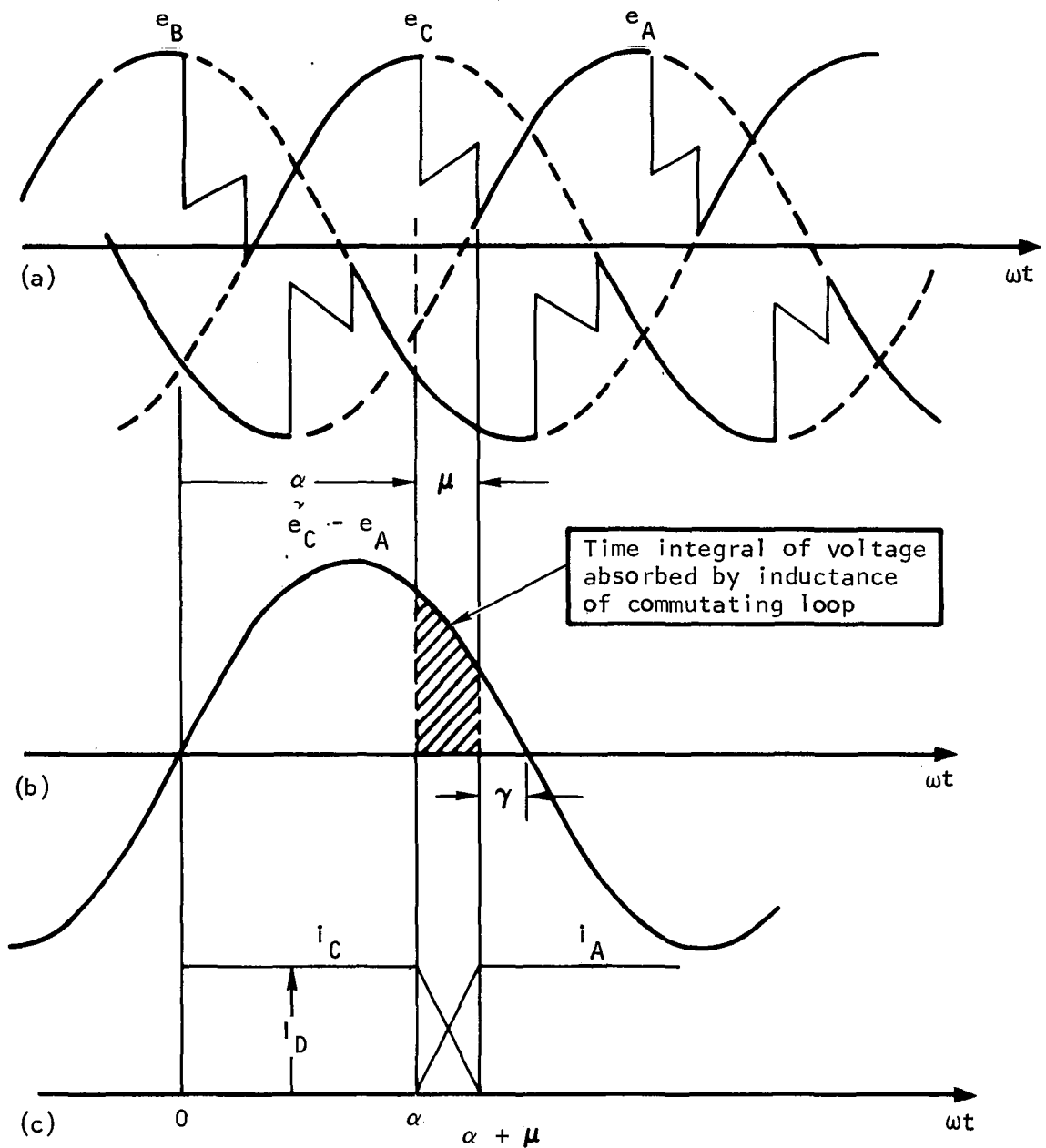
Figure 38.—Commutation of counter-emf controlled inverter.

$$E_{do} = \frac{3\sqrt{6}}{\pi}E_a \qquad\qquad\qquad (C7)$$

$$PF = 0.954 \; \frac{E_d}{E_{do}} \qquad\qquad\qquad (C8)$$

where μ = commutation angle

     $X_{L,PU}$ = PM motor per-unit impedance

     L = PM motor line commutation inductance

     I_d = Average value of direct current from the dc source

     E_a = Rms line-to-neutral PM motor voltage

     E_d = Average value of the dc source voltage

     E_{do} = Average value of the dc source voltage excluding phase delay or commutation voltage reductions

     α = Phase control or angle of retard

     PF = PM motor total power factor

It becomes obvious that the application of these equations requires iterative calculations to establish final parameters acceptable to both inverter and PM motor design constraints. Typically the problem is the determination of the dc voltage (E_d) for a given PM machine voltage (E_a) and per-unit commutation impedance ($X_{L,PU}$) and a given turnoff time for the SCR.

Figure 39 shows the interrelationship of the various parameters and serves as an aid in evaluating their effect on inverter-PM motor interface. For example, operation at α = 120° with a $X_{L,PU}$ × PF value of 0.2 provides a margin angle of 35°. If the PM machine reactance is increased, the margin angle decreases to zero at $X_{L,PU}$ × P.F = 0.37. The minimum margin angle limit is given by the following equation.

$$\alpha = 360(tq)(f)$$

where   tq = SCR turnoff time, μsec.

     f = PM motor frequency, Hz

Thus, for the above example, the maximum PM motor frequency for an inverter SCR with a 60 μsec turnoff time would be 1851 Hz.
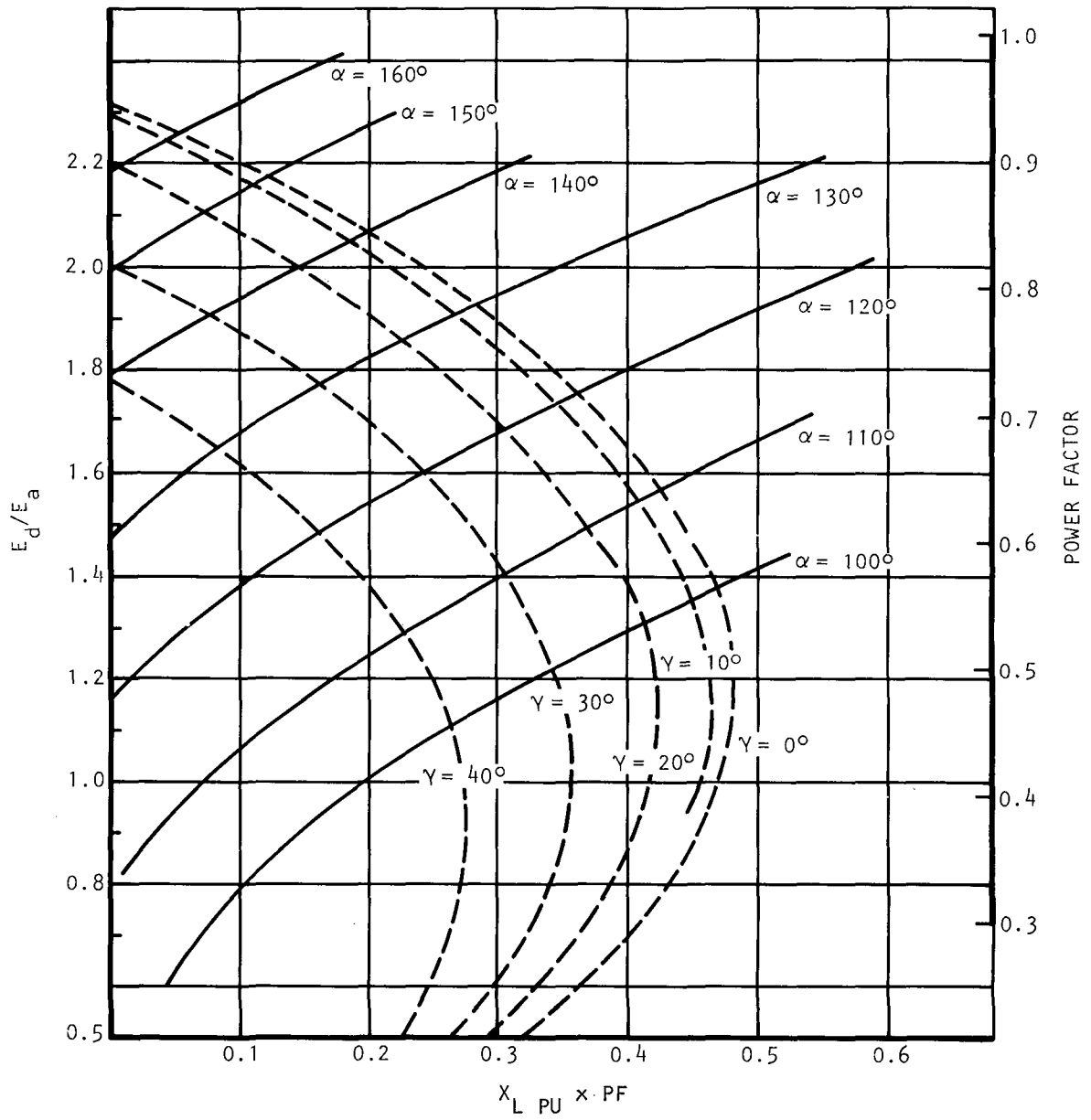
Figure 39.--Commutation parameters for ideal six-pulse inverter.

A-30590

APPENDIX D

THERMAL ANALYSIS OF ELECTRONICALLY COMMUTATED MOTOR

Motor Requirements

One of the basic requirements for the electronically commutated dc motor is that the power rating shall be that necessary to meet the following provisions:

(a) 2 hr at constant vehicle speed of 89 km/h (55 mph).

(b) 2 hr of repeated 120-s power cycles.

(c) 1 min at a vehicle speed of 48 km/h (30 mph) on a 10 percent grade immediately after operation under (a) and (b) above.

The provisions above were used as the baseline conditions for the thermal analysis and the losses for each are indicated in Table XI.

TABLE XI.—LOSSES IN WATTS FOR ELECTRONICALLY COMMUTATED DC MOTOR

Provision	Rpm	Copper	Tooth	Backiron	Rotor	Windage	Total
(a) 2 hr at 89 km/h	26,000	374	118	167	234	45	938
(b) 2 hr of repeating 120-s power cycles	See figure 39 for losses						
(c) 1 min at 48 km/h on a 10 percent grade	26,000	1039	106	151	276	45	1617

NOTE: Copper losses are given at 193°C (380°F)

Analysis

A steady-state and transient thermal analysis was performed on the
Phase I design with the provisions above. A totally enclosed air-over
motor design with a separately driven fan was assumed. Cooling air through
the stator gap and through the rotor slots was found necessary to comply
with motor temperature limits. The thermal model of rotor and stator and
a schematic flow diagram appear in figures 40 and 41, respectively. The
motor is enclosed with cooling air flow over the finned motor housing, as
shown in figure 41.

The first of each set of numbers in figure 40 represents the air inlet
half of the motor, while the numbers in parentheses represent the air
outlet half. The permanent magnet (nodes 1 and 38) are contained by a
sleeve (nodes 4 and 41). The stator stack winding nodes are represented
by nodes 6-7 and nodes 21-22, while the end turn windings are nodes 8-9
and 23-24. The end section winding nodes are 10-25.

The motor nodal model is prepared by means of the AiResearch Stator,
Armature, and LIM Thermal Model Generation Computer Program H0061. The
program connects each of the motor nodes by a conduction and convection
resistance array such that the motor thermal model may be combined with
the rest of the system to complete the model to be analyzed by the
AiResearch Thermal Analyzer Computer Program H0298. This program performs
conduction, convection, and radiation calculations and other heat transfer
mechanisms.

The motor losses for the 2-hr 89-km/h (55-mph) case and for the 1-
min 48-km/h (30-mph) case are shown in table XI. Figure 39 shows a
plot of the motor rpm and losses vs a function of time for the repeating
120-s cycle for 2 hr. All copper losses in the table are based on 193°C
(380°F) temperature. The actual losses used in the analysis, however,
vary as a function of temperature depending on the resistance character-
istics of copper.

In accordance with the 89-km/h (55-mph) motor requirement above, a
steady-state thermal analysis on the 2-hr 89-km/hr (55-mph) case was
performed. The design point parameters, i.e., the air flow rate, rotor-slot
sizing, etc., were determined such that the motor stays well within material
temperature limits. A transient thermal analysis on the 2-hr repeated cycle
case was also performed using determined design conditions from the 2-hr
89-km/h (55-mph) run. To save considerable computer time, the repeated
cycle was forced to reach steady-state condition within a cycle. The
time-averaged motor losses over a period of one cycle were calculated
from figure 39, the steady-state temperature profile of which was used
as an initial condition for the transient analysis. It was determined
from this procedure that the rate of temperature change after a 3-cycle
analysis was small, and therefore the steady-state condition was assumed to
be reached. To comply with the motor requirement, the worst temperature-
profile result of both the 2 hr 89-km/hr (55-mph) and repeated-cycle cases
was then used as an initial condition for the provision of 1-min 48-km/h
(30-mph) on a 10 percent grade.
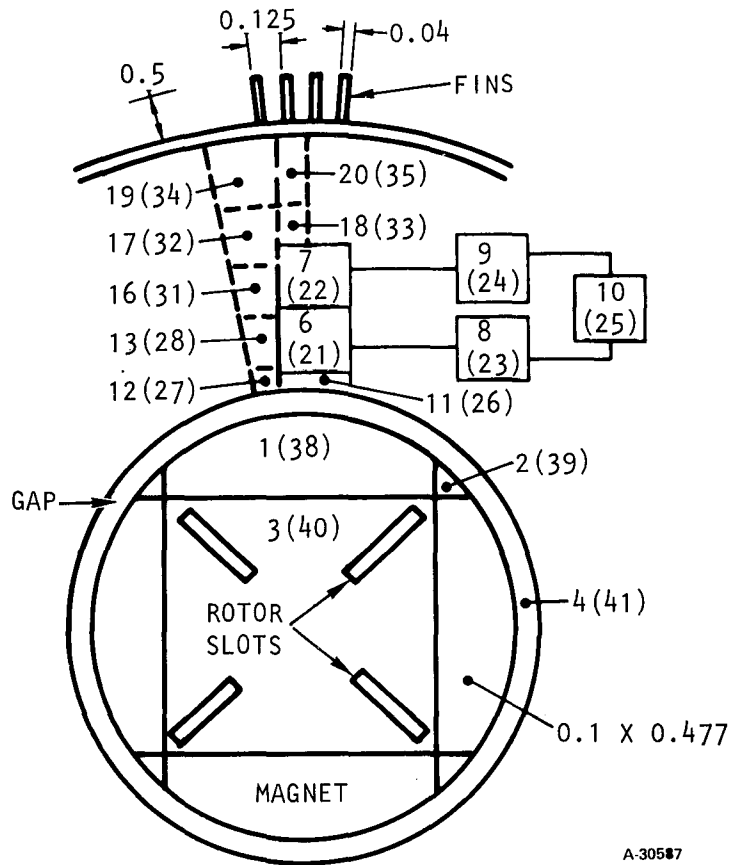
Figure 40.--Thermal nodal model of electronically commutated
dc motor for electric passenger vehicles.
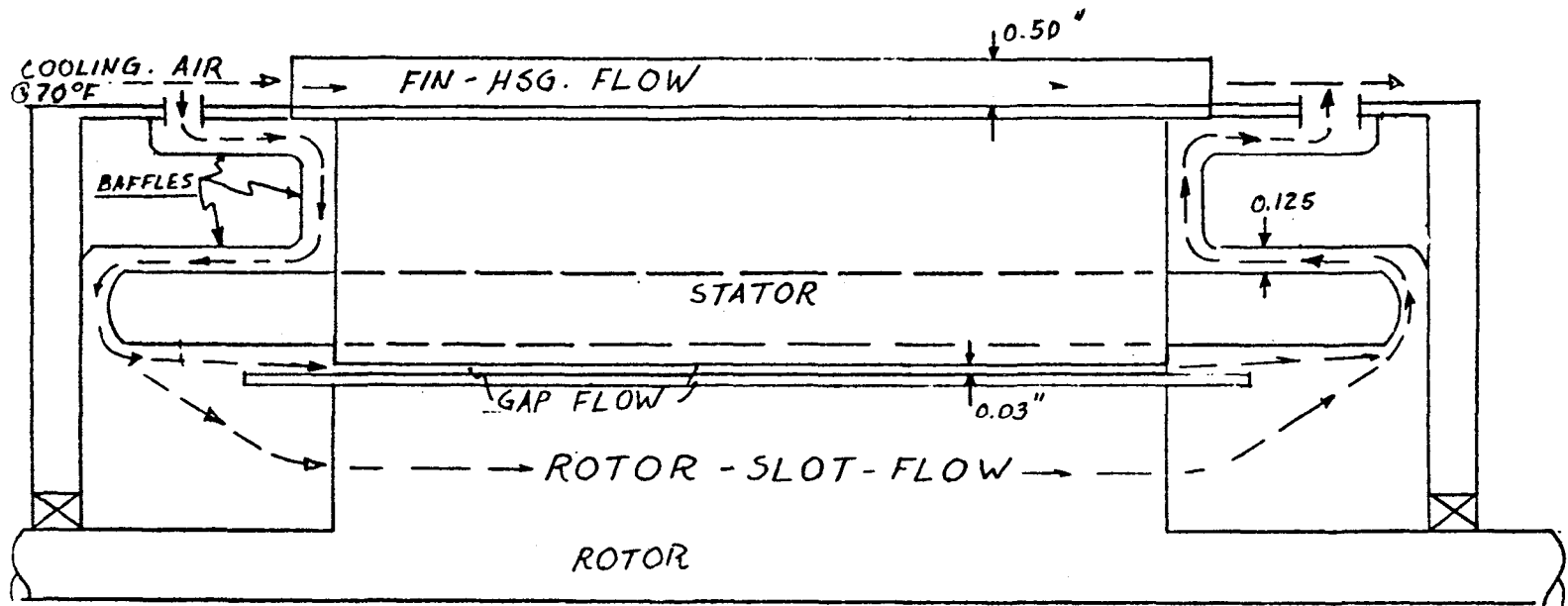
Figure 41.--Schematic cooling flow diagram of electronically commutated dc motor.

PAGE
75 &76
MISSING
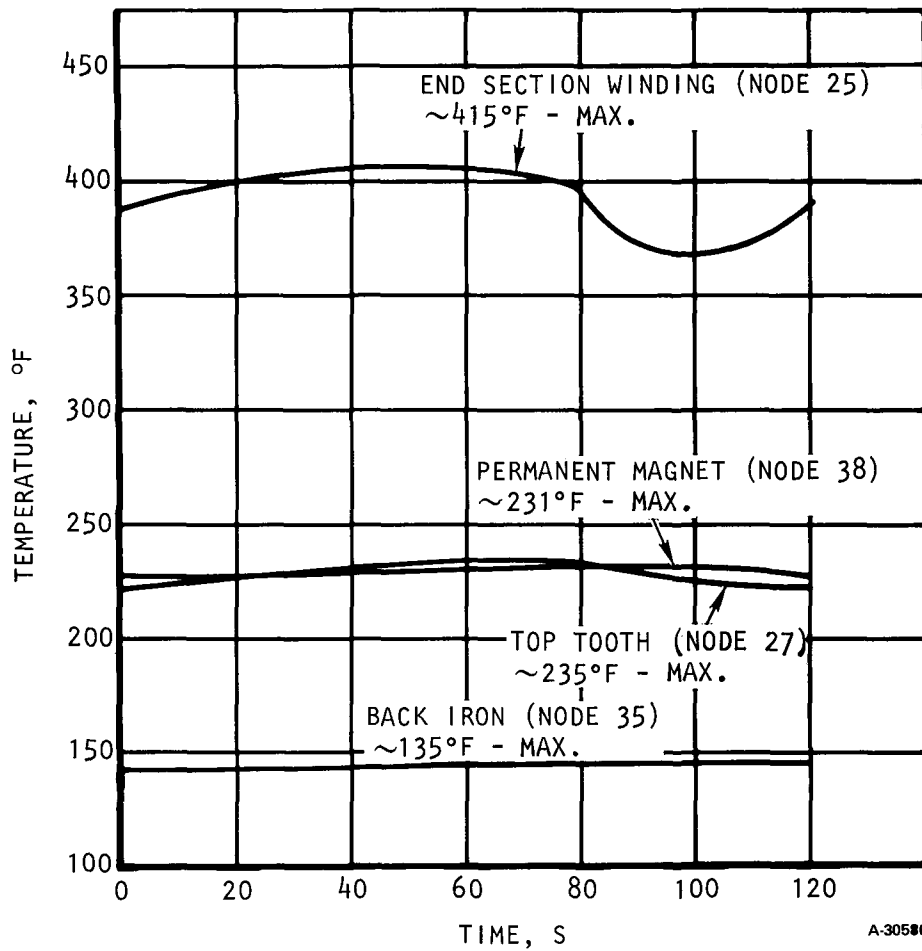
Figure 42.--Temperature-time profile of the
steady-state 120-s cycle.
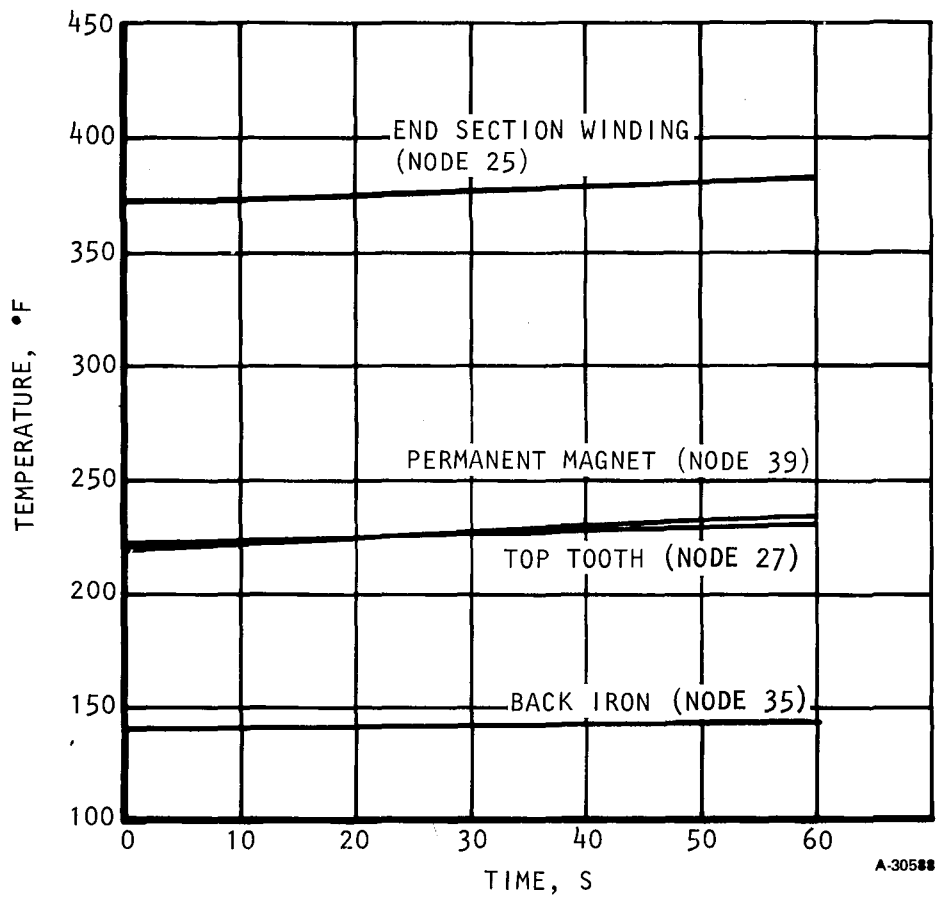
Figure 43.--Temperature-time profile of the 1-min, 30-mph run on a 10 percent grade.

Conclusion

With a fin-housing configuration of 3.06 mm (0.125 in.) spacing, a 12.3-mm (0.5-in.) fin height, and a 1.02-mm (0.04-in.) fin thickness, together with air cooling flow through the stator-rotor gap and through the design rotor slots, the electronically commutated dc motor complies with the maximum allowable temperature limits of the duty and motor requirements described above. With a total pressure drop of 45 Pa (2 in. H_2O), a 21°C (70°F) ambient condition, a 282-kg/hr (620-lb/hr) fin, a 4.54-kg/hr (10-lb/hr) gap, and a 9.09-kg/hr (20-lb/hr) rotor slot-air flow, corresponding to 4248 l/m (150 cfm), is the design point result of the analysis. A Rotron centrifugal blower, Type AS-508 simplex, is sufficient for the cooling requirements. The required power-input at an air volumetric rate of 4248 l/m (150 cfm) is about 120 W.

SPEED REDUCTION OF THE HIGH-SPEED MOTOR

Introduction

The high-speed motors being developed for vehicle applications may require a speed reducer in order to mate with available transmissions. The reduction required is approximately five to one. Two approaches have been evaluated: a gear reducer and a fixed-ratio traction drive.

Gear Reducer

The lightest and most efficient approach is a single-stage gear reduction. Helical reduction gearing is proposed to reduce audible noise, since noise represents the significant undesirable result of the gear reducer approach. Figure 44 shows a proposed single-stage helical gearhead mounted on a 40-hp (29.8-kW) (peak), 26,000-rpm, rare-earth-coablt permanent-magnet motor. The pinion is mounted directly on the end of the motor shaft. The output gear and spline are straddle-mounted on two ball bearings. The output gear and bearings are splash-lubricated. The estimated efficiency and weight are:

Efficiency >98 percent

Weight   <1.8 kg (4 lb)

Fixed-Ratio Traction Drive

The traction fixed-ratio drive (FRD) is a newly developed unit that can transmit fractional to very large horsepower at shaft speeds from zero to more than 150,000 rpm with ratios from 2:1 to about 25:1 in a single stage in either speedup or reduction. All power elements operate in pure rolling contact and run as quietly as high-quality roller bearings.

The unit is basically a modified planetary design with planets fixed to the housing. Input and output shafts are classified as coaxial; however, there is an offset between the two shafts.

Mechanical performance characteristics are symmetrical for either clockwise or counterclockwise rotation of the input shaft, and shaft rotation is nonself-locking.

The FRD houses a sun shaft, a ring, and the fixed planet rollers that transfer power between the ring and sun in either direction. The planet roller set consists of three rollers arranged in a triangle. One roller, the reaction roller, is larger than the other two. The two smaller rollers are loaded toward each other with preload springs. They are restrained from moving away from each other but may move toward each other. This planet arrangement positions the sun out of center from the ring in the direction of the two small rollers.

12.75

8.88

7.81
DIA

3.0
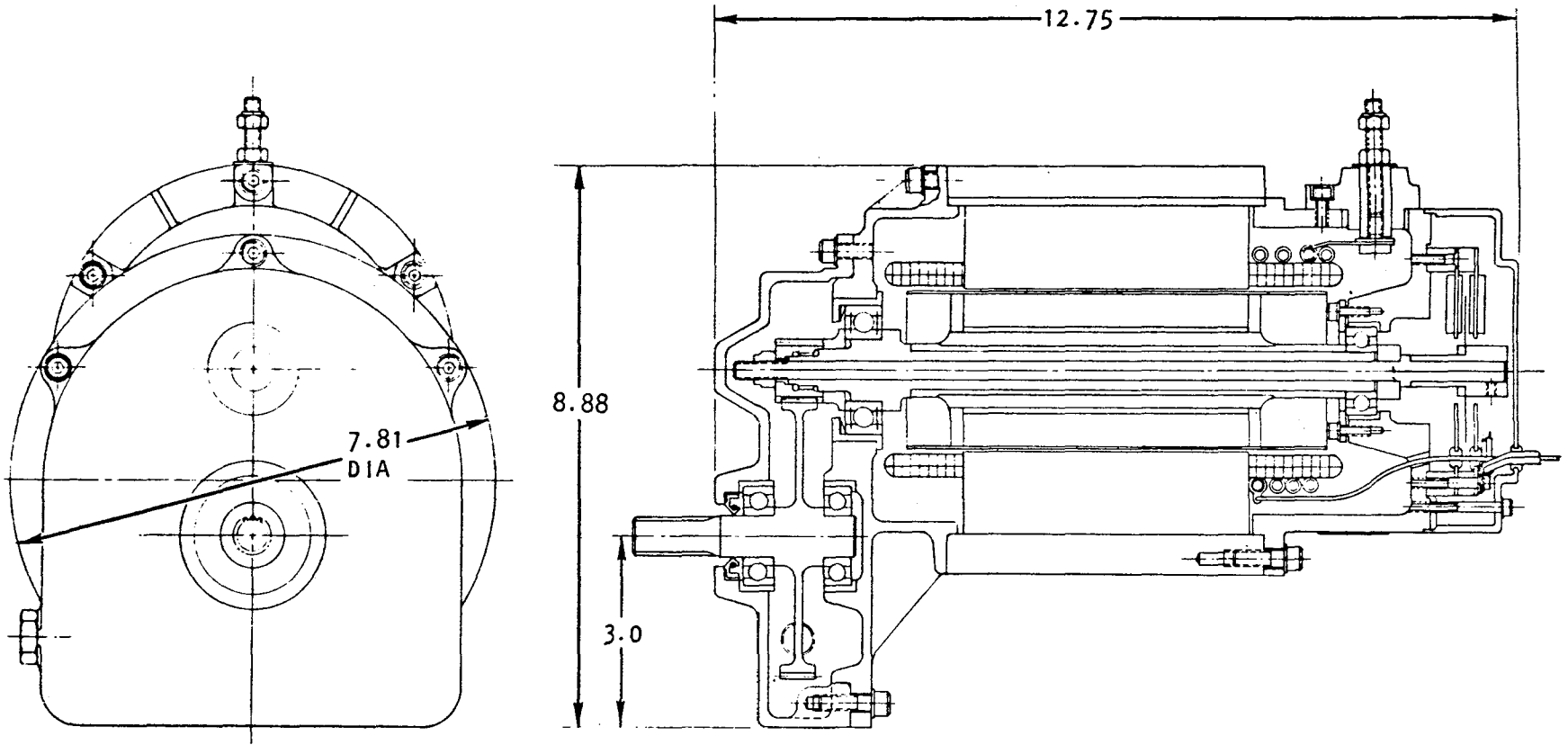
A-8025

Figure 44.--Proposed single-stage helical gearhead.

Loading of the traction contacts in response to torque load is accomplished as the sun tries to wedge one of the small rollers into the decreasing space between itself and the ring. The other small roller and the reaction roller are held from moving. The greater the torque, the greater the wedging effort on the small roller, and consequently, the greater the normal force on the traction contacts.

The amount of actual movement of the wedging roller is controlled by the resistance of the ring to three-point hoop deflection. This is generally kept very small.

The amount of offset between the sun and ring shafts is determined by the coefficient of traction available in the drive. This coefficient depends on the lubricant, rolling speed, and other factors that affect the elastohydrodynamic film within the traction contact.

The three-point wedging action of the planet rollers makes an excellent radial load bearing for both the sun shaft and ring. All reaction torques are contained in the design.

In this application, an 11.4-cm (4.5-in.) ID ring was chosen to fit conveniently into the 16.3-cm (6.4-in.) envelope of the motor (figure 45). The 2.235-cm (0.880-in.) diameter sun shaft provides a 5.20:1 reduction ratio (26,000 rpm to 5,000 rpm) with the proper allowance for traction creep loss. This preliminary design fits within the 16.3-cm (6.40-in.) meter motor envelope, and is 12.7 cm (5.0 in.) long.

Predicted reduction drive design life in B10 hours is 20,773 hr at 11 kW (15 hp)/20,000 rpm, and 1,385 hr at maximum power of 29.8 kW (40 hp)/26,000 rpm. These life figures include both traction and bearing fatigue life analysis.

These life figures may be excessive, but for this preliminary design analysis, they show that an acceptable sized traction reduction drive will have adequate life. During a detailed design, the drive size could be reduced to cut size and weight until a minimum acceptable B10 design life is reached.

The estimated efficiency and weight of the design shown is:

Efficiency >96 percent

Weight   <12 lb (5.45 kg)

The significant advantage of the approach is the elimination of audible noise as a concern.

Conclusion

A single-stage helical 5:1 reduction gearhead provides the most efficient and lightest weight method of obtaining the desired output shaft speed, and is the recommended initial solution.
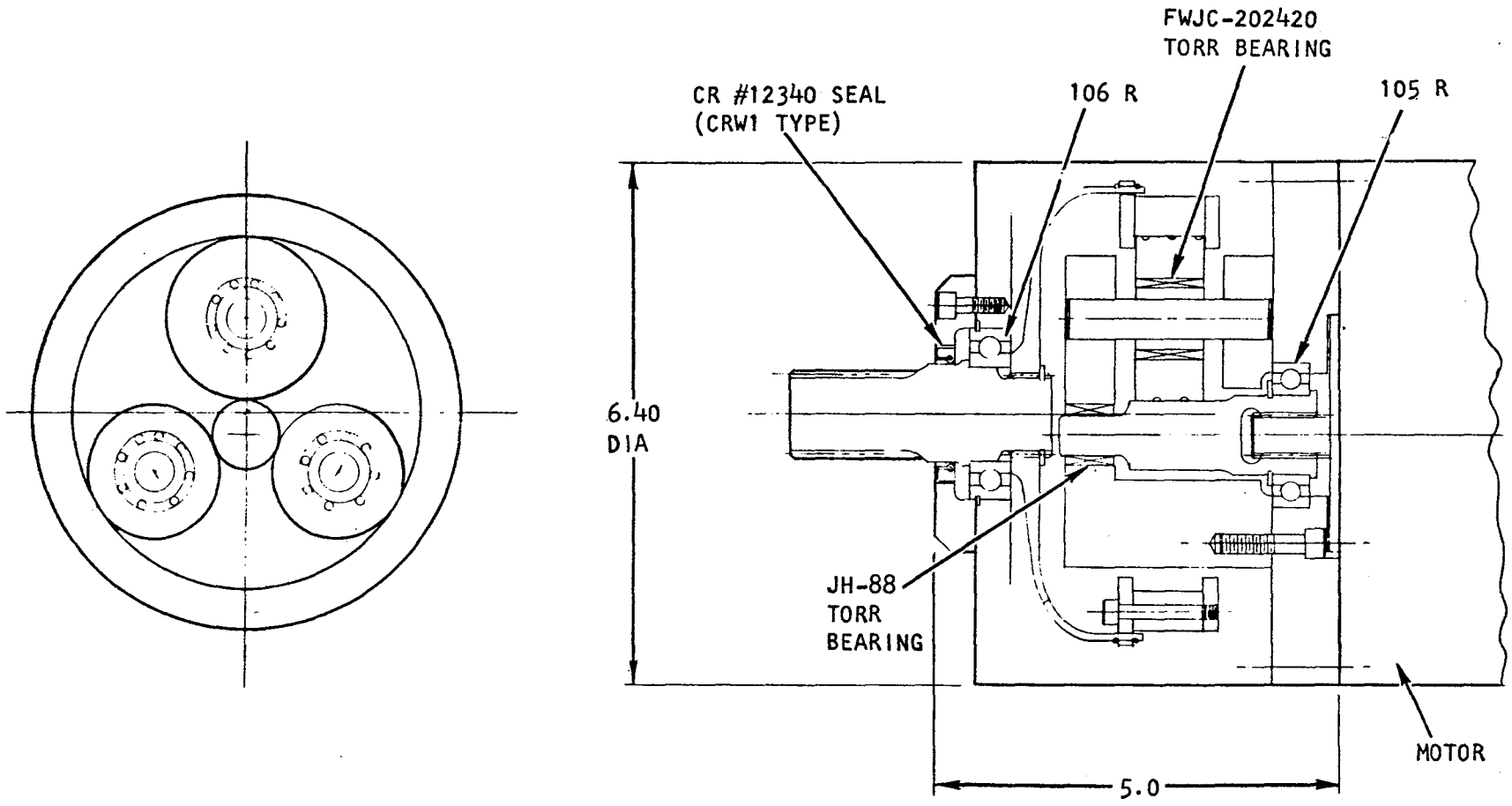
Figure 45.--Preliminary speed reducer design.

If noise levels using the helical gear approach prove to be excessive, a longer range program to develop a very low noise level traction drive could be considered. A significant additional noise reduction could be achieved at the expense of weight and efficiency.

APPENDIX F

IMPROVED PERMANENT MAGNET MACHINE USING LOW-COST, NONCRITICAL CERAMIC MAGNETS

Introduction

The motor developed under this contract employs high-cost magnets using critical materials. A study was made to determine the essential characteristics of the machine using noncritical, less costly magnet materials.

Magnet Material Comparison

Table XIII presents comparisons of three magnet materials that show Ceramic 8 (strontium ferrite) to be dramatically superior on the basis of dollars/joule. Since it provides less field energy per gram, operates at lower flux density, and is more adversely affected by temperature extremes than the other materials, savings resulting from the use of this material will be offset, to an extent, by the need to use more copper and iron in the motor and possibly by some constraints restricting application of abnormal loads at very low or very high temperatures to avoid demagnetization of the rotor magnets.

TABLE XIII.--COMPARISON OF MAGNET MATERIALS

	Ceramic 8 (strontium ferrite)	Cerium cobalt	Samarium cobalt
Cost, $/lb ($/kg)	2 (4.40)	68 (150)	140 to 150 (308 to 330)
Density, lb/cu in.	0.177	0.29	0.29
g/cm^3	4.9	8.03	8.03
Specific energy:			
Megagauss oersted	3.3	17.0	22.0
Joules/cm^3	0.0263	0.0168 max.	0.175
Joules/gram	0.00537	0.0168	0.0218
Cost $/joule	0.82	8.93	14.66

NOTE: Basic data were provided by Ceramic Magnetics, Inc., August 31, 1979. The cost ($/lb) is for large production orders and includes essential processing, but not special fabrication operations, which can vary considerably depending on size, shape, and tolerances. The cost for cerium cobalt was furnished by Shin-ETSU, May 1980.

Motor Design Comparisons

Comparisons of three motor designs are presented in table XIV. Motor 1 is an optimized version of the improved motor using a new lamination and rotor configuration, updated reactance computation, and 22 MGO magnets.

Motor 2 is a design using Shin-ETSU B85 (cerium cobalt). A precise description of the low-temperature B-H curve was not available, but the manufacturer recommended a design limit for B_D and Hd, which is believed to assure stability and which was observed in this design. It was not possible to meet the design limits with a 4-pole design, but a 6-pole design did meet the limits. The 6-pole design is feasible because for a given commutation reactance, the demagnetizing mmf per unit length of the pole magnet is much less than for a 4-pole design. A disadvantage of the 6-pole design is that the higher operating frequency will increase the losses in the inverter. To achieve inverter losses equivalent to the samarium cobalt machines, machine speed would have to be reduced to 17,333 rpm and size would increase about 40 percent.

Motor 3 is an optimized design using Ceramic 8 (strontium ferrite, 3.3 MGO). This design has been checked for short-circuit stability at 18°C (0°F); however, the analysis did not include examination of local regions within the magnet that may possibly be subjected to higher demagnetization intensity than the average perceived by the bulk of the magnet. Before building a machine, a computer flux plot should be undertaken to determine whether a design change to avoid regional demagnetization is required.

Conclusions

Although samarium cobalt magnets produce the lightest weight motor, machines of equivalent peak rating and efficiency can be made using alternate materials.

The lower cost of alternate rare earths, such as cerium cobalt, is approximately offset by the added quantity of magnet material required, and therefore no significant cost advantage is realized.

Ceramic 8 (strontium ferrite) is dramatically lower in cost. A 15.9-kg (35-lb) penalty in iron, copper, and aluminum resulting from the use of this material may be acceptable. A Ceramic 8 permanent magnet machine may therefore be a viable alternate to rare-earth-cobalt designs. Figures 46 and 47 show the Ceramic 8 design of table XIV.

TABLE XIV.—COMPARISON OF THREE MOTOR DESIGNS

	Samarium cobalt	Cerium cobalt B85	Ceramic 8
No. of poles	4	6	4
Magnet energy product at 68°F	22 MGO	17 MGO	3.3 MGO
Magnet weight, kg (lb)	0.677 (1.49)	1.47 (3.27)	3.78 (8.32)
Magnet approximate cost, $	225	215	16
Rating, rpm	26,000	26,000	22,000
V_{L-N} (induced, 3d)	55.85	58.00	56.64
A, ac	190.2	190.2	190.2
Pf (apparent)	-0.7536	-0.742	-0.7614
Net shaft power, kW (hp)	23.36 (31.32)	23.49 (31.5)	23.59 (31.63)
Weight, kg (lb)			
Electromagnetic	4.46 (9.84)	5.98 (13.18)	16.15 (35.6)
Estimated total	7 to 9 (15 to 20)	9 to 11 (20 to 25)	23 to 25 (50 to 55)
Losses, kW			
Copper	1.073	0.536	0.589
Eddy and stray	0.025	0.099	0.142
Windage and friction	0.083	0.103	0.428
Teeth	0.142	0.406	0.137
Core	0.252	0.421	0.347
Poles	0.0155	0.0375	0.0166
Damper	0.152	0.104	0.073
Total	1.74	1.71	1.73
Dimensions, cm (in.)			
Stack OD	10.066 (3.963)	9.581 (3.772)	13.475 (5.305)
Rotor OD	6.302 (2.481)	6.162 (2.426)	9.268 (3.649)
Hoop thickness	0.0823 (0.0324)	0.0937 (0.0369)	0.1674 (0.06591)
Stack length	10.305 (4.057)	15.133 (5.958)	4.196 (9.017)
Coil extension	2.837 (1.117)	2.096 (0.825)	4.196 (1.652)
Current density, $\frac{A}{m^2}$ $\frac{A}{in.^2}$	2.113×10^7 (13,630)	1.24×10^7 (8000)	6.2×10^6 (4000)
Commutation reactance, ohms	0.1965	0.185	0.2744

16.10 MAX

B

4.75 MAX
TYP

B
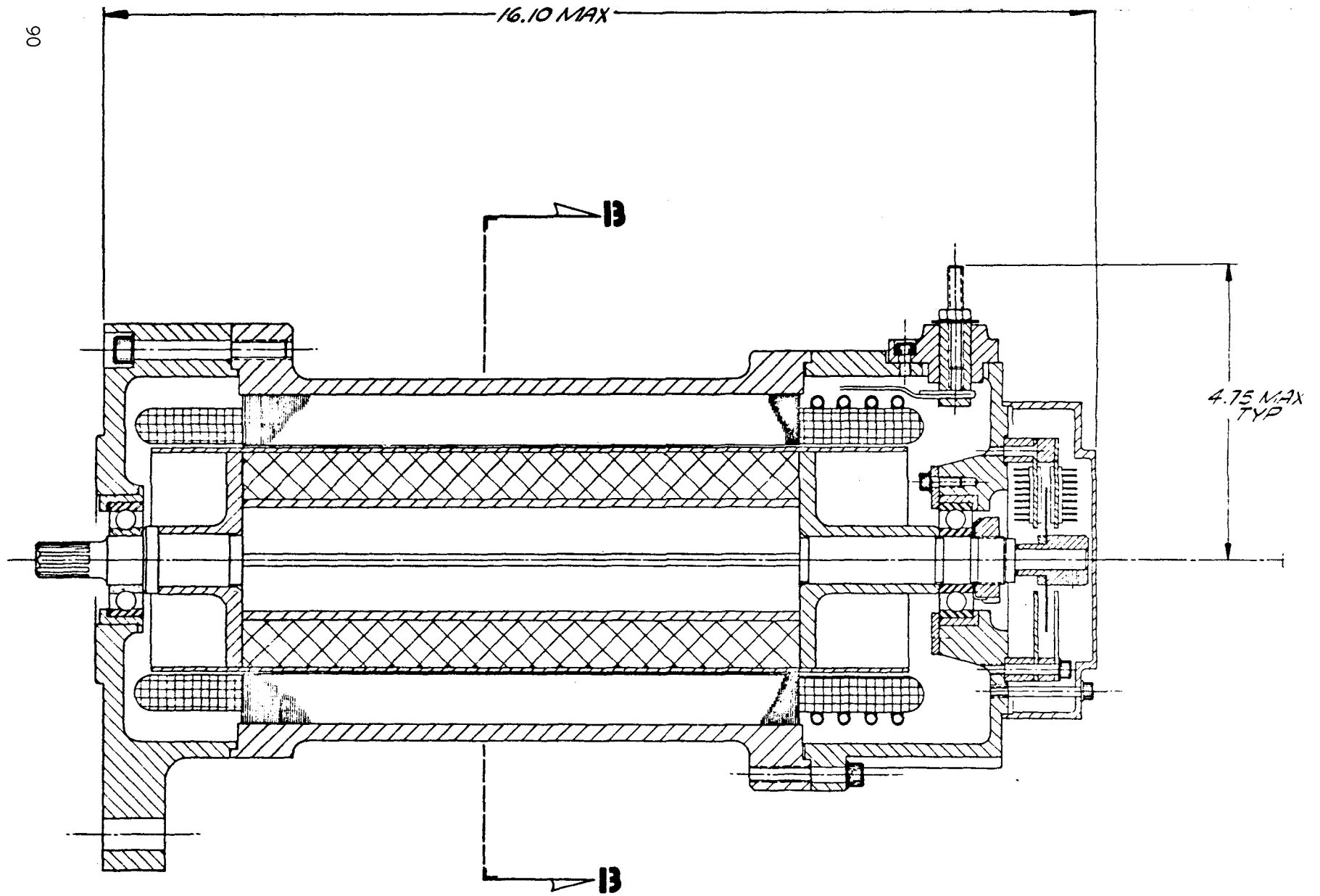
Figure 46.--Ceramic 8 design.
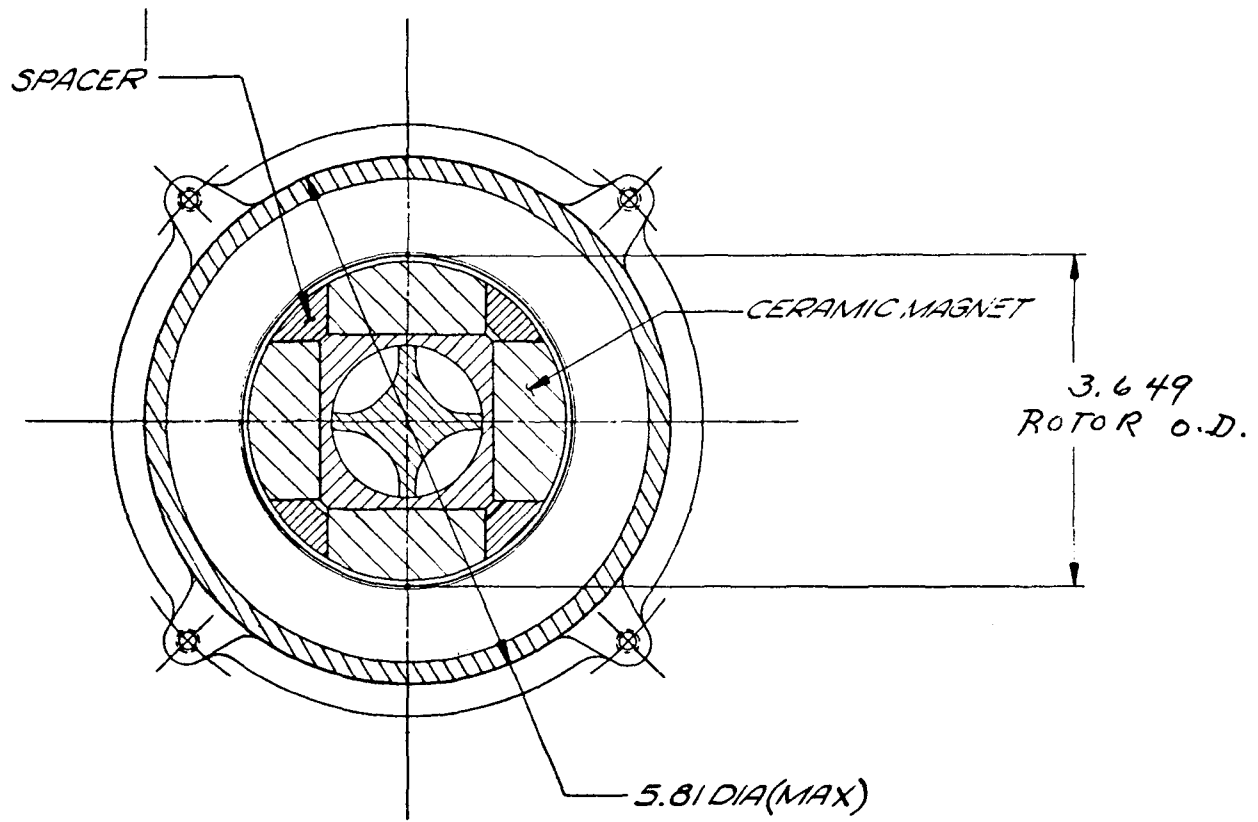
Figure 47.--Ceramic 8 design.

APPENDIX G

TABULATED TEST DATA FOR THE
ENGINEERING MODEL ELECTRONICALLY COMMUTATED
MOTOR

Tables XV and XVI present the essential test data taken during the test of the engineering model motor of Phase II as described in the Engineering Model Test section of this report. The estimated accuracies of the measurements are as follows:

Power ±2 percent

Torque ±2 in.-lb

Speed ±20 rpm

TABLE XV.--ENGINEERING MODEL IECM DRIVE MODE TEST RESULTS

Power			Operating point			Efficiency (calculated)		
dc input, kW	Motor input, kW	Motor output, kW	Speed, rpm	Torque		Motor, %	Controller, %	System, %
				in.-lb	N-m			
8.442	7.997	6.763	25620	22.31	2.521	84.6	94.7	80.1
13.278	12.800	11.175	25680	36.77	4.154	87.3	96.4	84.2
20.124	19.300	17.737	25800	58.09	6.564	91.9	95.9	88.1
29.277	28.620	25.590	25800	83.81	9.470	89.4	97.8	87.4
2.243	6.545	5.473	19080	24.24	2.739	83.6	90.4	75.6
10.101	9.305	7.967	18900	35.62	4.024	85.6	92.1	78.9
17.004	15.700	14.336	18780	64.51	7.288	91.3	92.3	84.3
25.238	23.340	20.630	18960	91.94	10.387	88.4	92.5	81.7
17.171	15.560	14.247	19200	62.7	7.084	91.6	90.6	83.0
5.891	5.496	4.405	13320	27.94	3.157	80.2	93.3	74.8
8.931	8.004	6.745	13440	42.41	4.791	84.3	89.6	75.5
14.318	12.880	10.880	13320	69.02	7.798	84.5	90.0	76.0
19.174	16.431	13.961	12960	91.03	10.285	85.0	85.7	72.8
13.070	11.240	9.708	12960	63.3	7.152	86.4	86.0	74.3
15.809	14.350	12.113	12840	79.72	8.894	84.4	90.8	76.7
3.460	2.774	2.075	6300	27.83	3.144	74.8	80.2	60.0
4.981	3.738	3.241	6360	43.06	4.865	86.7	75.1	65.1
9.354	7.078	5.454	6540	70.47	7.962	77.1	75.7	58.3
11.024	8.187	5.925	6540	76.55	8.649	72.4	74.3	53.8
8.203	6.038	4.787	6420	63.0	7.118	79.3	73.6	58.4

TABLE XVI.--ENGINEERING MODEL IECM BRAKE (GENERATOR) MODE TEST RESULTS

Power			Operating point			Efficiency (calculated)		
dc (1) output, kW	Motor (2) input, kW	Motor output, kW	Speed, rpm	Torque		Motor, %	Controller, %	System, %
				in.-lb	N-m			
23.586	26.874	26.100	26040	87.21	9.853	97.1	90.4	87.8
76.158	19.250	18.390	19560	83.16	9.395	95.5	88.0	84.0
12.462	14.775	13.770	19500	64.03	7.234	93.2	90.6	84.4
6.151	6.958	6.923	19500	30.15	3.406	99.5	88.8	88.4
3.378	4.218	3.950	19380	18.39	2.078	93.7	85.5	80.1
10.067	12.709	11.700	12990	82.67	9.340	92.1	86.0	79.2
7.242	9.066(3)	9.085(3)	12960	59.11	6.678	100(3)	79.9	79.9
3.294	4.588	4.315	13080	29.64	3.349	94.1	76.3	71.8
1.038	2.048	1.483	12840	13.48	1.523	72.4	70.0	50.7
4.008	6.118	5.594	6420	80.53	9.098	91.4	71.7	65.5
2.973	4.480	4.370	6480	58.42	6.600	97.6	68.0	66.4
1.378	2.448	2.445	6480	31.92	3.606	99.9	56.4	56.3
.351	1.161	1.053	6540	14.23	1.608	95.6	33.4	31.9

NOTES:

(1) 174 W additional loss to account for external power supplies has been included.

(2) Determined from power input to dynamometer.

(3) These measurements are subject to the instrumentation accuracies specified.

REFERENCES

1. Bedford, B. D.; and R. G. Hoft: Principles of Inverter Circuits. Wiley (New York), 1964.

2. Schaefer, Johannes: Rectifier Circuits: Theory and Design. Wiley (New York), 1965.

1. Report No. NASA CR-165601	2. Government Accession No.	3. Recipient's Catalog No.
4. Title and Subtitle Lightweight Electronically Commutated dc Motor for Electric Passenger Vehicles		5. Report Date September 1982
		6. Performing Organization Code 778-36-06
7. Author(s) E. F. Echolds and P. S. Walia		8. Performing Organization Report No. 81-18266
		10. Work Unit No.
9. Performing Organization Name and Address AiResearch Manufacturing Company The Garrett Corporation 2525 W. 190th Street Torrance, California 90509		11. Contract or Grant No. DEN 3-64
		13. Type of Report and Period Covered Contractor Report
12. Sponsoring Agency Name and Address U. S. Department of Energy Office of Vehicle and Engine R&D Washington, D.C. 20545		14. Sponsoring Agency Code-Report No. DOE/NASA/0064-1

16. Abstract

A program was conducted to develop a state-of-the-art, electronically commutated motor specifically designed for propulsion of electric vehicles with increased range, reduced energy consumption, and reduced life-cycle costs compared with conventional systems. The program was accomplished in two phases involving development and test of (1) a functional model breadboard converter and a rare-earth-cobalt, permanent-magnet (PM) motor, and (2) an engineering model converter and PM motor suitable for vehicle installations. The converter and motor achieved an 88 percent peak efficiency, a maximum output of 26 kW at 26,000 rpm, and a continuous rating of 15 kW. The system also regenerated power to the source during braking, with a demonstrated peak power available at the converter terminals of approximately 26 kW at 88 percent efficiency. Major conclusions included (1) the SAE J227a(D) driving cycle efficiency for the converter/motor is 86 to 88 percent when energy available for recovery at the converter terminals is included; (2) the converter initial cost is approximately five times that of the permanent magnet motor, but can be reduced by means of LSI logic and integrated liquid-cooled semiconductor packages; and (3) an electronically commutated motor with a liquid-cooded converter will operate reliably without service or maintenance for the life of a passenger vehicle.

17. Key Words (Suggested by Author(s)) Electric vehicle Electric propulsion Electronic commutation Permanent magnet motor Converter	18. Distribution Statement Unclassified - unlimited STAR Category 33 DOE Category UC-96		
19. Security Classif. (of this report) Unclassified	20. Security Classif. (of this page) Unclassified	21. No. of Pages	22. Price*